

# The Impact of Dams on Sediment Transport from the Parker River Watershed to the Plum Island Estuary:

Author: Xinyi Zeng

Persistent link: <http://hdl.handle.net/2345/bc-ir:108922>

This work is posted on [eScholarship@BC](#),  
Boston College University Libraries.

---

Boston College Electronic Thesis or Dissertation, 2020

Copyright is held by the author. This work is licensed under a Creative Commons Attribution 4.0 International License (<http://creativecommons.org/licenses/by/4.0>).

**THE IMPACT OF DAMS ON SEDIMENT  
TRANSPORT FROM THE PARKER RIVER  
WATERSHED TO THE PLUM ISLAND ESTUARY**

**Xinyi Zeng**

A thesis  
Submitted to the Faculty of  
the department of Earth and Environmental Sciences  
in partial fulfillment  
of the requirements for the degree of  
Master of Science

Boston College  
Morrissey College of Arts and Sciences  
Graduate School

August, 2020

© Copyright (2020) Xinyi Zeng

**THE IMPACT OF DAMS ON SEDIMENT TRANSPORT FROM THE PARKER  
RIVER WATERSHED TO THE PLUM ISLAND ESTUARY**

Xinyi Zeng

Advisor: Noah P. Snyder, Ph.D.

Though previous studies have shown saltmarsh adaptability to some degree of sea level rise (SLR), sediment supply is critical to sustaining saltmarshes as SLR accelerates. Land-use activities, such as dams, often influence watershed sediment transport and delivery to the coast. Previous studies have suggested that, even in small watersheds, dams can significantly impact coastal sediment budgets. The Parker River watershed (PRW) in northeastern Massachusetts hosts 20 dams and several natural lakes, and drains into the Plum Island Sound Estuary (PIE). This research aims to evaluate the impact of dams and sediment transport in the PRW. Three approaches were used: theoretical modeling of sediment transport patterns using digital elevation models; spatial analysis of suspended sediment concentration (SSC) and remote sensing data; and empirical calculations of reservoir trap efficiency.

Geomorphic modeling indicates that bankfull discharge can transport 20  $\mu\text{m}$  grains (silt) as wash load throughout the PRW. Sediment deposition might happen at Crane Pond and in reservoirs, but removing dams would not change this pattern. Both SSC data and observations of satellite images during high-flow events indicate low supply and transport of sediment throughout the PRW. The estimates of sediment yield ( $Y$ ) are low for the PRW. An empirical calculation indicates little-to-no trap efficiencies for all dams. Therefore, fluvial contribution to the sediment budget of the PIS estuary is limited and dam removals in the PRW are unlikely to change the rate of sediment delivery to the PIE. The proposed method of this study provides an additional scope to assess the

ecological benefits of removing a dam and could be easily replicated for other locations for similar assessment. Future studies should assess sediment dynamics and management practices from a more thorough perspective incorporating the riverine, estuarine and shelf system.

## **Acknowledgements**

I would like to first thank my thesis advisor Professor Noah Snyder for both providing me guidance and fostering my independence on my research. You consistently allowed me to develop my work, but also steered me towards right direction whenever I needed it.

Thank you to the Department of Earth and Environmental Sciences at Boston College (BC), for providing the educational opportunities and financial supports that allowed me to pursue this research and travel to conferences over my time at BC.

I am also gratefully indebted to my second reader, Professor Gail Kineke, who provided me many constructive comments at various stages of this research. Also, thank you to Carling Hay for serving on my committee.

I am also grateful to have a lab group that provided me friendship, support, and field assistance: Thank you, Samantha Dow, James LeNoir, Robin Kim, Sarah Jonathan, Megan Kopp, and Aleksandra Ostojic. Thank you to all my fellow grad students for being such a welcoming and supportive community.

I would also like to thank Beth Lambert, the director at the Massachusetts Division of Ecological Restoration (DER), who provided me the initial question that this research is hoping to address, and all my colleagues at DER who provided constructive feedbacks for this research.

Finally, I would like to express my profound gratitude to my parents who always provide unconditional support for me to pursue my dream. Your trust and encouragement help me overcome ups and downs in the process of writing this research and I would not be who I am without you. Thank you!

# Table of Contents

Acknowledgements .....	i
List of Figures .....	v
List of Tables .....	x
1 Introduction .....	1
2 Study Area.....	4
3 Background .....	8
3.1 The Future of SLR and Saltmarshes Adaptability to SLR.....	8
3.2 Sediment Availability and Marshland Resilience.....	12
3.3 Impact of Dams on Sediment Transport .....	14
3.4 Sediment Discharges and Sediment Yields from Previous Studies.....	16
4 Purpose and Scope.....	19
5 Research Methods.....	20
5.1 Theoretical Approach: Suspended-Sediment Transport Pattern .....	20
5.1.1 Calculations of Geomorphic Parameters and Geospatial Analysis.....	20
5.2 Field-based and Remote Sensing Approach: Observations of Hydrology and Sediment Transport .....	27
5.2.1 SSC Datasets and Suspended Sediment Yield.....	27

	5.2.2	Fieldwork and Lab Designs for SSC Spatial Pattern Analysis .....	29
	5.2.3	Remote Sensing Analysis .....	31
	5.3	Empirical Approach: Trap Efficiency.....	31
6		Results.....	33
	6.1	Theoretical Analysis: Suspended Sediment Transport Pattern .....	33
	6.1.1	Geomorphic Parameters and Geospatial Analysis .....	33
	6.1.2	Downstream Variations of Geomorphic Parameters.....	43
	6.1.3	Comparison of Shear Stress Change between the Dammed and Undammed Scenarios .....	47
	6.2	Field-based and Remote Sensing Analysis: Observations of Hydrology and Sediment Transport.....	47
	6.2.1	Suspended Sediment Yield .....	47
	6.2.2	SSC Spatial Pattern Analysis .....	52
	6.2.3	Remote Sensing Data Analysis .....	54
	6.3	Empirical Analysis: Trap Efficiency.....	59
7		Discussion .....	59
	7.1	Are Dams Trapping Sediment and therefore Reducing Sediment Load to the Estuary? 59	

7.2	What Portion of the Watershed can Contribute Sediments to the Estuary?.....	68
7.3	Sediment Sources to the PIS Estuary .....	72
7.4	Insights on Management .....	80
8	Conclusions .....	81
	Bibliography .....	84
	Appendix: Parameters and Constants.....	90

## List of Figures

Figure 1. (a) The study site, Parker River (blue-line polygon), is located in the northeastern Massachusetts about 40 km north of Boston tide gage (blue star) (MassGIS, 2017). The climatological station at the Lawrence Municipal Airport, MA (green star) locates slightly northwest of the watershed. (b) The study area (navy blue-lined polygon) is constrained to the part of the watershed (purple-lined polygon) without tidal influence. (c) A close-up map for the dammed reach (yellow-lined rectangle). SSC samples were collected at Parker River at Thurlow Street, River Street, Larkin Road, USGS gage (yellow star), and Parker River Dam, and Wheeler Brook at Larkin Road..... 3

Figure 2. The longitudinal profile (a) and the slope profile (b) of the Parker River main stem from mouth to head. The longitudinal profile with no data values and extreme pits and spikes removed (filtered LiDAR, blue line). Tide information is obtained from Plum Island South tide gage located close to the inlet of Plum Island Sound on the stage island and tidal datum is measured relative to mean lower low water (MLLW, magenta line). Mean high water (MHW) is 2.77 m above MLLW, mean higher-high water (MHHW, green line) is 2.89 m above MLLW, mean tide level (MTL, cyan line) is 1.43 m above MLLW, mean sea level (MSL) is 1.43 m above MLLW. 25-m-moving-average profile (25-point filter, black line), profile with minima connected (demprofile\_min, red line), and dams (black downward triangle) are indicated in the upper panel. Z\_space is the filter interval for slope calculation. .... 5

Figure 3. Surficial geology of the Parker River upland watershed and the Rowley River watershed (MassGIS, 2017)..... 6

Figure 4. Mean discharge ( $Q$ ) for each month at the USGS gage on Parker River at Byfield, MA (USGS, 2019). .... 7

Figure 5. Interannual variation in mean sea level resulted in this relationship between the observed productivity of the salt marsh macrophyte *Spartina alterniflora*, measured annually since 1984 (Morris 2000), and depth below mean high tide (MHT) of sites in the high (open circles) and low (solid circles) marsh. Depth below MHT was computed during the peak growing season months of July and August and is a highly significant predictor of productivity ( $r^2 = 0.81$ ,  $P < 0.0001$ ). Stable (solid line) or unstable (dashed line) combinations of equilibrium productivity,  $B$ , and depth,  $D$  are also shown for  $B = 155D - 1.855D^2 - 1364$  (from Morris et al., 2002)..... 9

Figure 6. Response of marsh elevation (a) and accretion rate (b) to a conservative sea-level acceleration (IPCC A1B scenario [Bindoff et al., 2007]). Heavy blue line denotes sea level at spring high water (Figure 2a) or the sea-level rise rate (Figure 2b). The other lines represent elevations of the simulated position of the marsh relative to spring high water for different models (Morris et al., 2002; Temmerman et al., 2003; D'Alpaos et al., 2007; Kirwan and Murray, 2007; Mudd et al., 2009). Because each model predicts a slightly different initial elevation relative to sea level, Kirwan et al. have normalized each model to a common equilibrium elevation at time zero. Because sea-level rise rates tend to exceed accretion rates, marsh elevations adjust to sea-level acceleration by becoming lower relative to sea level (i.e., more inundated) (Figure 2a), which enhances vertical accretion (Figure 2b). (Experimental conditions: spring tidal range = 1 m, suspended-sediment concentration = 30 mg L<sup>-1</sup>) (from Kirwan et al., 2010). .... 10

Figure 7. Response of (a) marsh elevation and (b) accretion rate to a rapid sea-level acceleration. Heavy blue line denotes sea level at spring high water (Figure 3a) or the sea-level rise rate (Figure 3b). The other lines represent elevations of the marsh relative to spring high water using different models (Morris et al., 2002; Temmerman et al., 2003; D’Alpaos et al., 2007; Kirwan and Murray, 2007; Mudd et al., 2009). In this model experiment, sea level accelerates according to Rahmstorf’s (2007) maximum scenario. Kirwan et al. (2010) have extrapolated Rahmstorf’s scenario from 2100 to 2200 AD using a 3rd degree polynomial fit. Marsh elevations tend to adjust to sea-level acceleration by becoming deeper relative to sea level, although the dashed black line denotes the lowest elevations at which vegetation can grow. Arrows denote the point in each model at which marsh elevations become too low to support vegetation. In most models, vegetation mortality leads to a decrease in accretion. However, mortality leads to a temporary increase in organic accretion in the Mudd model, and does not affect accretion in the Temmerman model. (Experimental conditions: spring tidal range = 1 m, suspended-sediment concentration = 30 mg L<sup>-1</sup>.) (from Kirwan et al., 2010). ..... 11

Figure 8. Map of Plum Island Estuary (Massachusetts) study area showing extent of pre-settlement marsh (blue shading) and post-settlement marsh (pink shading). Dates of marsh formation on map represent calibrated radiocarbon dates from basal peat (red dots), or dates estimated from peat thickness reported by McIntire and Morgan (1963) (yellow dots) and McCormick (1968) (blue dots). Positive dates indicate years A.D., negative dates indicate years B.C. (from Kirwan et al. 2011). ..... 13

Figure 9. Conceptual diagram depicting longitudinal profile of pre and post impoundment conditions and volume of stored sediment (modified from McCusker & Daniels, 2008). The blue arrow demonstrates the direction of water flow. Scenarios without dams will be synthesized through connecting A and B in longitudinal profiles..... 15

Figure 10. The Strahler stream order is a common way in hydrology to define the size of a river or stream (Horton, 1945; Strahler, 1952; Strahler, 1957). Each segment of a stream or a river within a river network is treated as a node in a tree, with the next segment downstream as its parent. When two first orders come together, they form a second-order stream. The figure represents a stream order of 5 (modified from Wikipedia, 2011). ..... 17

Figure 11. The logarithmic relation between annual peak stream-flow and recurrence interval at the USGS gage (01101000) on Parker River at Byfield, MA (USGS, 2018a). ..... 24

Figure 12. Lab set up for SSC measurements. Equipment from left to right: a 1000-mL graduated cylinder, a conical flask with a filter cup and an opening that could be connected to the lab vacuum through a tube, and Whatman 47-mm GF/F glass-fiber filters. .... 30

Figure 13. The aerial photo of the Crane Pond in 2001 with the inlet location position indicated (red arrow) (MassGIS, 2019). ..... 32

Figure 14. The longitudinal profile of the Parker main stem (a). The distribution of basal shear stress ( $\tau_b$ ) for bankfull discharge ( $Q_{bf}$ ) [red point: > 50 Pa; yellow point: 10 - 50 Pa; green point: < 10 Pa] (b). All  $\tau_b$  are above  $\tau_c$  (critical shear stress) for 20  $\mu\text{m}$  (0.05 Pa) and 200  $\mu\text{m}$  (0.15 Pa). Color shading emphasizes the splitting classes and is consistent with the following figures. The  $d\tau_b/dx$  calculated with central difference (c), 5 points average (d), and 9 points average (e) with

positive value as red, negative value as blue and zero as grey. Gray banding indicates the location of Crane Pond. ....	35
Figure 15. The distribution of basal shear stress ( $\tau_b$ ) for bankfull discharge ( $Q_{bf}$ ) [red point: > 50 Pa; yellow point: 10 - 50 Pa; green point: < 10 Pa]. All $\tau_b$ values are above critical shear stress ( $\tau_c$ , Table 3) for 20 $\mu\text{m}$ and 200 $\mu\text{m}$ . The red rectangle indicates the Crane Pond. ....	36
Figure 16. The distribution of Shields parameter ratio ( $\phi\phi_c$ ) for 200 $\mu\text{m}$ grains at bankfull discharge ( $Q_{bf}$ ) [green points: >1]. The red rectangle indicates the Crane Pond. ....	37
Figure 17. The distribution of Shields parameter ratio ( $\phi\phi_c$ ) for 20 $\mu\text{m}$ grains at bankfull discharge ( $Q_{bf}$ ) [green points: >1]. The red rectangle indicates the Crane Pond. ....	38
Figure 18. The longitudinal profile of the Parker main stem (a). The distribution of Rouse number ( $P$ ) for 200 $\mu\text{m}$ grains at bankfull discharge ( $Q_{bf}$ ) [red: bed load; yellow: suspended load with 50% suspension; turquoise: suspended load with 100% suspension; green: wash load] (b). The change of Rouse number calculated with central difference (c), 5 points average (d), 9 points average (e) with positive values as blue, negative values as red, and zero as grey. Gray banding indicates the location of Crane Pond. ....	39
Figure 19. The distribution of Rouse number ( $P$ ) for 200 $\mu\text{m}$ grains at bankfull discharge ( $Q_{bf}$ ) for original profile [red: bed load; yellow: suspended load with 50% suspension; light green: suspended load with 100% suspension; green: wash load]. The red rectangular is highlighting the Crane Pond Wildlife Management area. ....	40
Figure 20. The longitudinal profile of the Parker main stem (a). The distribution of Rouse number ( $P$ ) for 20 $\mu\text{m}$ grains at bankfull discharge ( $Q_{bf}$ ) [turquoise: suspended load with 100% suspension; green: wash load] (b). The change of Rouse number ( $dPdx$ ) calculated with central difference (c), 5 points average (d), 9 points average (e) with positive values as blue, negative values as red, and zero as grey. Gray bandings indicates the location of Crane Pond. ....	41
Figure 21. The distribution of Rouse number ( $P$ ) for 20 $\mu\text{m}$ grains at bankfull discharge ( $Q_{bf}$ ) for original profile [green: wash load]. The red rectangular is highlighting the Crane Pond Wildlife Management area. ....	42
Figure 22. The distribution of the change of basal shear stress ( $d\tau_bdx$ ) for bankfull discharge ( $Q_{bf}$ ) [red point: positive change indicating erosional; beige point: no change; blue point: negative change indicating depositional]. The red rectangular is highlighting the Crane Pond Wildlife Management area. ....	44
Figure 23. The distribution of Rouse number change ( $dPdx$ ) for 200 $\mu\text{m}$ grains at bankfull discharge ( $Q_{bf}$ ) [red: negative change - erosional; beige: no change; blue: positive change - depositional]. The red rectangular is highlighting the Crane Pond Wildlife Management area. ...	45
Figure 24. The distribution of Rouse number change ( $dPdx$ ) for 20 $\mu\text{m}$ grains at bankfull discharge ( $Q_{bf}$ ) [red: negative change - erosional; beige: no change; blue: positive change - depositional]. The red rectangular is highlighting the Crane Pond Wildlife Management area. ....	46

Figure 25. The longitudinal profile of the Parker main stem (blue) and its simulated undammed scenario (orange) (a). Change in shear stress ( $\tau_{bdx}$ ) is identified throughout the longitudinal profile with positive values as red and negative values as blue for undammed (b) and dammed (c) scenarios. ....48

Figure 26. Suspended sediment rating curves at the Parker River Dam (LTER, blue) and USGS gage (modified from Nadeau, 2010, orange) are used for suspended sediment discharge estimate. Reference lines indicate the bankfull discharge at the USGS gage (light orange,  $4.6 \text{ m}^3 \text{ s}^{-1}$ ) and the LTER site (light blue,  $5.5 \text{ m}^3 \text{ s}^{-1}$ ). ....49

Figure 27. Sediment load at USGS gauge (orange dotted line) and Parker River Dam (LTER, blue dotted line) for each water year from 1947 to 2017. The average  $Q_s$  is  $120.3 \text{ Mg yr}^{-1}$  at USGS gage (orange line) and  $61.0 \text{ Mg yr}^{-1}$  at LTER site (blue line). Grey banding is indicating the 95 % confidence interval for the average calculation. ....50

Figure 28. Sediment yield at USGS gauge (orange dotted line) and Parker River Dam (LTER, blue dotted line) for each water year from 1947 to 2017. The average  $Y$  is  $2.3 \text{ Mg km}^{-2} \text{ yr}^{-1}$  at USGS gage (orange line) and  $1.0 \text{ Mg km}^{-2} \text{ yr}^{-1}$  at LTER site (blue line). Grey banding is indicating the 95% confidence interval for the average calculation. ....51

Figure 29. Dry sediment mass ( $m_{ds}$ , upper panel, orange dots), post-LOI sediment mass ( $m_s$ , middle panel, olive dots), and suspended sediment concentration (SSC, lower panel, brown dots) measured and calculated from a 250-mL water sample collected in 1-L bottles at the Parker River at Parker River Dam, Larkin Road, River Street, Newbury, MA, Thurlow Street, Georgetown, MA, Wheeler Brook at Larkin Road, Georgetown, MA, and USGS gage at Byfield, MA on October 26<sup>th</sup>, 2018. DI water was used as a blank reference. Yellow bandings indicate the uncertainty calculated from the accuracy of the measurement ( $\pm 2 \text{ mg}$  for  $m_{ds}$ , and  $m_s$  and  $\pm 7 \text{ mg/L}$  for SSC) and gray bandings indicate the 95% confidence intervals for the average of three samples at each site (dark gray line). The average daily flow ( $Q_d$ ) was  $0.40 \text{ m}^3/\text{s}$  and the weather was sunny with a temperature at 2-6 °C. ....53

Figure 30. Dry sediment mass ( $m_{ds}$ , upper panel, orange dots), post-LOI sediment mass ( $m_s$ , middle panel, olive dots), and suspended sediment concentration (SSC, lower panel, brown dots) measured and calculated from a 250-mL water sample collected in 1-L bottles at Parker River at the Parker River Dam, Larkin Road, River Street, Newbury, MA, Thurlow Street, Georgetown, MA, Wheeler Brook at Larkin Road, Georgetown, MA, and USGS gage at Byfield, MA on May 14<sup>th</sup>, 2019. DI water was used as a blank reference. Yellow bandings indicate the uncertainty calculated from the accuracy of the measurement ( $\pm 0.2 \text{ mg}$  for  $m_{ds}$  and  $m_s$ , and  $\pm 0.7 \text{ mg/L}$  for SSC) and gray bandings indicate the 95% confidence intervals for the average of three samples at each site (dark gray line). The average daily flow ( $Q_d$ ) was  $1.68 \text{ m}^3/\text{s}$  and the weather was light rain with a temperature at 5-6 °C. ....55

Figure 31. (a) High discharge event between March 28<sup>th</sup>, 2017 to April 17<sup>th</sup>, 2017 at Parker River. Orange dots are 15-min discharges ( $Q_{15\text{-min}}$ ) measured at the USGS gauge, Byfield, MA with the peak discharge ( $Q_{\text{peak}}$ ) at  $7.362 \text{ m}^3/\text{s}$  ( $RI=2.52$  years). Blue bars are precipitations measured at Lawrence Municipal Airport, MA. Grey lines annotated the time with available satellite images from Planet.com. (b) (c) satellite images from Planet.com. Ice cover (red rectangle) presented on Crane Pond on March 30<sup>th</sup>, 2017 and the inlet is indicated (red arrow) (b). ....56

Figure 32. (a) High discharge event between April 16<sup>th</sup>, 2018 to April 25<sup>th</sup>, 2018 at Parker River. Orange dots are 15-min discharges ( $Q_{15\text{-min}}$ ) measured at the USGS gauge, Byfield, MA with the peak discharge ( $Q_{\text{peak}}$ ) at 4.927 m<sup>3</sup>/s ( $RI=1.62$  years). Blue bars are precipitations measured at Lawrence Municipal Airport, MA. Grey lines annotated the time with available satellite images from Planet.com. (b) satellite images from Planet.com with the inlet location indicated (red arrow).  
.....57

Figure 33. (a) Three consecutive high discharge events between November 4<sup>th</sup>, 2018 to December 9<sup>th</sup>, 2018 at Parker River. Orange dots are 15-min discharges ( $Q_{15\text{-min}}$ ) measured at the USGS gauge, Byfield, MA with the peak discharge ( $Q_{\text{peak}}$ ) at 6.513 m<sup>3</sup>/s ( $RI=2.17$  years). Blue bars are precipitations measured at Lawrence Municipal Airport, MA. Grey lines annotated the time with available satellite images from Planet.com. (b-g) satellite images from Planet.com with the inlet location indicated (red arrow).....58

Figure 34. Aerial photos of Crane Pond from 1990s to 2018 signaling little to no delta evolution (MassGIS, 2019) with the inlet location indicated (red arrow). The figure for 2016 was impacted by cloud cover. ....60

Figure 35. The reservoir area ( $A$ , red line) and reservoir extent (red dots) determined by the slope jump in the minimum profile.....61

Figure 36. The corresponding trap efficiency ( $Te$ ) for each dam given capacity-inflow ratio ( $C/I$ ) (modified by Verstraeten and Poesen, 2000 from Brune, 1953). The red triangle with number one inside denotes the trap efficiency and capacity-inflow ( $C/I$ ) ratio for the Parker River Dam, Newbury, MA when the reservoir area is determined using the reservoir polygons in the USGS 25k water bodies. All reservoir areas determined using LiDAR DEM and other reservoir areas from USGS 25k water bodies are not identifiable using this graph because the  $C/I$  ratios are less than 0.001.....62

Figure 37. The reservoir area ( $A$ , red line) determined by reservoir polygons in USGS 25k water bodies. ....63

Figure 38. The Landsat Scenes in 1-2-3 [Blue-Green-Red] of Plum Island Sound (PIS) on March 18<sup>th</sup>, 2014 ( $SSC = 1.72$  mg/L) (a) and April 3<sup>rd</sup>, 2014 ( $SSC = 9.72$  mg/L) (b) (EarthExplorer, 2020). ....70

Figure 39. The relationship between  $SSC$  and  $Q_d$  at the Parker River Dam (LTER site). The blue line indicates the log-regression relationship between the two variables and the grey band shows the 95% confidence interval. The light blue reference line indicates the bankfull discharge (vertical, 5.5 m<sup>3</sup>/s) and the splitting line for the highest four  $SSCs$  (horizontal, 10 mg/L) at Parker River Dam. ....73

Figure 40. The Landsat Scenes in band 1-2-3 [Blue-Green-Red] of Plum Island Sound and Merrimack River mouth on September 2<sup>nd</sup>, 2011 (after Hurricane Irene) (Earth Explorer, 2020).  
.....78

Figure 41. The sediment rating curve for the USGS gage at Lowell, MA (USGS 01100000) on the Merrimack River. Light blue lines indicate the  $Q_d$  during Hurricane Irene (882 m<sup>3</sup>/s) and its corresponding  $Q_{sd}$  (1069 Mg/d) estimated from this curve.....79

## List of Tables

Table 1. Land use of the Parker River watershed in 2016 (MassGIS, 2017).....	5
Table 2. Surficial geology of the Parker River watershed and the Rowley River watershed (MassGIS). .....	6
Table 3. Results of $\varphi_c$ , $\tau_c$ , and $w_s$ for 20 $\mu\text{m}$ and 200 $\mu\text{m}$ grains. ....	24
Table 4. Implication of Rouse Number Values (Whipple, 2004).....	26
Table 5. The calculation for the empirical analysis based on the reservoir areas determined by the interpolated minimum slope profile.....	64
Table 6. The calculation for the empirical analysis based on the reservoir areas determined by the connected minimum profile.....	65

## 1 Introduction

Saltmarshes provides important ecological services, including flood abatement, carbon and nutrient sequestration, water quality maintenance, landscape appeal, and habitat for fish, shellfish, and wildlife (DER, 2014). As sea level rise (SLR) leads to the inundation of coastal regions, one of the biggest concerns is the adaptability of saltmarshes. Previous studies (e.g., Kirwan et al., 2010) have shown that saltmarshes adapt to some degree of SLR; however, when the inundation no longer allows vegetation growth, marshlands transition to subtidal mudflats. The rate of sediment supply to coasts and the movement of coastal sediments control whether saltmarshes accrete or erode under the accelerating SLR (Kirwan et al., 2010).

Rivers supply sediments to the coast and human activities can change sediment yields by modifying the characteristics of watersheds and river channels. In particular, dams can decrease the grade and velocity of rivers, trap sediments in impoundments, and decrease sediment supply to the coasts significantly. Most previous studies (e.g., Wang et al., 2007; Syvitski et al., 2009; Kemp et al., 2016) focus on large rivers, such as the Mississippi River and the Yangtze River, where high discharges can mobilize more and larger sediments to the river mouth, and thus the impact of dams on sediment transport are more significant. Only a few studies (e.g., Willis & Griggs, 2003; McCusker & Daniels, 2008) have investigated the effect of dams on small rivers, and suggested that dams could be a major factor impacting coastal erosion in these watersheds.

The Parker River watershed in northeastern Massachusetts hosts 17 dams and several natural lakes (Fig. 1). The river drains into the Plum Island Sound (PIS) estuary (Fig. 1), the largest intertidal marsh in the northeastern US. The tidal portion of the Parker River and PIS estuary lies within the boundary of the Parker River/Essex Bay Area of Critical Environmental Concerns (ACEC), which was designated in 1979. The status engages local communities to work with state

agencies and other organizations to preserve environmental quality, historic character, and associated economic values. The Parker River-PIS estuary possess valuable marine resources and provide important habitats for valuable fish, shellfish, and bird species (Buchsbaum et al., 2002). Multi-stakeholder efforts have long existed to actively assess the environmental issues and develop management plans (e.g., Rickards et al., 2002; Executive Office of Environmental Affairs, 2005; Schottland et al., 2017; Kelder, 2018). Many earlier efforts focused on the issues of water supply, water quality, habitats, and land use (e.g., Rickards et al., 2002; Executive Office of Environmental Affairs, 2005), while more recent planning start to address concerns over climate change, sea level rise, and human made structures as barriers to streamflow (e.g., Schottland et al., 2017; Kelder, 2018; DER, 2020).

However, these assessments lack a holistic analysis on the relationship among infrastructure, streamflow, sediment transport, and the consequential impact of marsh resilience. More specifically, the impacts of dams are only assessed on two dimensions: ecological impacts and infrastructure failure risks (e.g., Schottland et al., 2017; Kelder, 2018; DER, 2020). It is yet unclear whether the dams on the Parker River have impacts on the sediment dynamics of the whole watershed and thus the resilience of marshes. Thus, this study looks to fill the knowledge gap in current assessment through answering two questions: (1) Are dams trapping sediments and therefore reducing sediment load to the estuary? (2) What portion of the watershed can contribute sediments to the estuary? The estimated impact of dams on the sediment transport and the capacity of the watershed as a sediment source provide insights on land use practices and dam removal decisions in this region to help the resilience of saltmarshes in the PIS estuary.

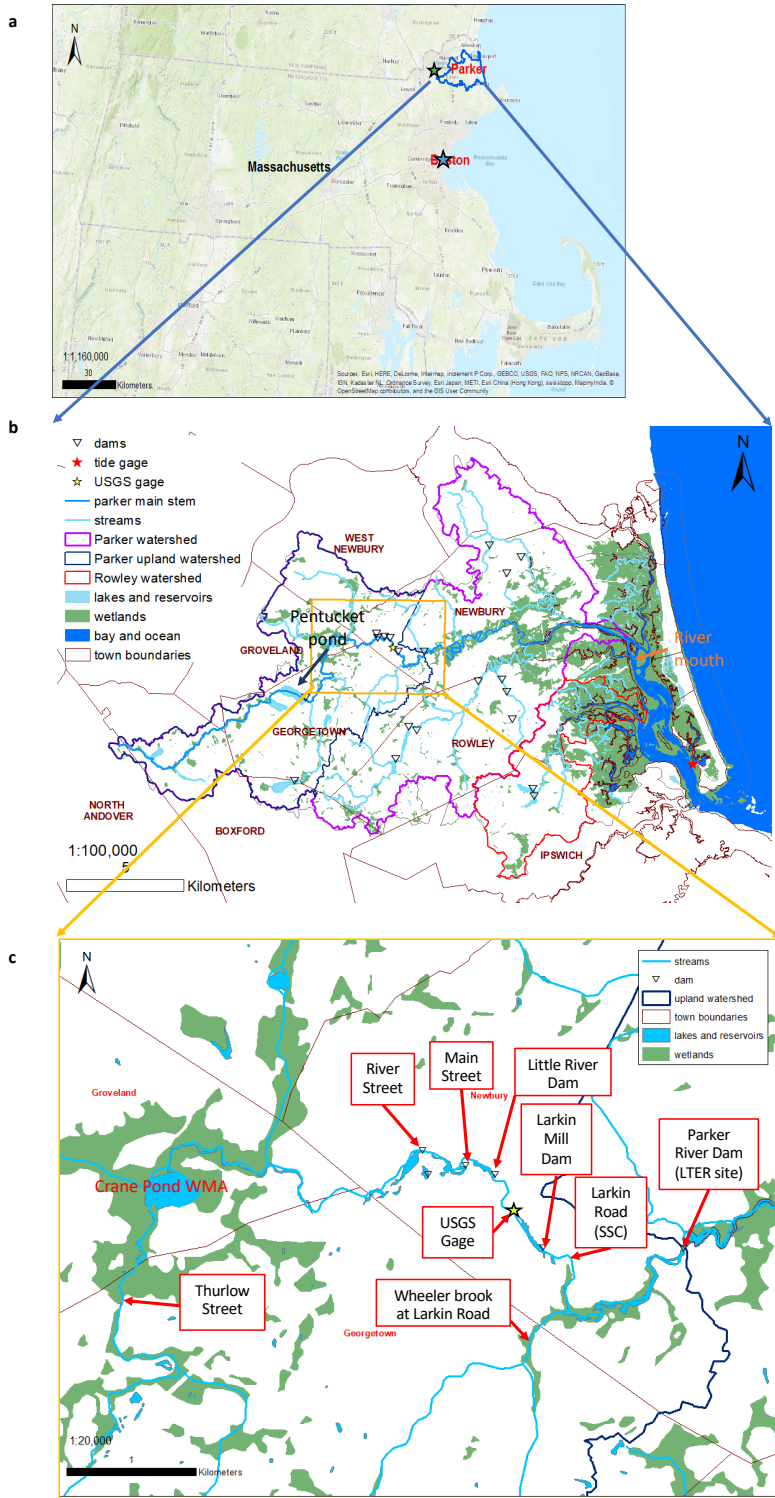


Figure 1. (a) The study site, Parker River (blue-line polygon), is located in the northeastern Massachusetts about 40 km north of Boston tide gage (blue star) (MassGIS, 2017). The climatological station at the Lawrence Municipal Airport, MA (green star) locates slightly northwest of the watershed. (b) The study area (navy blue-lined polygon) is constrained to the part of the watershed (purple-lined polygon) without tidal influence. (c) A close-up map for the dammed reach (yellow-lined rectangle). SSC samples were collected at Parker River at Thurlow Street, River Street, Larkin Road, USGS gage (yellow star), and Parker River Dam, and Wheeler Brook at Larkin Road.

## 2 Study Area

The Parker River is located in the northeastern Massachusetts with a total drainage area of 149.5 km<sup>2</sup> (Fig. 1a). The river originates in wetlands in Boxford, and flows 34 km into the PIS (Fig. 1b). A total of 18 dams are located in the watershed, including seven on the main stem. Six of these dams are concentrated in a segment of 0.5 km long and I will refer to this region as the dammed reach (Fig. 1b-c). The mean tidal range is 2.6 m (NOAA, 2018), with tidal influence extending up to the Parker River Dam (Fig. 2a). I define the upland watershed as the drainage basin upstream of the Parker River Dam (63.5 km<sup>2</sup>, Fig. 1b) and constrain my analysis to this area.

The basin contains several lakes, which are natural locations for sediment deposition. The studied basin has little agricultural land (2%) and bare land (1%), which limits the opportunity for soil erosion from cleared lands (Table 1; MassGIS, 2017). Water bodies consist of 4% of the basin, wetlands occupy 8%, and forests take up 50% (Table 1; MassGIS, 2017). The surficial geology of the watershed includes glacial-age sand and gravel deposits, till or bedrock, fine-grained deposits, and floodplain alluvium (Fig. 3, Table 2). The river is mostly sand and gravel-bedded upstream of Crane Pond and transitions to mud-bedded or bedrock at and downstream of Crane Pond. The low relief landscape (the highest elevation = 109 m) provides low energy to erode sedimentary deposits and bedrock. The mean annual precipitation is 1.0 m (USGS, 2019) and mean annual flood is 5.89 m<sup>3</sup> s<sup>-1</sup> (USGS, 2019) measured at the USGS gage (Fig. 1b, c). The mean annual discharge is 1.1 m<sup>3</sup> s<sup>-1</sup> (Granato et al., 2017) and the highest mean monthly flow occurs in spring (Fig. 4).

The Parker River is ideal for this study for several reasons: (1) it supplies sediment to the salt marshes in the PIS ecosystem, one of the first coastal sites in the National Science Foundation's (NSF) Long Term Ecological Research Network; (2) it has many dams and lakes that might impact the sediment transport; and (3) its location is easily accessible for field measurements.

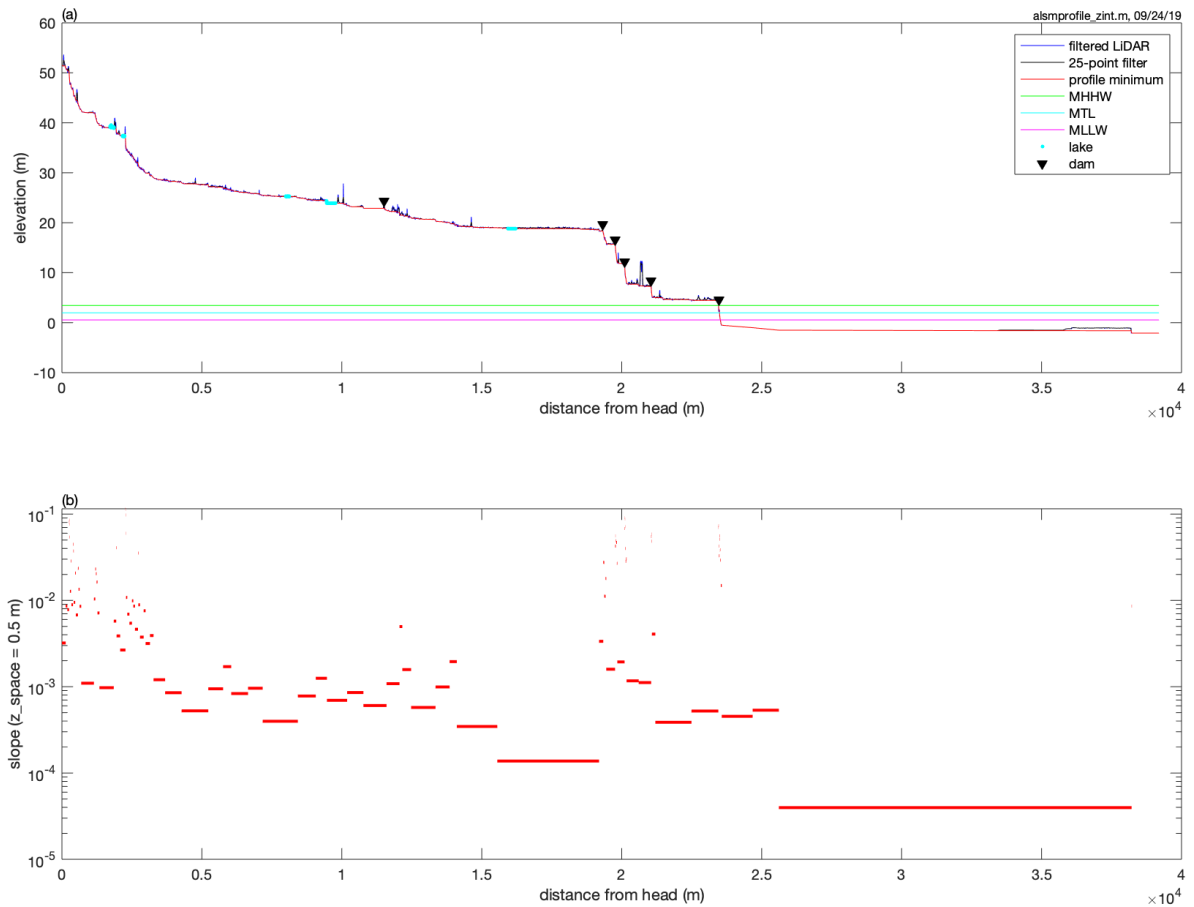


Figure 2. The longitudinal profile (a) and the slope profile (b) of the Parker River main stem from mouth to head. The longitudinal profile with no data values and extreme pits and spikes removed (filtered LiDAR, blue line). Tide information is obtained from Plum Island South tide gage located close to the inlet of Plum Island Sound on the stage island and tidal datum is measured relative to mean lower low water (MLLW, magenta line). Mean high water (MHW) is 2.77 m above MLLW, mean higher-high water (MHHW, green line) is 2.89 m above MLLW, mean tide level (MTL, cyan line) is 1.43 m above MLLW, mean sea level (MSL) is 1.43 m above MLLW. 25-m-moving-average profile (25-point filter, black line), profile with minima connected (demprofile\_min, red line), and dams (black downward triangle) are indicated in the upper panel. Z\_space is the filter interval for slope calculation.

Table A. Land use of the Parker River watershed in 2016 (MassGIS, 2017).

	Impervious	Agriculture	Forest	Wetland	Bare land	Developed Land	Water	Total
<i>Area (km<sup>2</sup>)</i>	13.1	1.2	31.7	5.2	0.5	9.1	2.7	63.5
<i>%Area</i>	21%	2%	50%	8%	1%	14%	4%	100%

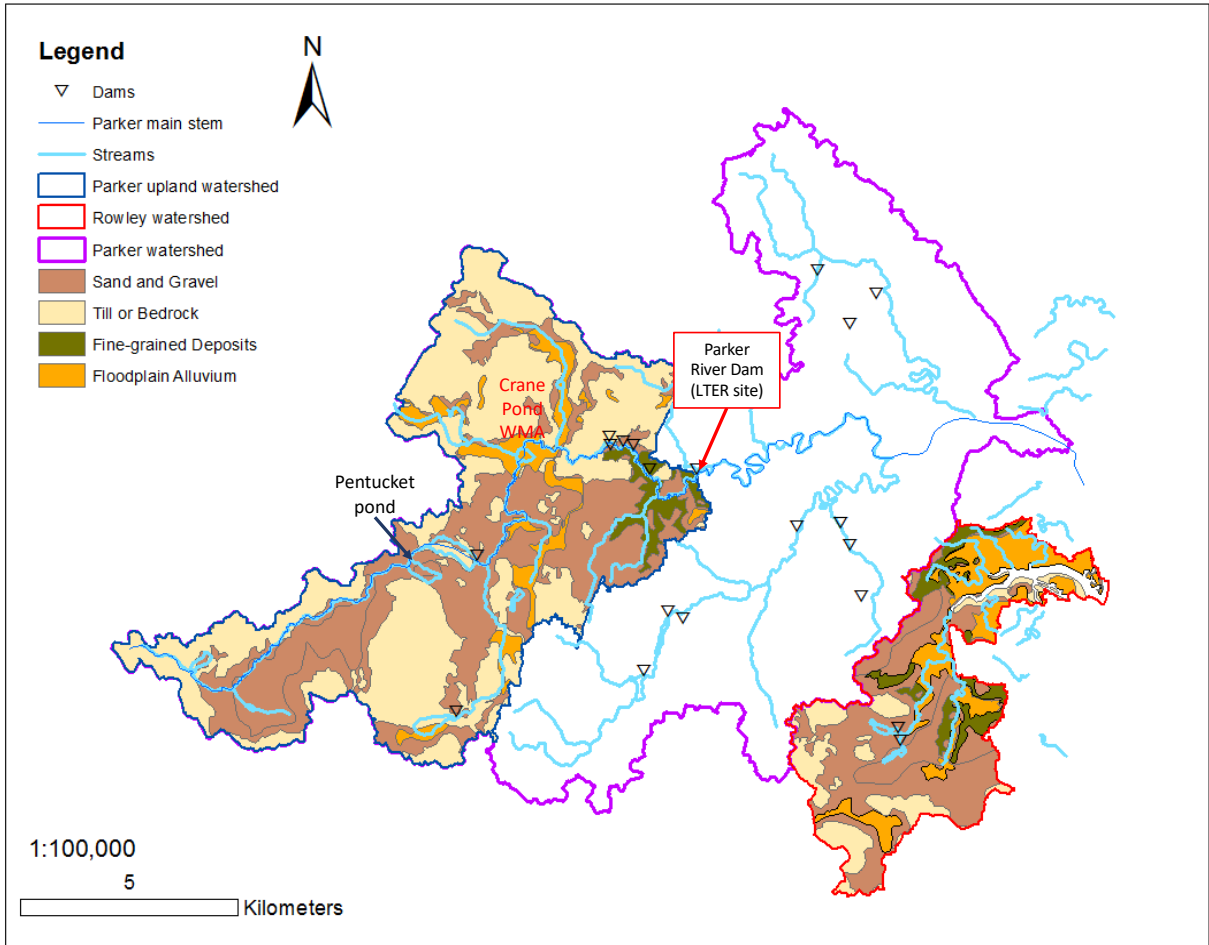


Figure 3. Surficial geology of the Parker River upland watershed and the Rowley River watershed (MassGIS, 2017).

Table B. Surficial geology of the Parker River watershed and the Rowley River watershed (MassGIS).

WATERSHED	SAND AND GRAVEL DEPOSITS	TILL OR BEDROCK	OR FINE-GRAINED DEPOSITS	FLOODPLAIN ALLUVIUM	TOTAL AREA
PARKER RIVER (KM <sup>2</sup> )	12.3	4.4	2.4	5.5	24.6
PARKER RIVER (%)	50%	18%	10%	22%	100%
ROWLEY RIVER (KM <sup>2</sup> )	25.2	31.7	1.9	4.7	63.5
ROWLEY RIVER (%)	40%	50%	3%	7%	100%

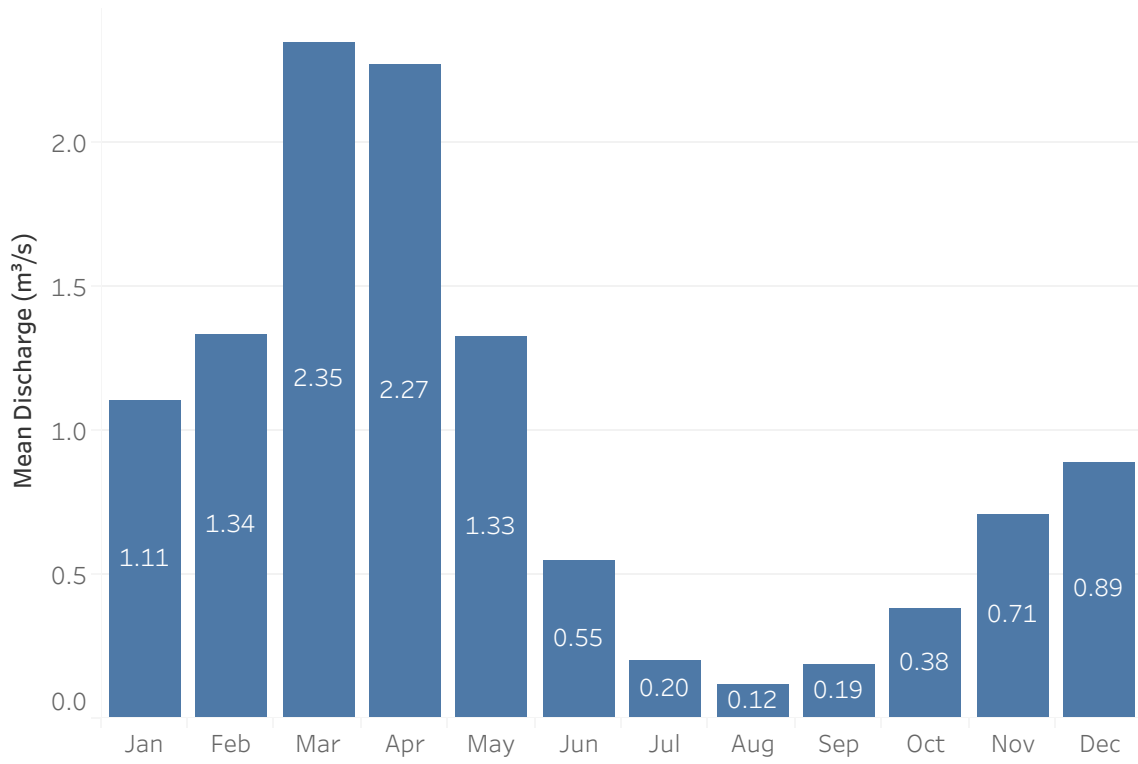


Figure 4. Mean discharge ( $Q$ ) for each month at the USGS gage on Parker River at Byfield, MA (USGS, 2019).

### 3 Background

#### 3.1 The Future of SLR and Saltmarshes Adaptability to SLR

As a result of anthropogenic climate change, the rate of SLR has accelerated since the Industrial Revolution. The estimated global average SLR rate increased from 1.1-1.9 mm yr<sup>-1</sup> between 1900-1990 to 2.8-3.1 mm yr<sup>-1</sup> between 1993-2010 (e.g., Church and White, 2011; Jevrejeva et al., 2014; Hay et al., 2015; Dangendorf et al., 2017). The future of SLR in northeastern Massachusetts might be more severe: the average rate of sea level rise increased to about 2.8 mm yr<sup>-1</sup> in the 20<sup>th</sup> Century (Hopkinson et al., 2018), while the rate for 2000-2017 at Boston tide gauge (5.85 mm yr<sup>-1</sup>; NOAA, 2017; Fig. 1) is almost double the global mean rate. The acceleration of SLR in the northeastern US is also 3-4 times faster than the global mean (Sallenger et al., 2012; Boon, 2012), while the effect of the glacial-isostatic adjustment remains minimal (Park et al., 2002). SLR exacerbates inundation and erosion in coastal habitats and poses a threat to the long-term existence of marshlands. Though some studies suggest that wetland loss is inevitable (e.g., McFadden et al., 2007; Craft et al., 2009), marshes could adapt to some extent of SLR through eco-geomorphic feedbacks (Fig. 5): when water depth increases, sediment trapping is more efficient and aboveground biological production will increase until water depth exceeds the suffocation threshold of vegetation, causing a drop of production with water-depth increase. Kirwan et al. (2010) modelled marsh elevation response to two different SLR scenarios (Fig. 6 and 7). When SLR accelerates moderately, the accretion rate of marshes can keep up with increasing SLR rate (Fig. 6b). The modeled elevation of marshlands accommodates SLR, maintaining a water depth that still allows plant growth (Fig. 6a). However, if SLR rate continues to increase almost linearly (Fig. 7b), marshland elevation cannot stay abreast with the vegetation limit level and can

no longer support any plant growth (Fig. 7a). As a result, water depth increases, reflecting a transition from marshlands into subtidal mudflats (Fig. 7a).

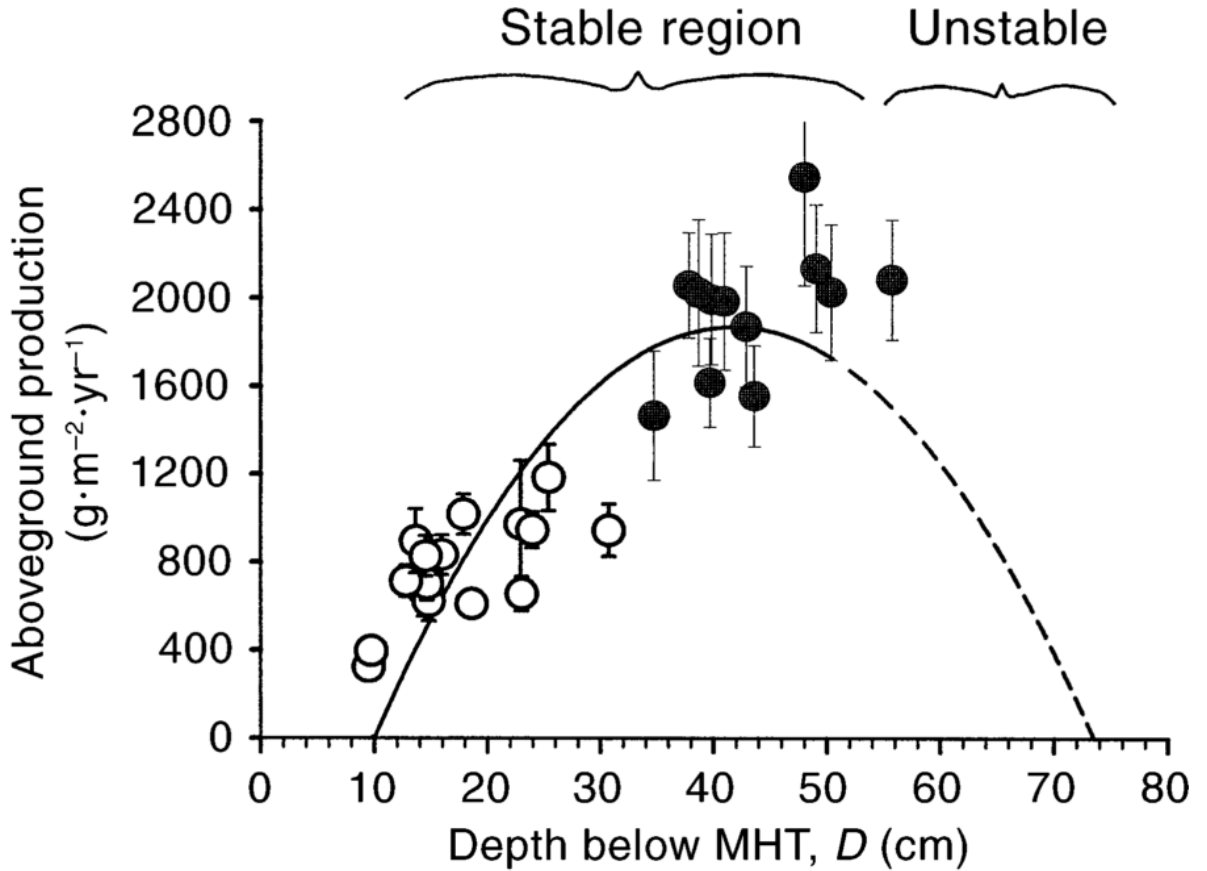


Figure 5. Interannual variation in mean sea level resulted in this relationship between the observed productivity of the salt marsh macrophyte *Spartina alterniflora*, measured annually since 1984 (Morris 2000), and depth below mean high tide (MHT) of sites in the high (open circles) and low (solid circles) marsh. Depth below MHT was computed during the peak growing season months of July and August and is a highly significant predictor of productivity ( $r^2=0.81$ ,  $P < 0.0001$ ). Stable (solid line) or unstable (dashed line) combinations of equilibrium productivity,  $B$ , and depth,  $D$  are also shown for  $B = 155D - 1.855D^2 - 1364$  (from Morris et al., 2002).

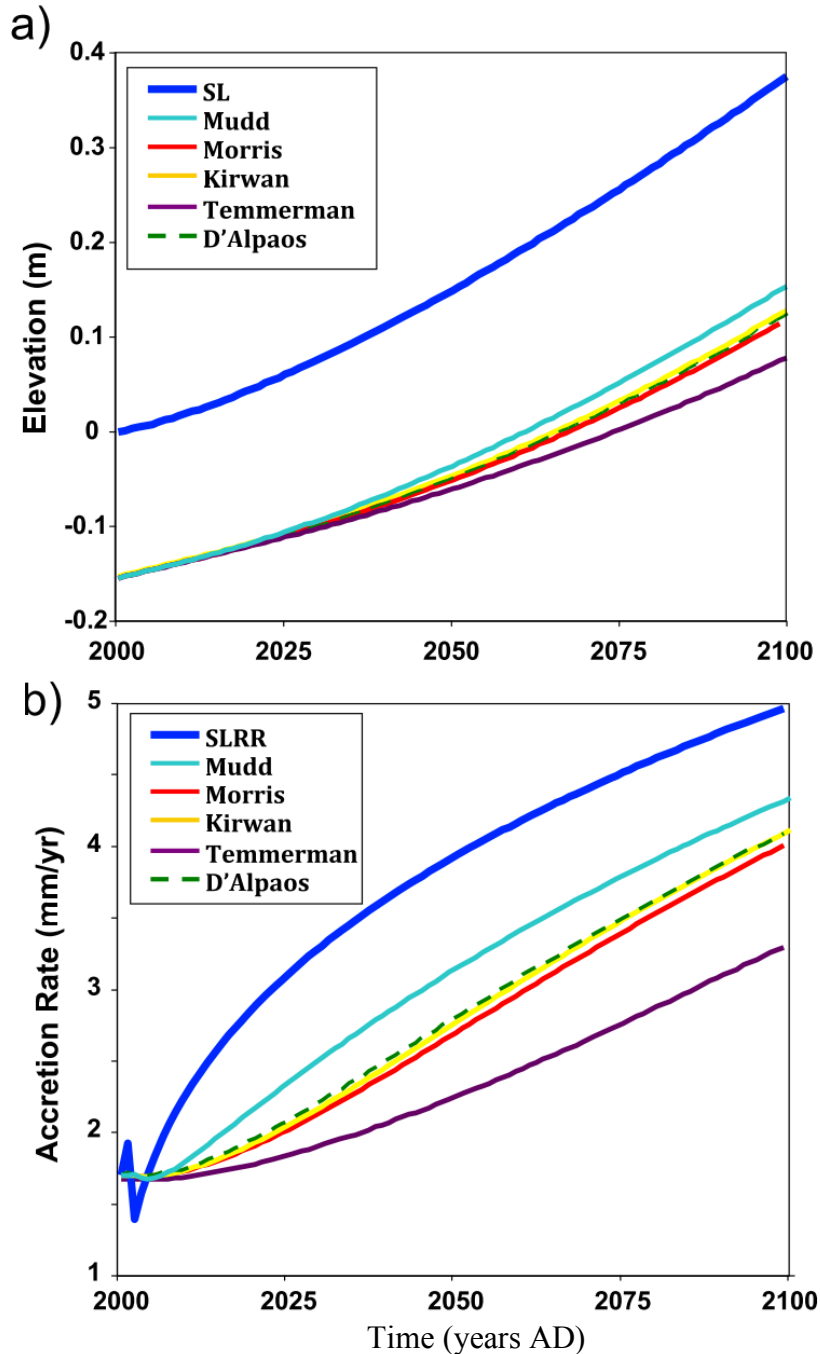


Figure 6. Response of marsh elevation (a) and accretion rate (b) to a conservative sea-level acceleration (IPCC A1B scenario [Bindoff et al., 2007]). Heavy blue line denotes sea level at spring high water (Figure 2a) or the sea-level rise rate (Figure 2b). The other lines represent elevations of the simulated position of the marsh relative to spring high water for different models (Morris et al., 2002; Temmerman et al., 2003; D'Alpaos et al., 2007; Kirwan and Murray, 2007; Mudd et al., 2009)). Because each model predicts a slightly different initial elevation relative to sea level, Kirwan et al. have normalized each model to a common equilibrium elevation at time zero. Because sea-level rise rates tend to exceed accretion rates, marsh elevations adjust to sea-level acceleration by becoming lower relative to sea level (i.e., more inundated) (Figure 2a), which enhances vertical accretion (Figure 2b). (Experimental conditions: spring tidal range = 1 m, suspended-sediment concentration = 30 mg L<sup>-1</sup>) (from Kirwan et al., 2010).

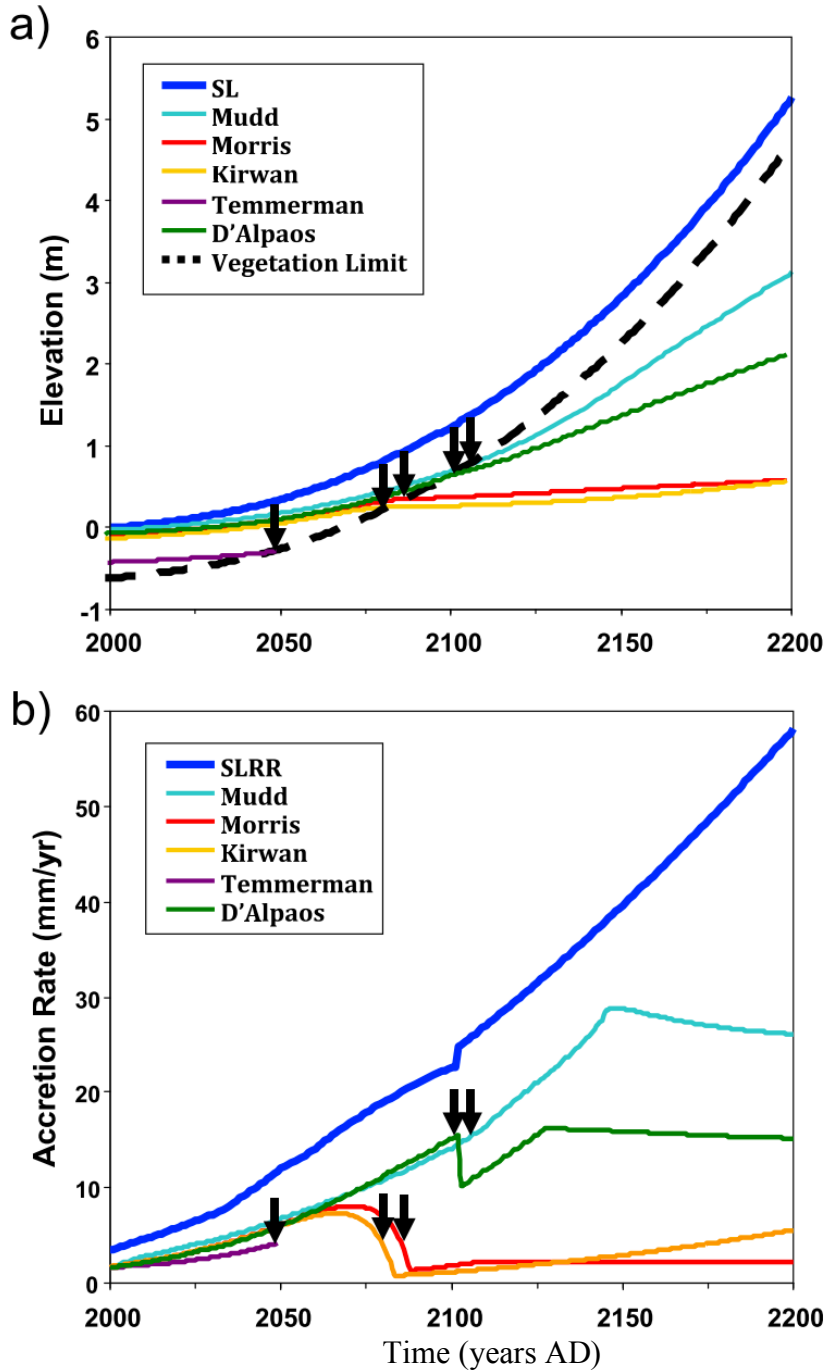


Figure 7. Response of (a) marsh elevation and (b) accretion rate to a rapid sea-level acceleration. Heavy blue line denotes sea level at spring high water (Figure 3a) or the sea-level rise rate (Figure 3b). The other lines represent elevations of the marsh relative to spring high water using different models (Morris et al., 2002; Temmerman et al., 2003; D'Alpaos et al., 2007; Kirwan and Murray, 2007; Mudd et al., 2009). In this model experiment, sea level accelerates according to Rahmstorf's (2007) maximum scenario. Kirwan et al. (2010) have extrapolated Rahmstorf's scenario from 2100 to 2200 AD using a 3rd degree polynomial fit. Marsh elevations tend to adjust to sea-level acceleration by becoming deeper relative to sea level, although the dashed black line denotes the lowest elevations at which vegetation can grow. Arrows denote the point in each model at which marsh elevations become too low to support vegetation. In most models, vegetation mortality leads to a decrease in accretion. However, mortality leads to a temporary increase in organic accretion in the Mudd model, and does not affect accretion in the Temmerman model. (Experimental conditions: spring tidal range = 1 m, suspended-sediment concentration = 30 mg L<sup>-1</sup>). (from Kirwan et al., 2010).

### 3.2 Sediment Availability and Marshland Resilience

Sediment availability impacts accretion rate through biological and physical processes, and thus is critical to the survival of marshlands. Applying different suspended sediment concentrations (*SSC*) to the same set of models yields different threshold SLR rates from a few millimeters per year ( $SSC = 1\text{--}10 \text{ mg L}^{-1}$ ) to several centimeters per year ( $SSC = 30\text{--}100 \text{ mg L}^{-1}$ ) (Kirwan et al., 2010). Kirwan et al. (2010) predicted a threshold SLR rate of about  $5 \text{ mm yr}^{-1}$  for marshes in the PIS Estuary given a 3 m tidal range and  $3 \text{ mg L}^{-1}$  *SSC*.

Two major processes dominate the sediment supply to marshlands: fluvial processes of the watershed and tidal processes of offshore shelf. This study focuses on the former. The previous study of Kirwan et al. (2011) demonstrated 6 to 9 km<sup>2</sup> wetland expansion in the PIS during the period of European settlement (~1850), when sediment load was presumed high due to land clearing in the Rowley River watershed (Fig. 8). Sediment cores were collected from the marshes surrounding the Rowley River and developed age-depth models to estimate the age at the bottom of the core (Fig. 8; Kirwan et al., 2011). The younger age area was explained as new expanded marsh from European settlement (Fig. 8; Kirwan et al., 2011). Furthermore, Kirwan et al. (2011) showed that marshland could expand with an increase of *SSC* by 1-2 orders of magnitude (from 1 mg/L to 10 mg/L under  $1 \text{ mm yr}^{-1}$  SLR) and the later return of *SSC* to previous level will lead to little change in marshland. This sequence implies that current marshland lost would not be replaced unless *SSC* increases by 1-2 orders of magnitude.

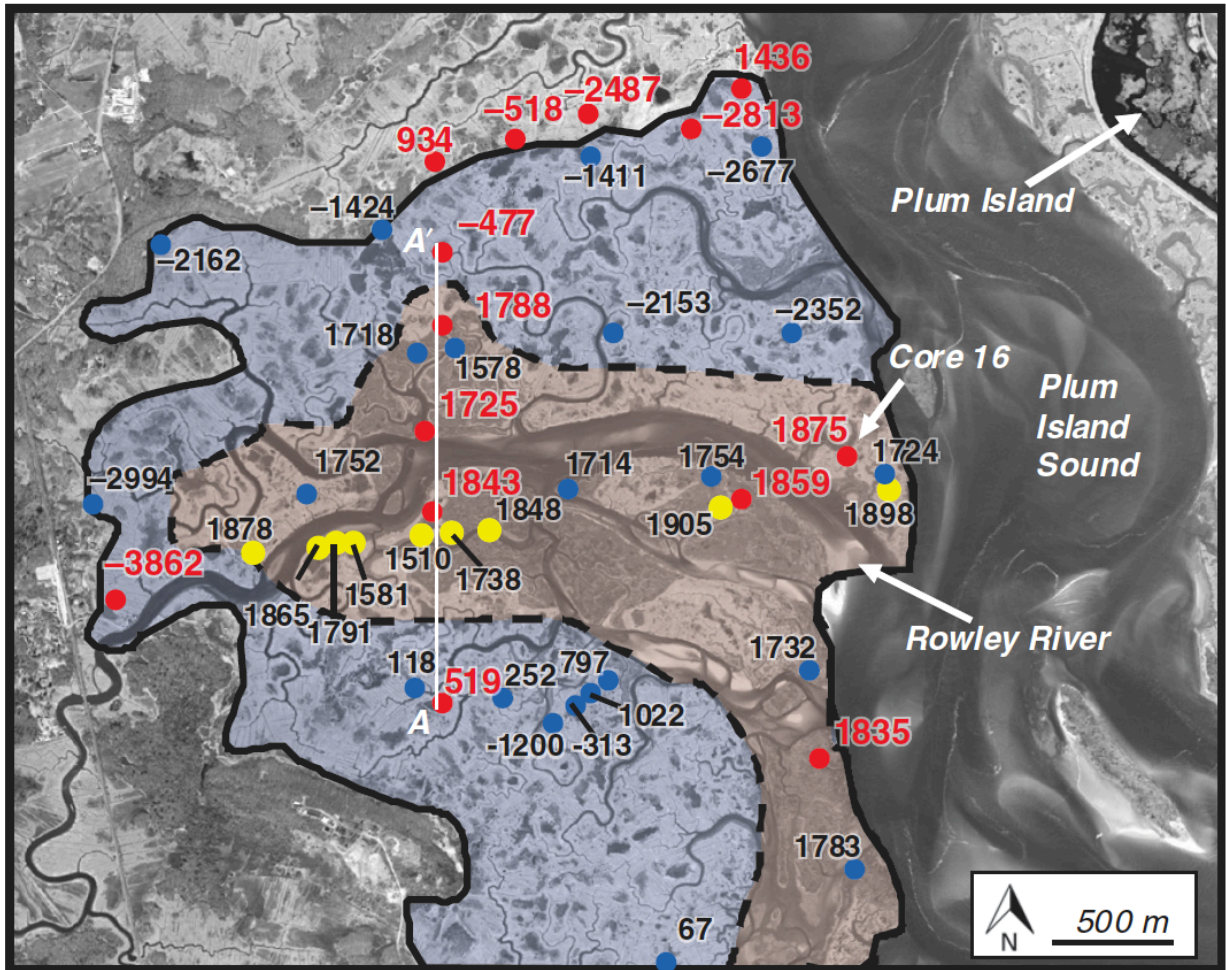


Figure 8. Map of Plum Island Estuary (Massachusetts) study area showing extent of pre-settlement marsh (blue shading) and post-settlement marsh (pink shading). Dates of marsh formation on map represent calibrated radiocarbon dates from basal peat (red dots), or dates estimated from peat thickness reported by McIntire and Morgan (1963) (yellow dots) and McCormick (1968) (blue dots). Positive dates indicate years A.D., negative dates indicate years B.C. (from Kirwan et al. 2011).

However, the results of Kirwan et al. (2011) are controversial. As pointed out by Priestas et al. (2012), high precision historical maps since 1780 show evidence of marsh loss that contradicts the proposed marsh expansion, and applying two age-depth curves for cores collected by previous researchers with no radiocarbon dates might bias the results. Kirwan and Murray (2012) responded the objections of Priestas et al. (2012), stating that historic maps are consistent with their stratigraphic record if marsh expansion began in 1700s, and that excluding the estimated marsh age of undated cores would still lead to the same conclusion of marsh expansion from their 14 directly radiocarbon dated cores.

Despite evidence for increased sediment loads as a result of past land clearing, the watersheds of the PIS Estuary is still sediment starved. The Parker River watershed is a low-relief, paraglacial landscape, where geomorphic features and sediments were formed directly or indirectly from glacial processes (Forbes and Syvitski, 1994). Kasprak et al. (2014) demonstrated that sediment exports from logging sites to channels along some parts of paraglacial coastal Maine were restricted by low gradient landscape. Paraglacial features such as lakes and bogs also provide additional opportunities for sediment trapping and reduce the modern sediment loads of New England rivers (Meade, 1982). It is likely that a fraction of the Parker River watershed is incapable of contributing sediments to the estuary.

### **3.3 Impact of Dams on Sediment Transport**

Prior studies demonstrated various ways that sediment discharge could be influenced by human-induced changes including deforestation, agricultural practices, and dams and reservoirs (e.g., Wang et al., 2007; Syvitski et al., 2009; Restrepo et al., 2015; Kemp et al., 2016; Nienhuis et al., 2020). Particularly, dams create reservoirs (Fig. 9) that decrease the slope and velocity upstream. Thus, the sedimentation rate often increases at these locations, and the sediment load

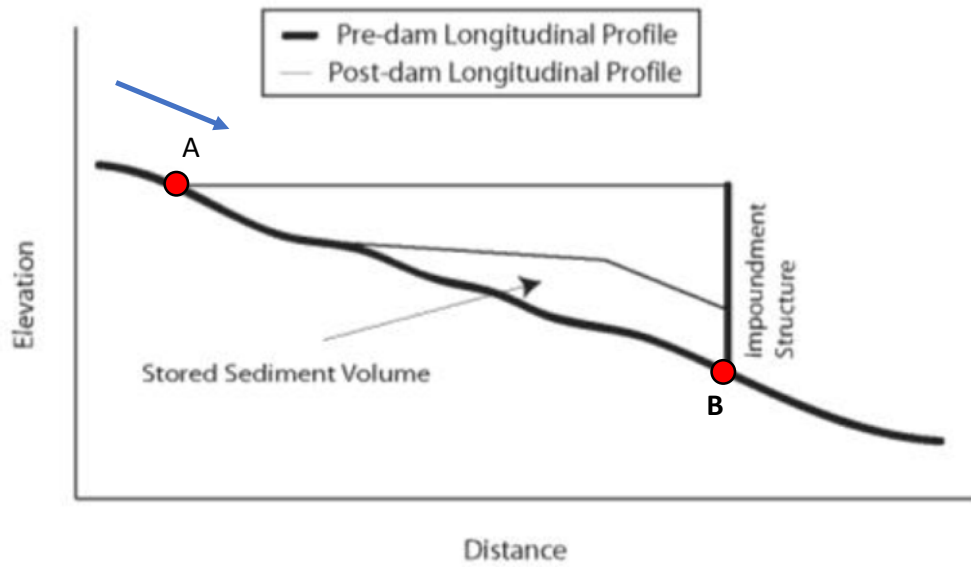


Figure 9. Conceptual diagram depicting longitudinal profile of pre and post impoundment conditions and volume of stored sediment (modified from McCusker & Daniels, 2008). The blue arrow demonstrates the direction of water flow. Scenarios without dams will be synthesized through connecting A and B in longitudinal profiles.

downstream decreases. Syvitski et al. (2009) reported an average 44% decline in sediment supply to world's 33 major deltas as a result of dam and reservoir construction. Modelling 11,000 coastal deltas worldwide with a process-based ternary diagram, Nienhuis et al. (2020) demonstrated that 970 deltas were found to have a >50% decrease in fluvial sediment flux and a collective land loss of  $12 \pm 4 \text{ km}^2 \text{ yr}^{-1}$  as a result of river damming.

Most previous studies on the influence of dams on river sediment supply to the coast (e.g., Panin and Jipa, 2002; Yang et al., 2005; Dada et al., 2018) focus on large rivers, which have a Strahler stream order of 5 or larger (Fig. 10), high availability of mobile sediments, and a large discharge to carry a significant quantity of sediment to the river mouth. Only a few studies (e.g., Willis and Griggs, 2003; McCusker and Daniels, 2008) have attempted to investigate the effect of dams on smaller rivers (Strahler stream order  $\leq 4$ ). McCusker and Daniels (2008) estimated a total yearly volumetric sedimentation rate of five dams to be  $7664 \text{ m}^3 \text{ yr}^{-1}$ , about 6.5% of the total coastal erosion estimate in Connecticut. It is thus possible that adding the  $\sim 4000$  additional dams in Connecticut, the sedimentation rate would approximate the amount of coastal erosion. No significant correlation was found between impoundment age, watershed area, dam height and sedimentation rate, indicating that the influence of dams on sediment flux should be consistent regardless of their ages, upstream watershed sizes and dam heights (McCusker and Daniels, 2008). Following McCusker and Daniels (2008), my research focuses on the influence of dams on the sediment transport of the Parker River, in Massachusetts.

### **3.4 Sediment Discharges and Sediment Yields from Previous Studies**

Previous studies have estimated sediment discharge ( $Q_s$ , unit:  $\text{Mg yr}^{-1}$ ) and sediment yield ( $Y$ , unit:  $\text{Mg km}^{-2} \text{ yr}^{-1}$ ) that could provide some insights on the sediment transport capacity of the Parker River to the estuary. Hopkinson et al. (2018) quantified the input of sediments from rivers

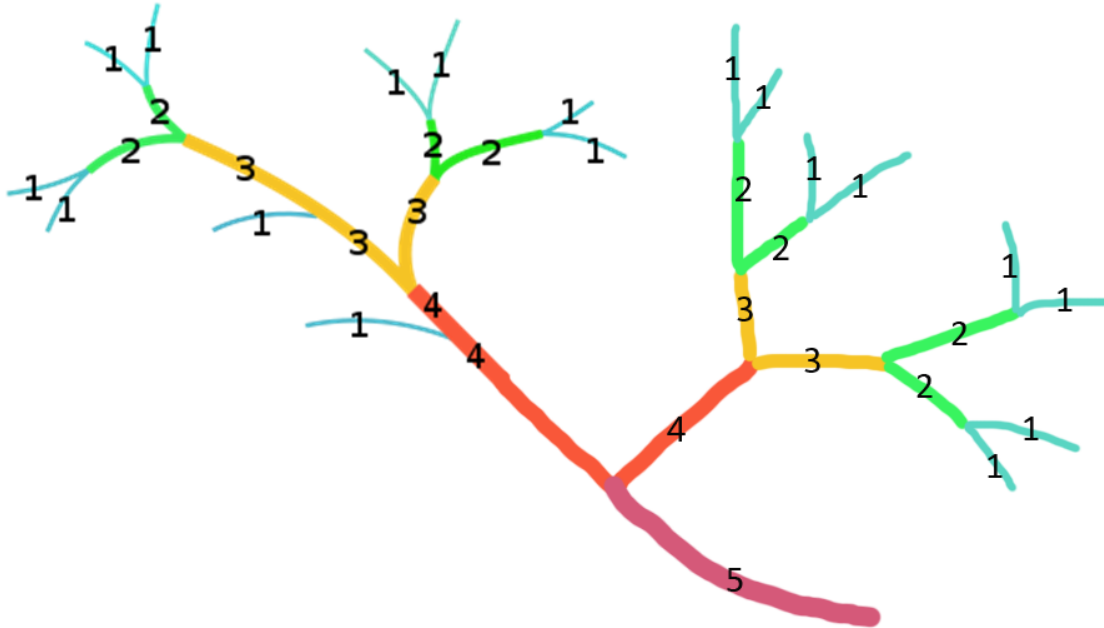


Figure 10. The Strahler stream order is a common way in hydrology to define the size of a river or stream (Horton, 1945; Strahler, 1952; Strahler, 1957). Each segment of a stream or a river within a river network is treated as a node in a tree, with the next segment downstream as its parent. When two first orders come together, they form a second-order stream. The figure represents a stream order of 5 (modified from Wikipedia, 2011).

and marsh edge erosion for the PIS estuary. Using *SSC* data collected by the Plum Island Ecosystems Long Term Ecological Research Network (LTER) and the USGS discharge data for the Parker and Ipswich Rivers, a mean annual load of 2,656 Mg yr<sup>-1</sup> was estimated between 2007 and 2014 (Hopkinson et al., 2018). An additional 554 Mg yr<sup>-1</sup> of organic matter were estimated, assuming that 10% of the total dissolved organic carbon flocculates when in contact with the high salinity estuarine water (Hopkinson et al., 2018). As the organic matter fraction of marsh sediments is 0.3, Hopkinson et al. (2018) speculated from previous studies that the accretion of organic matter on marsh surface is associated with not only net belowground production of refractory roots and rhizome tissues but also deposition during tidal inundation. While an estimated input of 32,299 Mg yr<sup>-1</sup> of sediments is necessary to maintain marsh level under a SLR rate of 2.8 mm yr<sup>-1</sup>, the fluvial input (3,210 Mg yr<sup>-1</sup>) only contribute to 10% of the marsh accretion need (Hopkinson et al., 2018). Using high resolution ocean color orthophotographs to model *SSC* from multispectral remote sensing reflectance, Zhang et al. (2020) analyzed the dominant drivers of *SSC* within the PIS estuary and attributed 19% of *SSC* variations to the Parker River discharge, with the potential to increase *SSC* by 5-10-fold during extreme river floods.

Past literatures have reported the range of *Y* to be 5 - 1,460 Mg km<sup>-2</sup>yr<sup>-1</sup> for 24 gaged rivers and 800 watersheds throughout the US (Lane et al., 1997) and a global mean of 120 Mg km<sup>-2</sup>yr<sup>-1</sup> (Syvitski et al., 2005). Ames (2018) calculated the mean of stream gauging *Y* for glaciated and unglaciated basins in the northeastern United States, yielding values of 36.8 Mg km<sup>-2</sup> yr<sup>-1</sup> and 50.5 Mg km<sup>-2</sup> yr<sup>-1</sup> respectively. Nadeau (2010) constructed a sediment rating curve at the USGS gauge on the Parker River at Byfield, MA (yellow star, Fig. 1) and estimated that at least 400 Mg of suspended sediments passed through the outlet of USGS gauge from June 9<sup>th</sup>, 2008 to June 7<sup>th</sup>, 2010. This value yields a *Y* of 3.7 Mg km<sup>-2</sup>yr<sup>-1</sup>, which is about an order smaller than the values

estimated in the Ames (2018) study. Hopkinson et al. (2018) reported a similarly low overall  $Y$  ( $3.1 \text{ Mg km}^{-2}\text{yr}^{-1}$ ) from the Ipswich and Parker River watersheds. This comparison suggests that the Parker River is likely not an important sediment source for the PIS estuary. One aspect of my research is to evaluate  $Y$  values estimated by previous studies with additional data.

#### **4 Purpose and Scope**

This research will answer two major questions:

- (1) Are dams trapping sediments and therefore reducing sediment load to the estuary?
- (2) What portion of the watershed can contribute sediments to the estuary?

I combine three perspectives to study the sediment transport of the Parker River. In the theoretical approach, I leveraged the use of digital elevation models (DEM) and geomorphic parameters to model the pattern of potential sediment sources and sinks along the main stem Parker River. The present-day dammed conditions were compared with a scenario with the dams removed. The field-based analysis then looked to confirm the predicted pattern with field measurements of SSC and remote sensing data, and to quantify the sediment delivery capacity of the Parker River watershed with calculations of  $Y$  and  $Q_s$ . Lastly, the empirical approach quantified trap efficiency ( $T_e$ ) of the five dams in the dammed reach to evaluate how much sediment could be transported downstream of these dams. The outcomes together help evaluate whether removing dams in the dammed reach is a worthwhile decision to increase suspended sediment sources for the PIS estuary and the resilience of saltmarshes under SLR.

From these two research questions, three competing hypotheses exist for these two questions and provide insights on the worthiness of removing dams from a marsh-sediment replenishment perspective:

(1) Upstream dams have no impact on the sediment supply of the Parker River watershed to the PIS and thus, no role in influencing the threshold sea level rate and resilience of salt marshes.

(2) Upstream dams cause a difference in sediment supply of the Parker River watershed to the PIS, but the difference in sediment supply is insignificant compared to coastal erosion.

Two possible indications could be derived from this scenario.

a. If the relative difference in sediment supply between dammed and undammed conditions is small, this result might indicate that removing dams will not significantly increase sediment supply to the coast.

b. If the relative difference in sediment supply between dammed and undammed conditions is large, but the sediment supply from the upland watershed is very small in the synthesized undammed situations, then this result might indicate that the sediment supply from the Parker River watershed is not the major source of sediment supply for the PIS.

(3) Upstream dams cause a difference in sediment supply of the Parker River watershed to the PIS, and the difference is comparable to the amount of coastal erosion. This scenario would indicate a necessity to remove dams upstream for the purpose of salt marsh preservation.

## **5 Research Methods**

### **5.1 Theoretical Approach: Suspended-Sediment Transport Pattern**

#### **5.1.1 Calculations of Geomorphic Parameters and Geospatial Analysis**

DEM data were used to model the sediment transport patterns of the main stem Parker River. Previous studies demonstrated the simplicity and applicability of DEM data to investigate river

morphology and sediment transport (e.g., Snyder, et al., 2000; Snyder, 2009; Snyder, et al., 2013; Gartner et al., 2015). Snyder et al. (2000) used USGS 30 m DEM data to analyze the shear stress model of bedrock-channel incision in response to tectonic forcing. Gartner et al. (2015) developed a model to predict locations of sediment sources and sinks based on downstream gradient in stream power using 10 m DEMs. In both studies, the DEMs allow for simple and accurate wide-range drainage-area measurements.

Snyder (2009) summarized several benefits of LiDAR DEM data for fluvial sediment transport analysis. Standard DEMs, where resolution depends on the map contour interval (typically 3 - 20 m) and density (set by landscape gradient), generated spatially variable inaccuracy in geometric measurements. In contrast, with pixel sizes of 0.5 - 5 m and the ability to measure heights down to 5 - 20 cm, LiDAR DEMs yielded an excellent resolution of river channel morphology and fluvial features. The measurements from LiDAR DEMs were comparable to those of high-precision but time-consuming field surveys.

Furthermore, LiDAR DEMs are particularly useful for coarse gravel-bedded river channels. Previous studies (Wilkins & Snyder, 2011; Snyder et al., 2013) developed a model based on geometric and hydrologic parameters to predict bed grainsize in coarse gravel-bedded river channels. LiDAR DEMs were used to take geometric measurements of slope ( $S$ ) and channel width ( $w$ ). Because the widths of coarse gravel-bedded river channels were on the order of 10 m, only the resolution of LiDAR DEMs could allow for accurate measurements. However, the limitation of LiDAR DEMs was also obvious: the flow-routing algorithms based on adjacent pixels are computationally intensive for large ( $>100 \text{ km}^2$ ) drainage basins (Snyder, 2009). Thus, drainage area ( $A$ ) measurements in the Parker River watershed ( $212 \text{ km}^2$ ) were computed using standard DEMs.

Two DEM datasets were used to estimate sediment transport patterns: 1-m LiDAR bare-earth DEMs from MassGIS (2017) and 10-m standard DEMs from USGS (2017). In ArcGIS, channel centerlines were modified from a MassGIS dataset, using orthophotographs and topographic maps as guides. Using the channel centerlines and 1-m LiDAR DEMs, elevation was extracted every meter along the channels to plot the longitudinal profiles for the main stem of the Parker River (Fig. 2). The values of  $S$  were calculated from the longitudinal profile in MATLAB using the methods of Snyder (2009) (Eqn. (1)):

$$S = \frac{dz}{dx}, \quad (1)$$

where  $z$  is elevation (unit: m) and  $x$  is distance (unit: m). The values of  $A$  are measured from 10-m standard DEMs every 100 m along the channels.

The sediment transport model used in this research assumed that sediment transport scales with basal shear stress ( $\tau_b$ ). Basal shear stress ( $\tau_b$ ) is the force per unit area acting to transport sediment in the channel. Assuming a steady, uniform flow and the conservation of mass,  $\tau_b$  (unit: Pa) was calculated by combining the depth-slope product equation with the Manning's friction equation (Eqn. (2)):

$$\tau_b = \rho g n^{3/5} \left[ \frac{Q}{w} \right]^{3/5} S^{7/10}, \quad (2)$$

where  $\rho$  is density of water ( $\rho = 1000 \text{ kg m}^{-3}$  at  $20^\circ\text{C}$ ),  $g$  is acceleration by gravity ( $9.81 \text{ m s}^{-2}$ ),  $n$  is a channel roughness coefficient ( $\sim 0.04$  for gravel-bedded rivers based on Barnes, 1967), and  $Q$  is discharge (unit:  $\text{m}^3 \text{ s}^{-1}$ ) (Wilkins and Snyder, 2011).

I used bankfull condition to calculate  $\tau_b$ . Bankfull discharge ( $Q_{bf}$ ) represents a flood whose magnitude and frequency are most effective in shaping the morphology of the river and thus is appropriate for evaluating sediment transport. The values of  $Q_{bf}$  were calculated using drainage area ( $A$ , unit:  $\text{m}^2$ ) (Eqn. (3)):

$$Q_{bf} = k_q A^c, \quad (3)$$

where  $k_q = \frac{Q_{bf}}{A}$  at the USGS gage, Byfield, MA and,  $c$  is a constant that depends on how much of the watershed contributes water to the channel during a rainfall event (Wilkins and Snyder, 2011). Bent and Waite (2013) estimated that the averaged recurrence interval ( $RI$ ) for  $Q_{bf}$  among Massachusetts' rivers was 1.53 years and this value of  $RI$  was used to calculate  $Q_{bf}$  at the USGS gage with a logarithmic regression between  $RI$  and annual peak discharge (Fig. 11). The value of  $c$  was assumed to be one because the Parker River watershed is small enough to assume that major rainstorms typically encompass the entire watershed and  $Q_{bf}$  increases linearly with  $A$  (Dunne and Leopold, 1978). I calculated bankfull channel width ( $w_{bf}$ ) using the power law equation (Eqn. (4)):

$$w_{bf} = k_w A^e, \quad (4)$$

where  $k_w$  ( $1.918 \times 10^5 m^{1.2382}$ ) and  $e$  (0.4038) are both empirically determined constants from Bent and Waite (2013).

Shields parameter ( $\varphi$ ), a dimensionless parameter that can be compared to the critical values to determine whether sediments of a specific size can be entrained by a certain flow, was calculated using Eqn. (5):

$$\varphi = \frac{\tau_b}{(\rho_s - \rho)g d}, \quad (5)$$

where  $\rho_s$  is sediment density ( $2650 \text{ kg m}^{-3}$ , density of quartz and feldspar) and  $d$  is sediment size (unit: m). The input values of  $d$  were informed by the descriptive sediment sizes from marshes in the PIS estuary (See Fig. 1 from Kirwan et al., 2011):  $200 \mu\text{m}$  was used to represent fine-sand-sized grains and  $20 \mu\text{m}$  for silt-sized grains. I compared  $\varphi$  with the critical value ( $\varphi_c$ , Table 3) derived from the Shields diagram (See Fig. 6.9 from Middleton and Southard, 1984). For channel

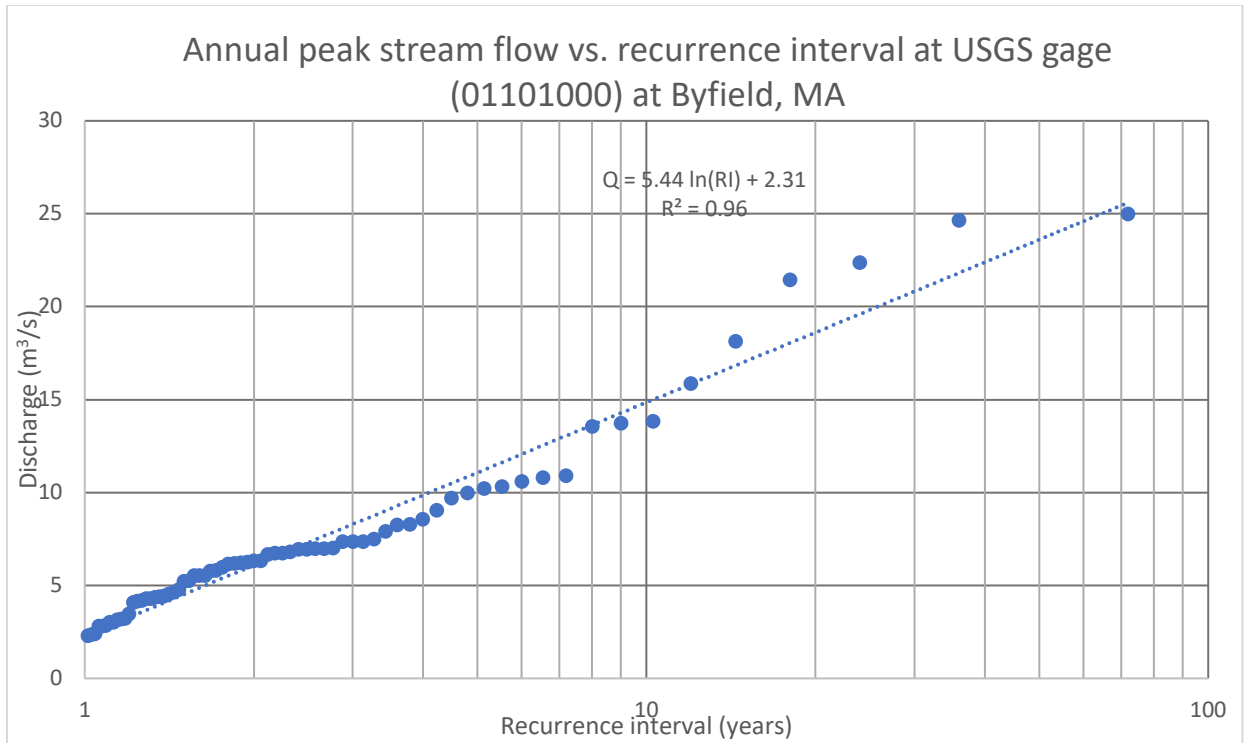


Figure 11. The logarithmic relation between annual peak stream-flow and recurrence interval at the USGS gage (01101000) on Parker River at Byfield, MA (USGS, 2018a).

Table C. Results of  $\varphi_c$ ,  $\tau_c$ , and  $w_s$  for 20  $\mu\text{m}$  and 200  $\mu\text{m}$  grains.

Grain sizes	20 $\mu\text{m}$	200 $\mu\text{m}$
$\varphi_c$	0.15	0.05
$\tau_c$ (Pa)	0.05	0.16
$w_s$ ( $\text{m s}^{-1}$ )	$3.6 \times 10^{-4}$	$3.6 \times 10^{-2}$

sections with  $\varphi > \varphi_c$ , sediments on the bed are set in motion. The Rouse number ( $P$ ) was calculated using Eqn. (6):

$$P = \frac{w_s}{\kappa u^*}, \quad (6)$$

where  $w_s$  (unit:  $\text{m s}^{-1}$ ) is settling velocity of the selected  $d$ ,  $\kappa$  is von Karman constant (0.41), and  $u^*$  (unit:  $\text{m s}^{-1}$ ) is the shear velocity.  $w_s$  is a function of  $d$  (Eqn. (7); Stokes, 1851; Table 3):

$$w_s = \frac{(\rho_s - \rho)}{18 \mu} g d^2, \quad (7)$$

where  $\mu$  is molecular viscosity ( $0.001 \text{ kg m}^{-1} \text{ s}^{-1}$  for water at  $20^\circ \text{C}$ ).  $u^*$  is a proxy for  $\tau_b$ , defined as:

$$u^* = \sqrt{\frac{\tau_b}{\rho}}. \quad (8)$$

The sediment transport mode of the selected  $d$  was evaluated based on the value of  $P$  (Table 4). A value of 2.5 was commonly used in previous studies (e.g., Bagnold, 1966; Van Rijn, 1984) to distinguish bed load and suspended load, while 1.2 was used for the split between incipient suspended load [referred to as 50 % suspension] and suspended load [referred to as 100% suspension] (e.g., Fredsøe and Deigaard, 1992; Borsje et al., 2014) and 0.8 was established for the boundary of wash load (e.g. Paola et al., 1999; Hill et al., 2016).

The Exner's downstream gradient approach was used to understand the pattern of sediment transport: an increase in  $\tau_b$  or decrease in  $P$  downstream reflects locations with a positive sediment flux change (erosion); whereas, a decrease in  $\tau_b$  or decrease in  $P$  downstream reflects locations with a negative sediment flux change (deposition) (Gartner et al., 2015). The downstream change of  $\tau_b$  ( $\frac{d\tau_b}{dx}$ ) and  $P$  ( $\frac{dP}{dx}$ ) were calculated in three ways: the difference between the upstream point and downstream point relative to the station (central difference), the average of 5 central differences centered around the station (5-point average), the average of 9 central differences

Table D. Implication of Rouse Number Values (Whipple, 2004).

$P > 2.5$	bedload
$1.2 < P < 2.5$	suspended load: 50% suspension
$0.8 < P < 1.2$	suspended load: 100% suspension
$P < 0.8$	wash load

center around the station (9-point average). The results of each parameter,  $\frac{d\tau_b}{dx}$ , and  $\frac{dP}{dx}$  were plotted on maps in ArcGIS to estimate locations of sediment deposition (i.e. sinks) and erosion (i.e. sources). A hydraulic model based on cross section surveys (such as HEC-RAS) would provide a more detailed analysis of the influence of dams on sediment transport, as was done by Wade (2008) for one of the dams on the Parker River (Larkin Mill Dam). The methods used in this study were less spatially resolved, but more efficient to apply over the entire channel networks.

To investigate the effect of dams on sediment loads, I repeated the same analysis on a simulated undammed scenario. I distributed the steep elevation change at the site of the dam over the length of the flatwater impoundment upstream to simulate the river channel without dams (Fig. 9). This smoothing was informed by measurements of dam's geometry (height, width and length) from LiDAR DEMs and field measurements. The patterns of  $\frac{d\tau_b}{dx}$  were compared between the dammed and undammed scenarios to understand how sediment transport might change with dam removal.

## **5.2 Field-based and Remote Sensing Approach: Observations of Hydrology and Sediment Transport**

### **5.2.1 SSC Datasets and Suspended Sediment Yield**

The field-based analysis first aimed to quantify  $Y$  of the Parker River watershed using  $SSC$  data. Two sets of historical data were used to calculate  $Y$ :  $SSC$  data at the Parker River Dam at Central Street, Newbury, MA from the LTER project (dataset available from Wollheim and Hopkinson, 2016), and  $SSC$  data at the USGS gage at Byfield, MA (USGS, 2018b; Fig. 1). The LTER scientists measured 238  $SSCs$  from 1993 to 2015. The range of daily mean flow discharge ( $Q_d$ ) spanned from  $1.6 \times 10^{-3} \text{ m}^3\text{s}^{-1}$  ( $RI = 0.65$  years) to  $14 \text{ m}^3\text{s}^{-1}$  ( $RI = 7.9$  years), and the  $SSC$  data spanned from  $0.1 \text{ mg/L}$  to  $39.8 \text{ mg/L}$ . The USGS dataset had 9 points from 2003 and the range

of  $Q_d$  spanned from  $1.9 \times 10^{-2} \text{ m}^3\text{s}^{-1}$  ( $RI = 0.66$  years) to  $4.3 \text{ m}^3\text{s}^{-1}$  ( $RI = 4.3$  years), and the  $SSC$  data spanned from  $1 \text{ mg/L}$  to  $22 \text{ mg/L}$ .

Based on the  $SSC$  data collection time, I obtained the  $Q_d$  (unit: cfs) at the USGS gage on the dates of data collection. I used Eqn. (3) to calculate  $Q_d$  at the first dam, where  $k_q$  is calibrated with  $Q_d$  at the USGS gage. I calculated daily sediment discharge ( $Q_{sd}$ , unit:  $\text{Mg d}^{-1}$ ) with  $SSC$  (unit:  $\text{mg L}^{-1}$ ) (Eqn. (9)):

$$Q_{sd} = SSC \left( \frac{\text{mg}}{\text{L}} \right) \times \frac{1 \text{ Mg}}{10^9 \text{ mg}} \times Q_d (\text{cfs}) \times \frac{1 \text{ L s}^{-1}}{0.035 \text{ cfs}} \times \frac{86400 \text{ s}}{1 \text{ d}}. \quad (9)$$

Using the same methods as Nadeau (2010), the sediment rating curves were developed through the linear regression of both datasets (Eqn. (10))

$$\log(Q_{sd}) = a \log(Q_d) + b, \quad (10)$$

and compared to explore the spatial variations on  $Q_{sd}$  for the same  $Q_d$  (unit:  $\text{m}^3 \text{ s}^{-1}$ ). Sediment discharge ( $Q_s$ , unit:  $\text{Mg yr}^{-1}$ ) is the sum of  $Q_{sd}$  calculated using suspended sediment rating curve in a year (Eqn. (11)):

$$Q_s = \sum_{i=1}^{365} Q_{sd\_i}. \quad (11)$$

$Q_s$  was calculated for each water year with available flow data (from 1945 to present) and the average for the whole dataset were calculated for both rating curves. Finally,  $Y$  was calculated using Eqn. (12).

$$Y = \frac{Q_s}{A}, \quad (12)$$

The results provided an estimate of the average amount of suspended load that the watershed delivered to the estuary annually. The values of  $Q_s$  and  $Y$  were compared to the values in Nadeau (2010), Ames (2018) and Hopkinson et al. (2018) to evaluate the sediment delivery capacity of the Parker River at different locations and how the  $Y$  compares with those of other rivers in northeastern US.

## 5.2.2 Fieldwork and Lab Designs for SSC Spatial Pattern Analysis

The second goal of the field-based analysis was to measure the spatial variations of *SSC* through the dammed reach to test the predictions of theoretical analysis. I collected 3 *SSC* samples at each of six locations with road crossings along the Parker River and one tributary on October 26<sup>th</sup>, 2018 and May 14<sup>th</sup>, 2019 (Fig. 1c). I used one-liter polypropylene wide-mouth bottles to take water samples from the water column around mid-channel (Davis, 2005) and measure suspended sediment mass ( $m_s$ ) and *SSC* in the lab. For each sample bottle, I used 250 mL to measure *SSC*. Whatman 47-mm GF/F glass-fiber filters (pore size = 0.7  $\mu\text{m}$ ) were pre-combusted at 450 °C for 4 hours to get rid of organic remnants in the filters and weighed. The volume of water samples ( $V_{ws} = 250 \text{ mL}$ ) were measured and a vacuum set up (Fig. 12) was used to filter this sample. Filtered sediments along with the filters were placed into individual pre-weighed crucibles and dried overnight in the oven at 105°C. The mass of dry sediments and organics ( $m_{ds}$ ) was measured as the difference between the measured values and the weights of the pre-weighed crucibles and filters. The dry samples were then combusted at 550°C in the furnace for four hours to burn off all organics. After cooling,  $m_s$  was measured as the difference between the measured values and the pre-weighed crucibles and filters. *SSC* was calculated (Eqn. (13)):

$$SSC = \frac{m_s}{V_{ws}}. \quad (13)$$

I compared *SSC* at these six locations for each event and used the variation in *SSC* between sites to evaluate whether sediment erosion or deposition occurs at each segment. The uncertainty was calculated based on the accuracy of the measuring equipment: mass was weighed using different accuracies (1 mg for samples on October 26<sup>th</sup>, 2018 and 0.1 mg for samples on May 14<sup>th</sup>, 2019) and volume was measured with 2 mL accuracy. The uncertainty of  $m_{ds}$  and  $m_s$  were 2 mg for samples on October 26<sup>th</sup>, 2018 and 0.2 mg for samples on May 14<sup>th</sup>, 2019. The uncertainty of

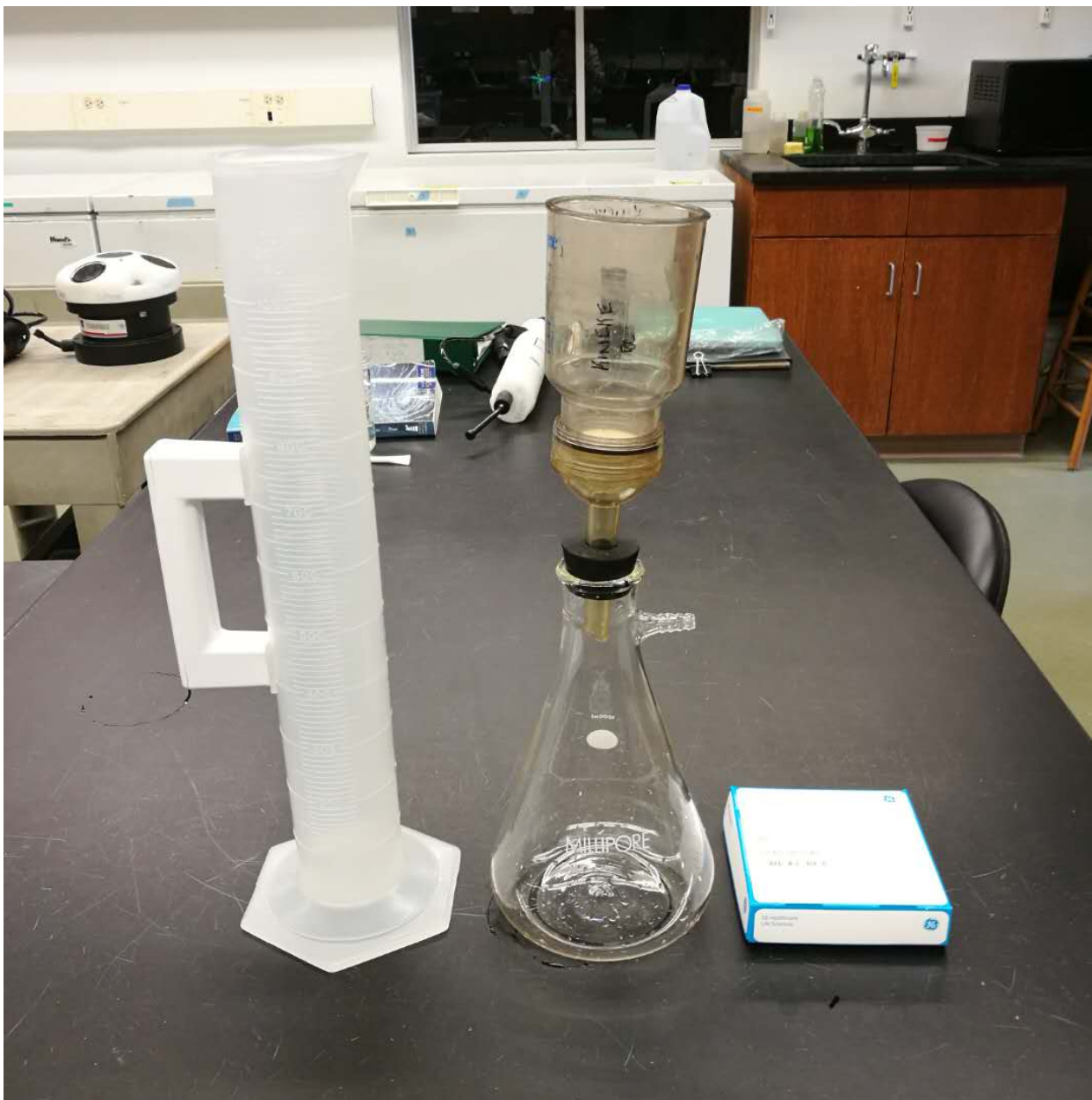


Figure 12. Lab set up for SSC measurements. Equipment from left to right: a 1000-mL graduated cylinder, a conical flask with a filter cup and an opening that could be connected to the lab vacuum through a tube, and Whatman 47-mm GF/F glass-fiber filters.

SSC (7 mg/L) was calculated using Eqn. (14) to be 7 mg/L for samples on October 26<sup>th</sup>, 2018 and 0.7 mg/L for samples on May 14<sup>th</sup>, 2019:

$$\Delta SSC^2 = \frac{\Delta m_s^2}{V_{ws}^2} - \frac{m_s}{V_{ws}^2} \Delta V_{ws}, \quad (14)$$

where  $\Delta SSC$  is the uncertainty of SSC,  $\Delta m_s$  is the uncertainty of  $m_s$ , and  $\Delta V_{ws}$  is the accuracy of  $V_{ws}$ . Averages for each location on each day were also calculated with 95% confidence intervals.

### 5.2.3 Remote Sensing Analysis

The third part of the field-based analysis looked for visual evidence of suspended sediment transport corresponding to precipitation events and geomorphic evolution in the past 25 years from aerial photos and satellite images. Crane Pond Wildlife Management Area (Fig. 1c) was selected as the ideal location to look for sediment transport evidence such as sediment plumes after high flows at the inlet to the pond, and active delta evolution (Fig. 13). I used 15-min  $Q$  data at USGS gauge at Byfield and hourly precipitation data from the station at the Lawrence Municipal Airport, MA (Fig. 1a). I screened highest flows from available hydrologic data and mined for remote sensing data during these periods of high flow. Satellite images with 3 m resolution were available starting from March 2016 to present at a frequency of every 2-3 days on Planet.com, and were used for finding instantaneous sediment response to high flows. Orthophotographs from 1995 to 2019, with resolution of 0.5-3 m, are available from MassGIS and USGS. These photographs were used to identify delta evolution at the inlet of Crane Pond. The results of this analysis were used as another method to determine the pattern of  $SSC$  variation across field sites.

### 5.3 Empirical Approach: Trap Efficiency

The empirical approach calculated trap efficiency ( $Te$ ) for each dam. Trap efficiency was first linked to the ratio between storage capacity and watershed drainage area ( $C/W$ ) using an



Figure 13. The aerial photo of the Crane Pond in 2001 with the inlet location position indicated (red arrow) (MassGIS, 2019).

empirically derived curve (Brown, 1943). However, different runoff volumes due to various hydrologic characteristics could result in different  $Te$  for basins with the same  $C/W$ . Brune (1953) solved this problem using the reservoir storage capacity-inflow ratio ( $C/I$ ) to predict  $Te$  and a stronger correlation was found. This curve is widely used by many previous studies (e.g., Merritts et al., 2011). In this study, I used the same approach to estimate  $Te$  for the five reservoirs in the dammed reach and evaluated capacities of these dams to trap sediments and reduce sediment yield going downstream.  $C/I$  was calculated as (Eqn. (15)):

$$\frac{C}{I} = \frac{V}{Q_{avg}}, \quad (15)$$

where  $Q_{avg}$  (unit:  $m^3 yr^{-1}$ ) is mean annual inflow and  $V$  is storage capacity (unit:  $m^3$ ) estimated using Eqn. (16):

$$V = \frac{A_d H_d}{2}, \quad (16)$$

where  $A_d$  is reservoir area (unit:  $m^2$ ) measured from the LiDAR DEM in ArcGIS, and  $H_d$  is height of the dam (unit: m). Trap efficiency ( $Te$ ) provided another means to evaluate the impact of dams on sediment supply and whether  $Y$  quantified from sediment rating curves will change significantly without dams.

## 6 Results

### 6.1 Theoretical Analysis: Suspended Sediment Transport Pattern

#### 6.1.1 Geomorphic Parameters and Geospatial Analysis

I analyzed geomorphic parameters ( $\tau_b$ ,  $\frac{\varphi}{\varphi_c}$ ,  $P$ ) at a 100-m interval for the main stem of the Parker River watershed. Most  $\tau_b$  values are below 10 Pa, with a few 10-50 Pa occurring at the headwalls of dams and steep reaches in the headwater region. Only one  $\tau_b$  value is slightly above

50 Pa and occurs at the steep headwall of the Parker River Dam (Fig. 14b, 15). High  $\tau_b$  indicates the steep spot in the stream profile and a high stream power to entrain sediments from the river bed, while low  $\tau_b$  indicates the opposite. The relatively low  $\tau_b$  values along the Parker River main stem indicate the low energy of the channel to move sediments.

I used two grain sizes, 200  $\mu\text{m}$  (fine sand) and 20  $\mu\text{m}$  (silt), with  $w_s$  of 36.0 mm/s and 0.4 mm/s, respectively, for the analysis of  $\frac{\varphi}{\varphi_c}$  and  $P$ . For the whole Parker River main stem,  $\frac{\varphi}{\varphi_c}$  values for 200  $\mu\text{m}$  and 20  $\mu\text{m}$  are all above 1 (Fig. 16, 17). As  $\frac{\varphi}{\varphi_c}$  values evaluate whether  $\tau_b$  values are large enough to entrain a certain grain size, the results of  $\frac{\varphi}{\varphi_c}$  indicate that  $\tau_b$  values for the main stem are large enough to entrain both grain sizes from the bed. For  $d = 200 \mu\text{m}$ ,  $P$  values vary from less than 0.8 to more than 2.5. For most stream sections, 200  $\mu\text{m}$  grains move at 50% suspension, and at the headwalls of dams and steep spots near the headwater as 100% suspended load and wash load, while only around the Crane Pond Wildlife Management area, 200  $\mu\text{m}$  grains move as bed load (Fig. 18b, 19). For  $d = 20 \mu\text{m}$ , all  $P$  values are below 0.8 and thus moved as wash load (Fig. 20b, 21). Thus, the sediment transport analysis suggests that grain sizes important to the construction of downstream saltmarshes (clay-silt sizes, informed by Fig. 1 from Kirwan et al., 2011) are not trapped along the main stem.

Despite the capability of the model results to quickly evaluate the sediment transport patterns along the whole stream profile, the model overestimates the stream power at the Crane Pond to move sediments because the lake environment violates the model assumption that fluvial processes are occurring. The variable  $w_{bf}$  is assumed as functions of  $A$ , but the actual  $w_{bf}$  values at the Crane Pond are much wider than empirically predicted values and thus actual values of  $\tau_b$  should be smaller than my results. Also, water depths within the pond, which are outside of fluvial channel scaling, might be underestimated and  $S$  values are essentially zero, and therefore  $\tau_b$  should be

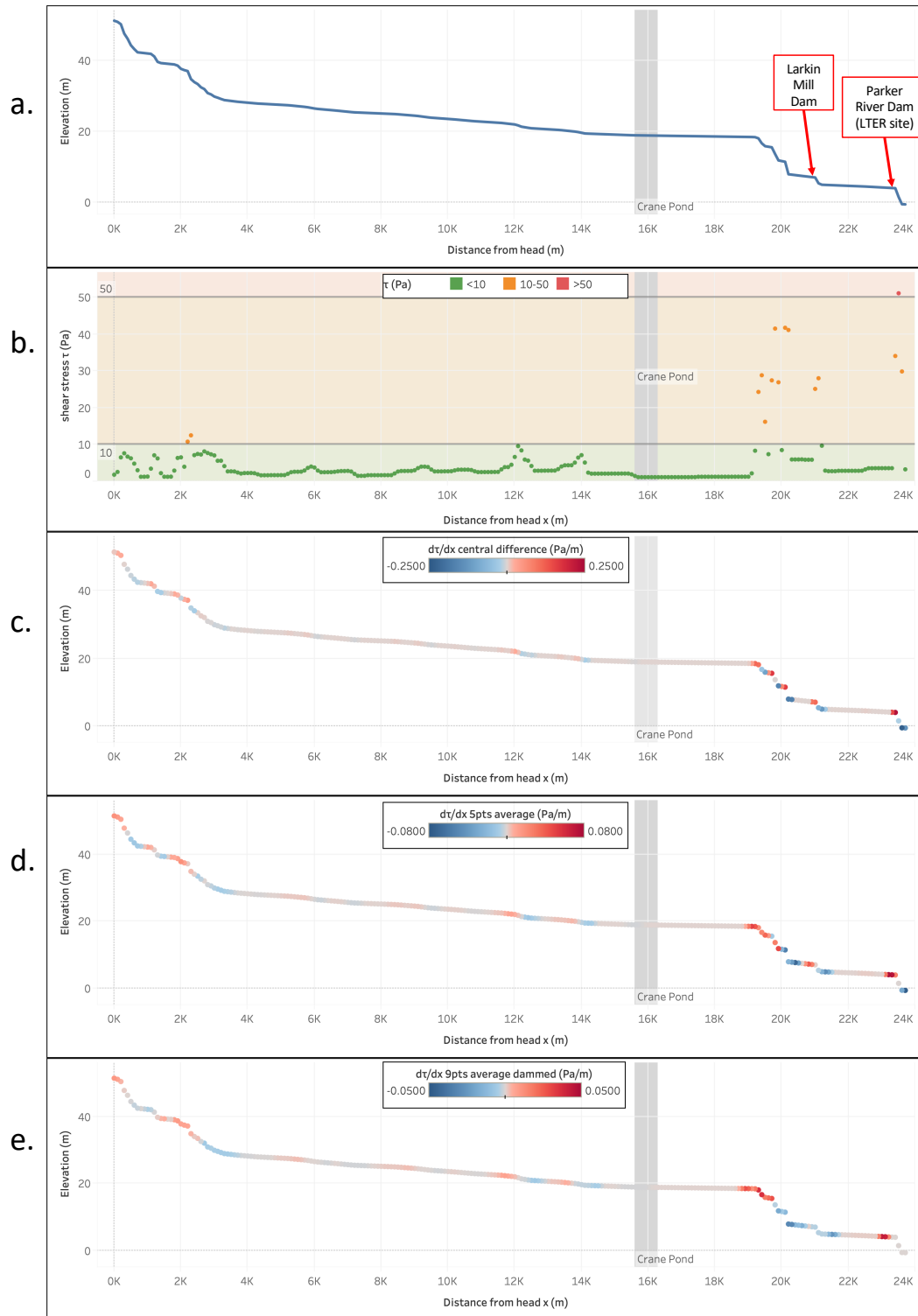


Figure 14. The longitudinal profile of the Parker main stem (a). The distribution of basal shear stress ( $\tau_b$ ) for bankfull discharge ( $Q_{bf}$ ) [red point: > 50 Pa; yellow point: 10 - 50 Pa; green point: < 10 Pa] (b). All  $\tau_b$  are above  $\tau_c$  (critical shear stress) for 20  $\mu$ m (0.05 Pa) and 200  $\mu$ m (0.15 Pa). Color shading emphasizes the splitting classes and is consistent with the following figures. The  $\frac{d\tau_b}{dx}$  calculated with central difference (c), 5 points average (d), and 9 points average (e) with positive value as red, negative value as blue and zero as grey. Gray banding indicates the location of Crane Pond.

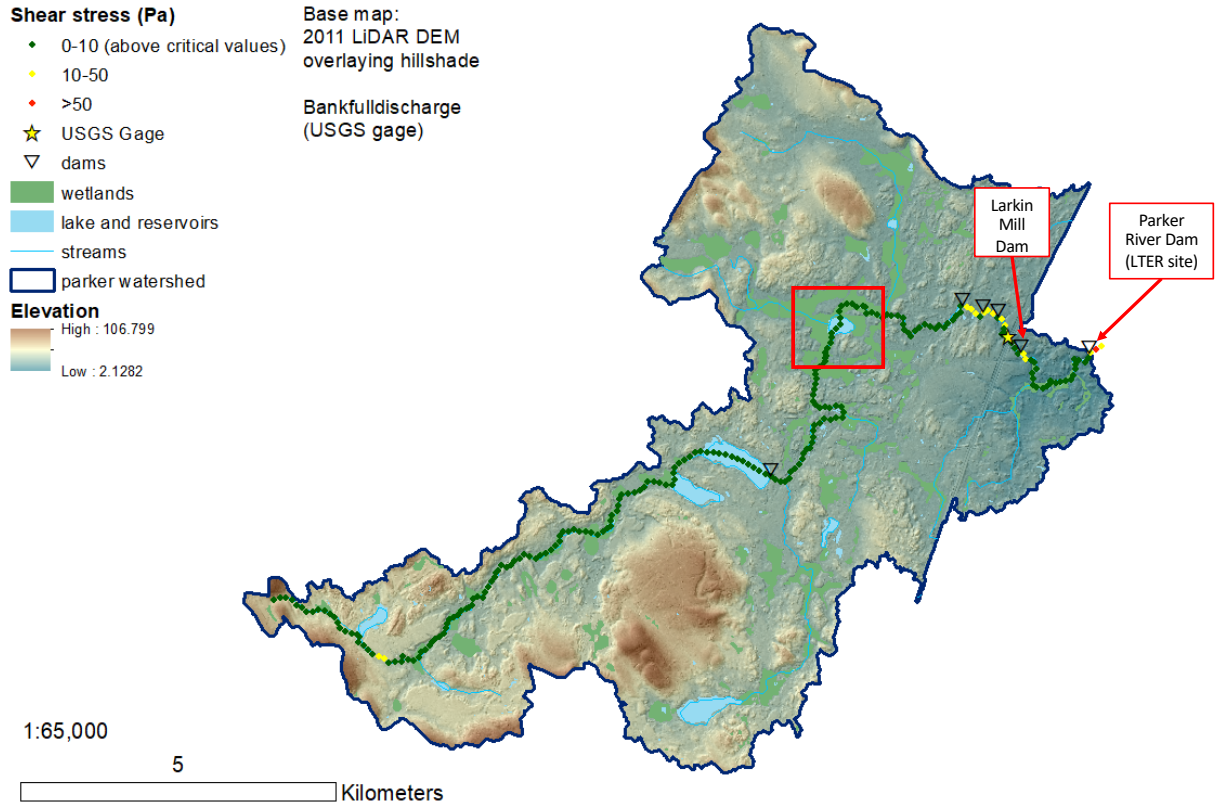


Figure 15. The distribution of basal shear stress ( $\tau_b$ ) for bankfull discharge ( $Q_{bf}$ ) [red point: > 50 Pa; yellow point: 10 - 50 Pa; green point: < 10 Pa]. All  $\tau_b$  values are above critical shear stress ( $\tau_c$ , Table 3) for 20  $\mu\text{m}$  and 200  $\mu\text{m}$ . The red rectangle indicates the Crane Pond.

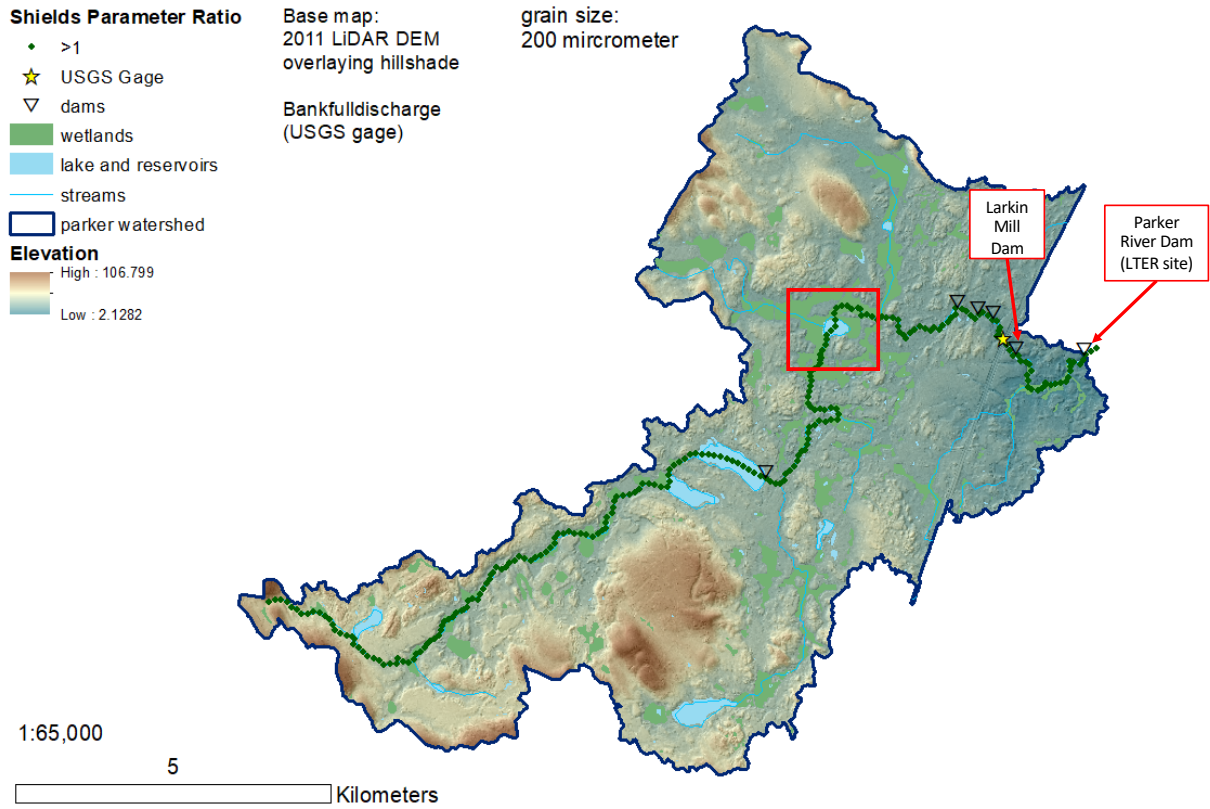


Figure 16. The distribution of Shields parameter ratio ( $\frac{\phi}{\phi_c}$ ) for 200  $\mu\text{m}$  grains at bankfull discharge ( $Q_{bf}$ ) [green points: >1]. The red rectangle indicates the Crane Pond.

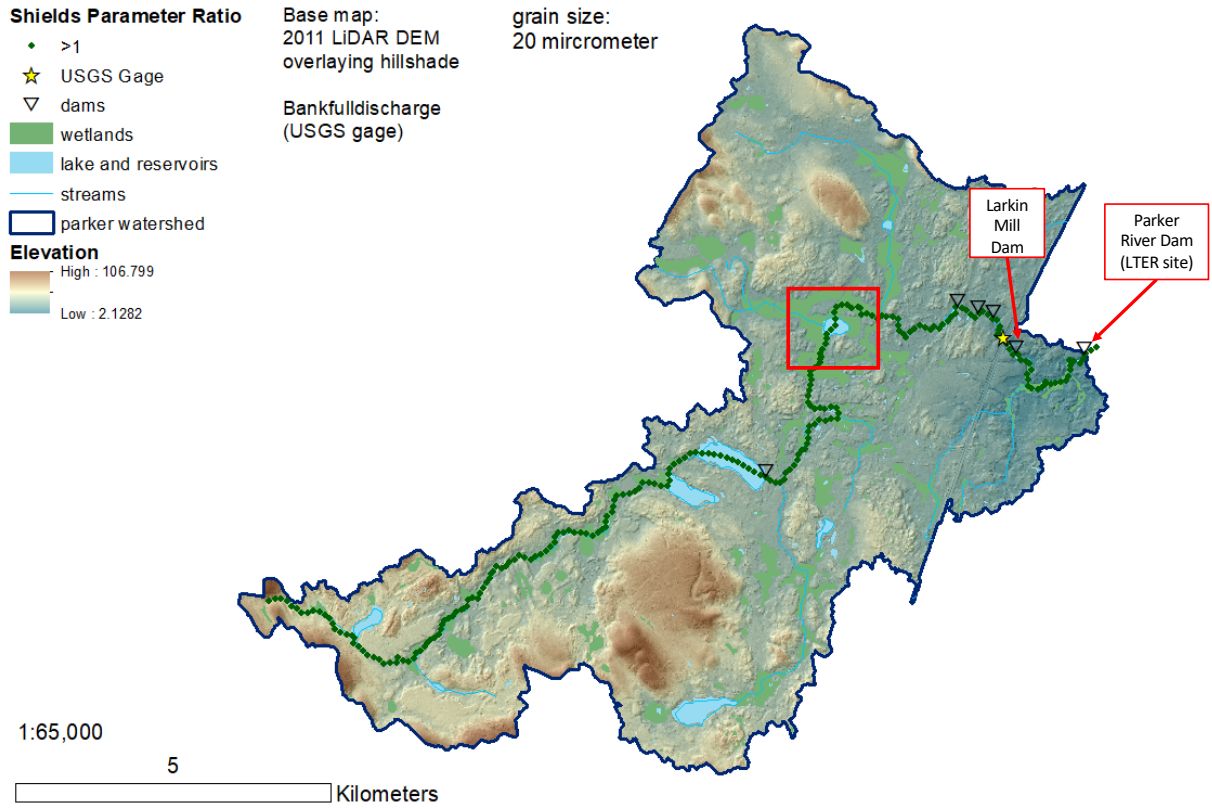


Figure 17. The distribution of Shields parameter ratio ( $\frac{\phi}{\phi_c}$ ) for 20  $\mu\text{m}$  grains at bankfull discharge ( $Q_{bf}$ ) [green points: >1]. The red rectangle indicates the Crane Pond.

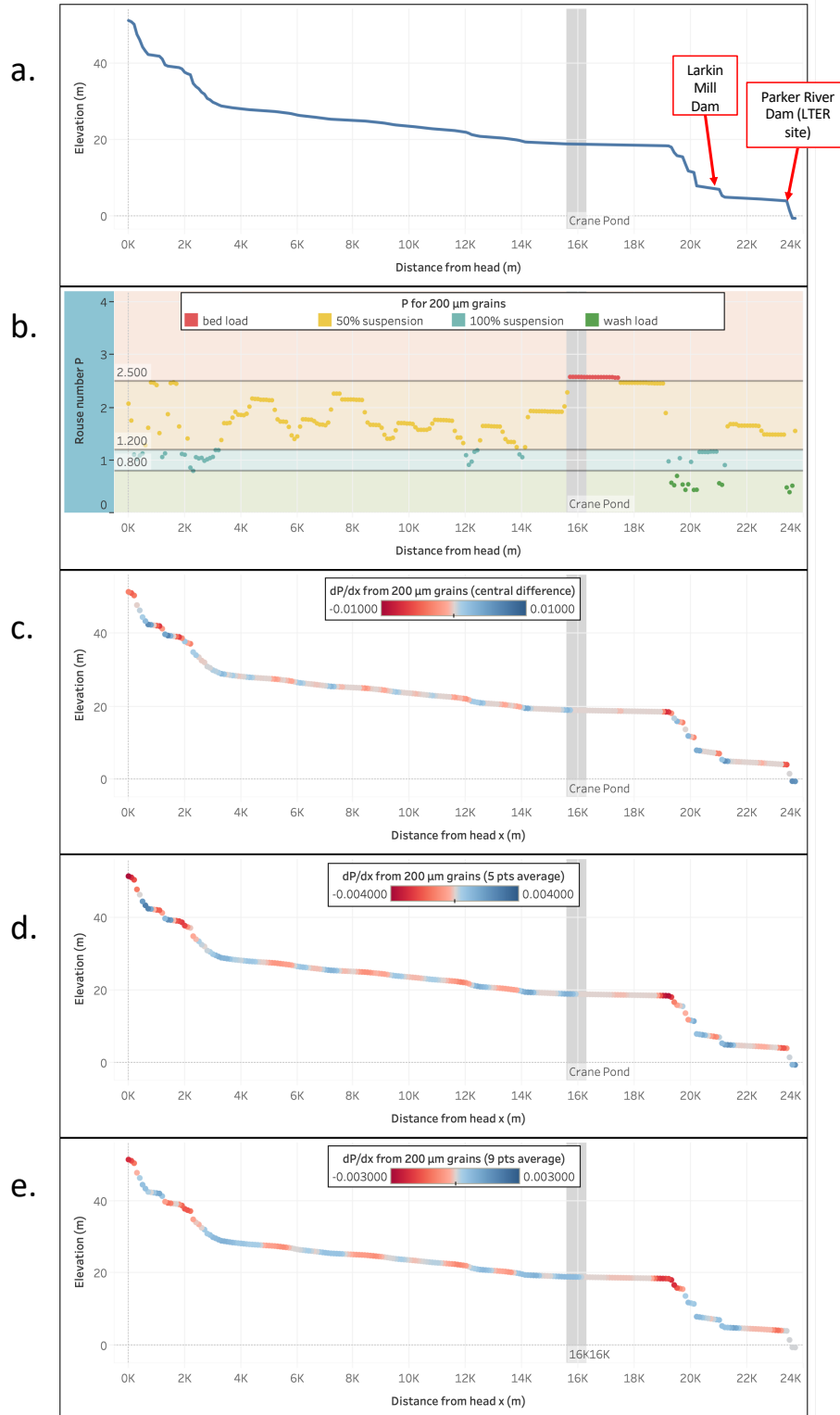


Figure 18. The longitudinal profile of the Parker main stem (a). The distribution of Rouse number ( $P$ ) for  $200\ \mu\text{m}$  grains at bankfull discharge ( $Q_{bf}$ ) [red: bed load; yellow: suspended load with 50% suspension; turquoise: suspended load with 100% suspension; green: wash load] (b). The change of Rouse number calculated with central difference (c), 5 points average (d), 9 points average (e) with positive values as blue, negative values as red, and zero as grey. Gray banding indicates the location of Crane Pond.

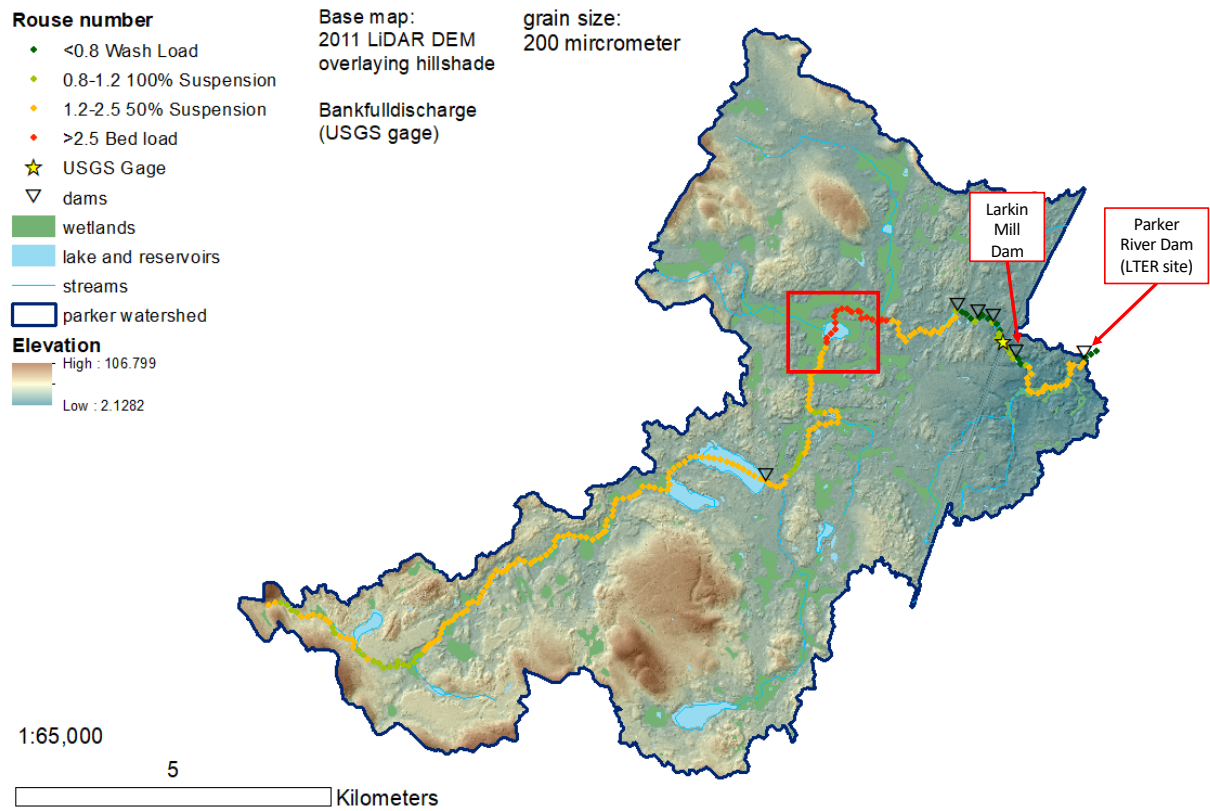


Figure 19. The distribution of Rouse number ( $P$ ) for 200  $\mu\text{m}$  grains at bankfull discharge ( $Q_{bf}$ ) for original profile [red: bed load; yellow: suspended load with 50% suspension; light green: suspended load with 100% suspension; green: wash load]. The red rectangular is highlighting the Crane Pond Wildlife Management area.

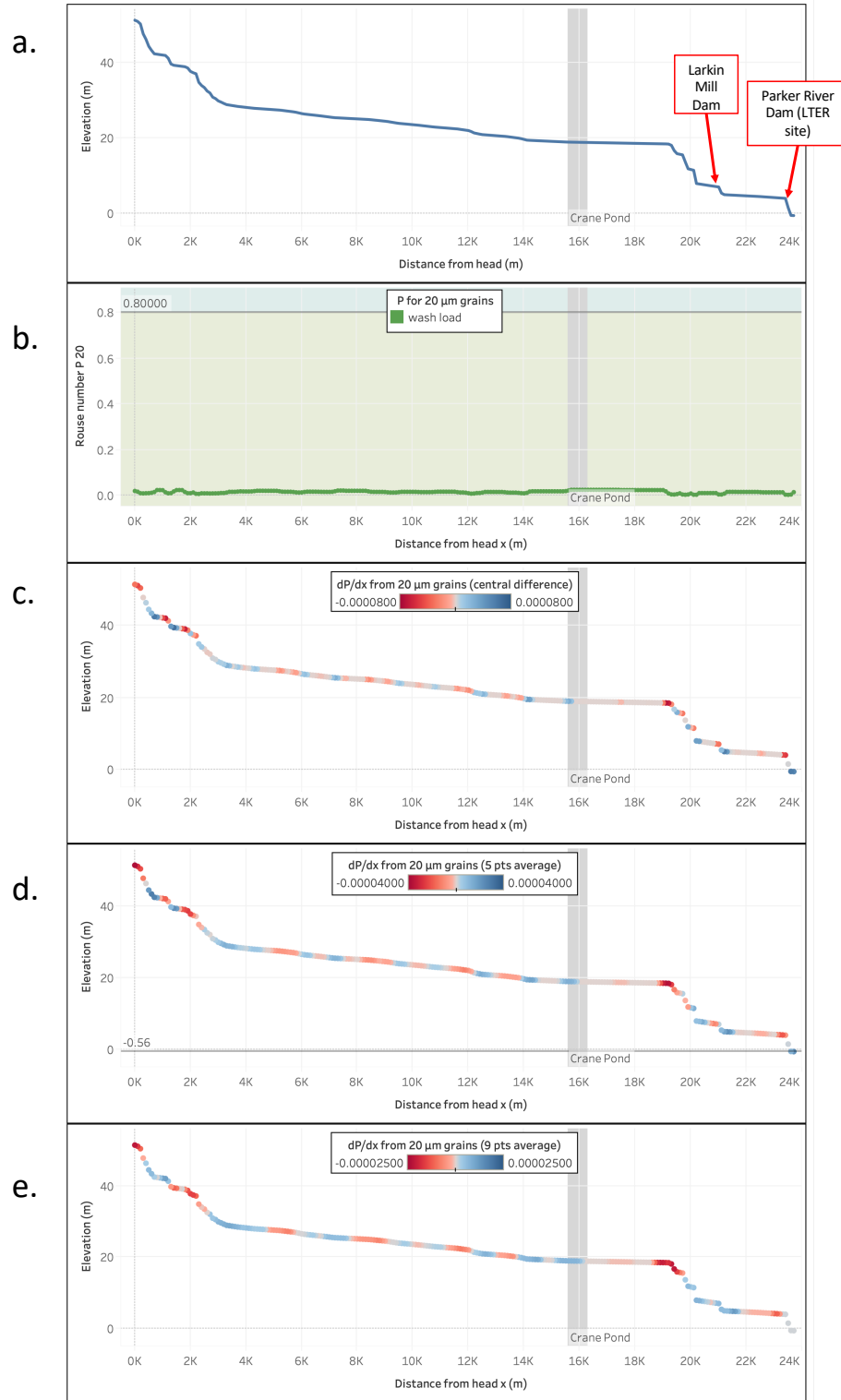


Figure 20. The longitudinal profile of the Parker main stem (a). The distribution of Rouse number ( $P$ ) for 20  $\mu\text{m}$  grains at bankfull discharge ( $Q_{bf}$ ) [turquoise: suspended load with 100% suspension; green: wash load] (b). The change of Rouse number ( $\frac{dP}{dx}$ ) calculated with central difference (c), 5 points average (d), 9 points average (e) with positive values as blue, negative values as red, and zero as grey. Gray bandings indicates the location of Crane Pond.

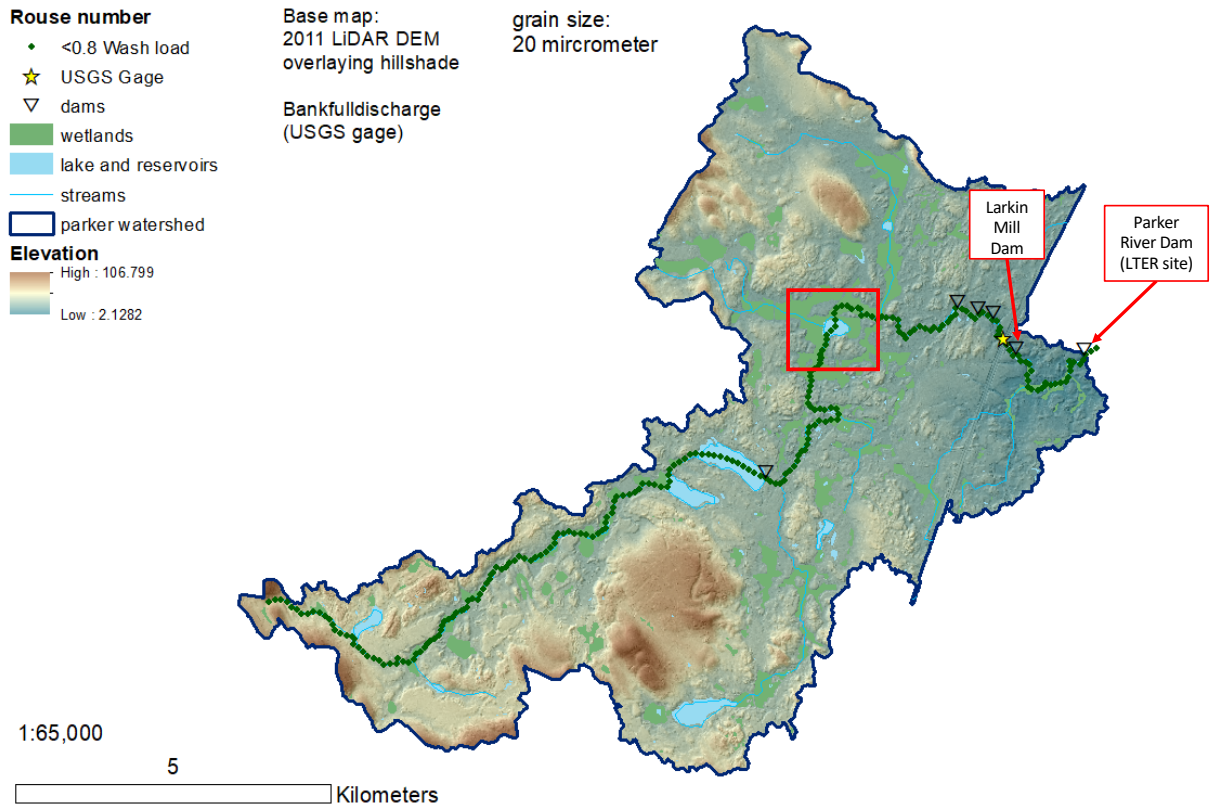


Figure 21. The distribution of Rouse number ( $P$ ) for 20  $\mu\text{m}$  grains at bankfull discharge ( $Q_{bf}$ ) for original profile [green: wash load]. The red rectangular is highlighting the Crane Pond Wildlife Management area.

lower than estimated. I expect that suspended and bedload sediments are trapped in the flat-water environment of Crane Pond and surrounding wetlands.

### 6.1.2 Downstream Variations of Geomorphic Parameters

Downstream variations of geomorphic parameters were calculated as central difference, 5 points average, and 9 points average (Fig. 14, 18, 20 c-e). These variations indicate the potential locations of sediment deposition and erosion: negative  $\frac{d\tau_b}{dx}$  and positive  $\frac{dP}{dx}$  values indicate sediment deposition (blue), positive  $\frac{d\tau_b}{dx}$  and negative  $\frac{dP}{dx}$  values indicate sediment erosion (red), little to no change indicates transport (light gray) (Fig. 14, 18, 20 c-e). Averaging over more points smooths out fluctuations between positive and negative values over a short distance and dampens the amplitudes of fluctuations (Fig. 14, 18, 20 c-e).

The signals of  $\frac{d\tau_b}{dx}$  are most substantial at the dammed reach (more intense red and blue in Fig. 14 c-e), while those of  $\frac{dP}{dx}$  demonstrate more noise over the whole reach (Fig. 18, 20 c-e). The pattern of  $\frac{dP}{dx}$  is consistent for the two grain sizes, but the amplitude differs by two orders of magnitude (Fig. 18, 20 c-e). The smaller amplitude of  $\frac{dP}{dx}$  indicates less distinguishable change in sediment transport modes and a higher chance of overamplifying signs of sediment deposition and erosion. Using 9-point averages, the spatial variation (Fig. 22-24) predicts erosion upstream of the Parker River Dam, Little River Dam and the River Street dam at the dammed reach, while deposition occurs downstream of the Larkin Mill Dam, Little River Dam, and the Main Street Dam. These results indicate that sediment trapping might take place in the reservoirs of the Parker River Dam and the Larkin Mill Dam.

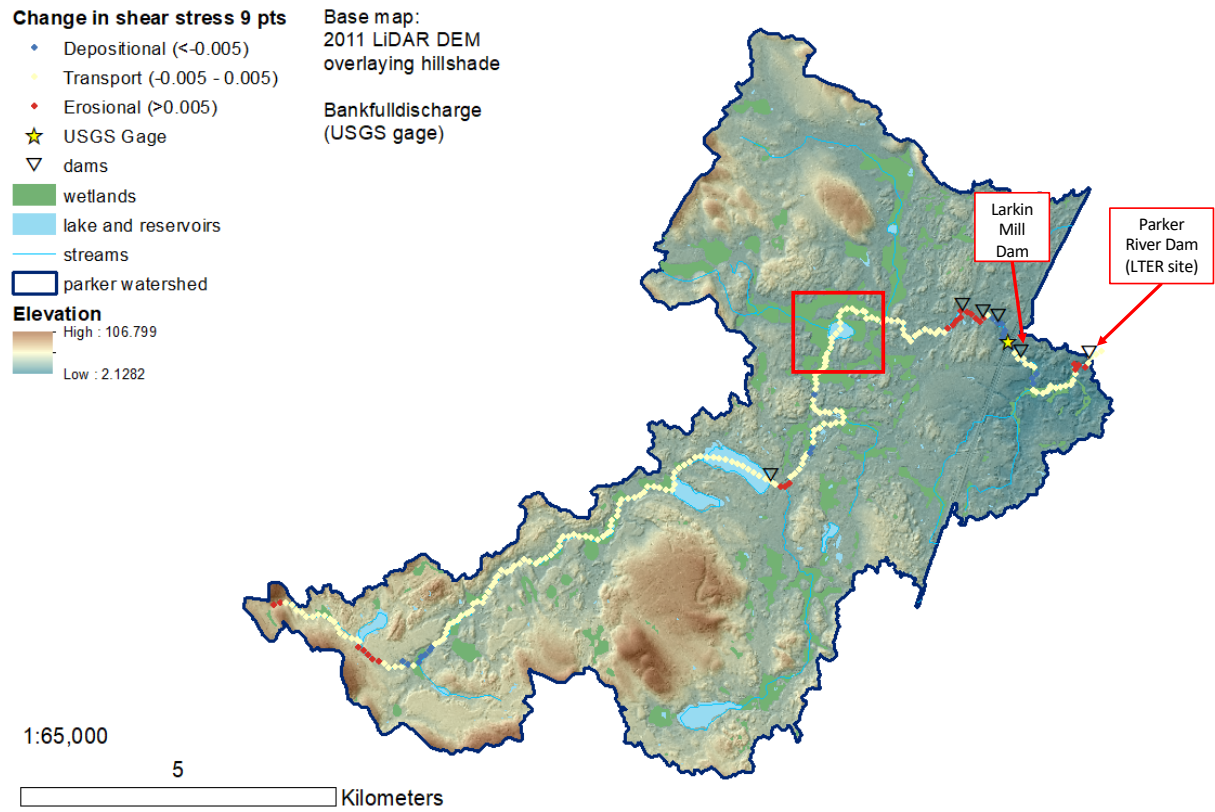


Figure 22. The distribution of the change of basal shear stress ( $\frac{d\tau_b}{dx}$ ) for bankfull discharge ( $Q_{bf}$ ) [red point: positive change indicating erosional; beige point: no change; blue point: negative change indicating depositional]. The red rectangular is highlighting the Crane Pond Wildlife Management area.

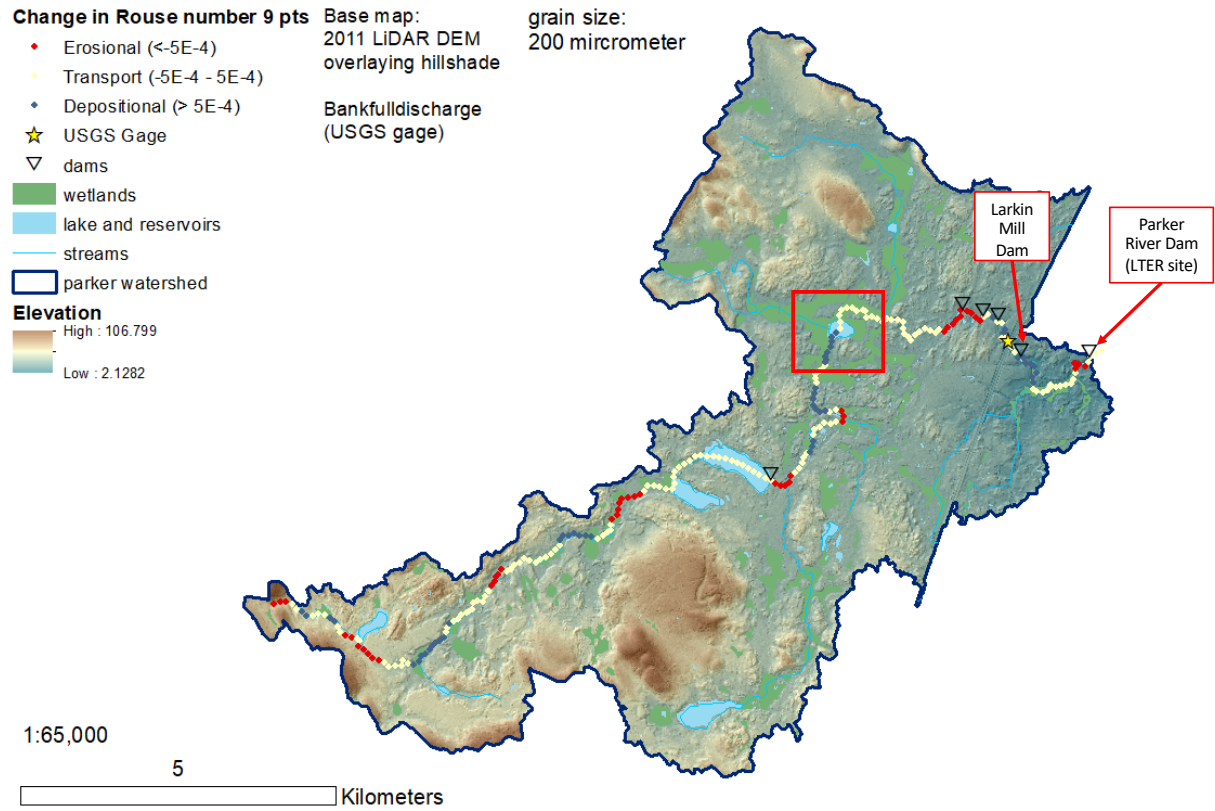


Figure 23. The distribution of Rouse number change ( $\frac{dP}{dx}$ ) for 200  $\mu\text{m}$  grains at bankfull discharge ( $Q_{bf}$ ) [red: negative change - erosional; beige: no change; blue: positive change - depositional]. The red rectangular is highlighting the Crane Pond Wildlife Management area.

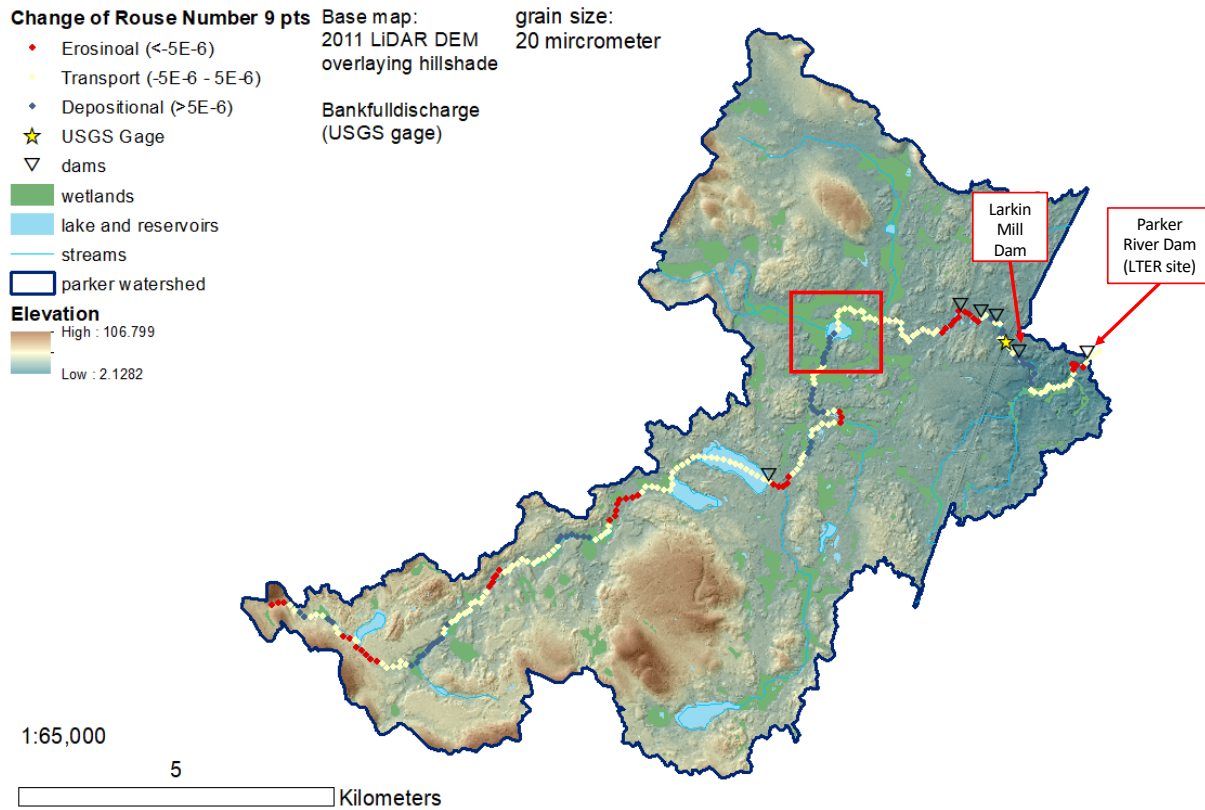


Figure 24. The distribution of Rouse number change ( $\frac{dP}{dx}$ ) for 20  $\mu\text{m}$  grains at bankfull discharge ( $Q_{bf}$ ) [red: negative change - erosional; beige: no change; blue: positive change - depositional]. The red rectangular is highlighting the Crane Pond Wildlife Management area.

### 6.1.3 Comparison of Shear Stress Change between the Dammed and Undammed Scenarios

I developed a longitudinal profile with the dams removed to calculate geomorphic parameters (Fig. 25 a). Since the general patterns of geomorphic parameters are relatively consistent, I used the 9-point average  $\frac{d\tau_b}{dx}$  to compare the dammed and undammed scenarios. Over the dammed reach, the predicted patterns of erosion and deposition are consistent between the two scenarios (Fig. 25 b-c). Thus, removing the dams would not significantly change the sediment transport pattern. Even though erosion might occur over a wider range at the Parker River Dam site after dam removals, deposition is predicted downstream of the first dam and thus any sediments eroded might not be transported much farther downstream.

## 6.2 Field-based and Remote Sensing Analysis: Observations of Hydrology and Sediment Transport

### 6.2.1 Suspended Sediment Yield

Suspended sediment rating curves were calibrated at two locations: Central Street, Newbury, MA (LTER) and the USGS gage at Byfield, MA (Fig. 26). Both regressions are statistically significant with P-values smaller than 0.05 (Fig. 26). The LTER curve ( $R^2=0.853$ ) has a stronger correlation between  $Q_{sd}$  and  $Q_d$  than the USGS curve ( $R^2=0.797$ ), most likely because it is constrained by more observations. The USGS curve is slightly steeper than the LTER curve with similar y-intercepts (Fig. 26). The difference between the two rating curves is not statistically significant because the confidence intervals for the two curves overlap, suggesting that the transport capacity of the basin is not significantly different at these two locations.

The values of  $Q_s$  and  $Y$  were calculated using these two sediment rating curves for each water year from 1947 to 2017 (Fig. 27-28). The average  $Q_s$  is  $120.3 \text{ Mg yr}^{-1}$  at the USGS gage and  $61.0$

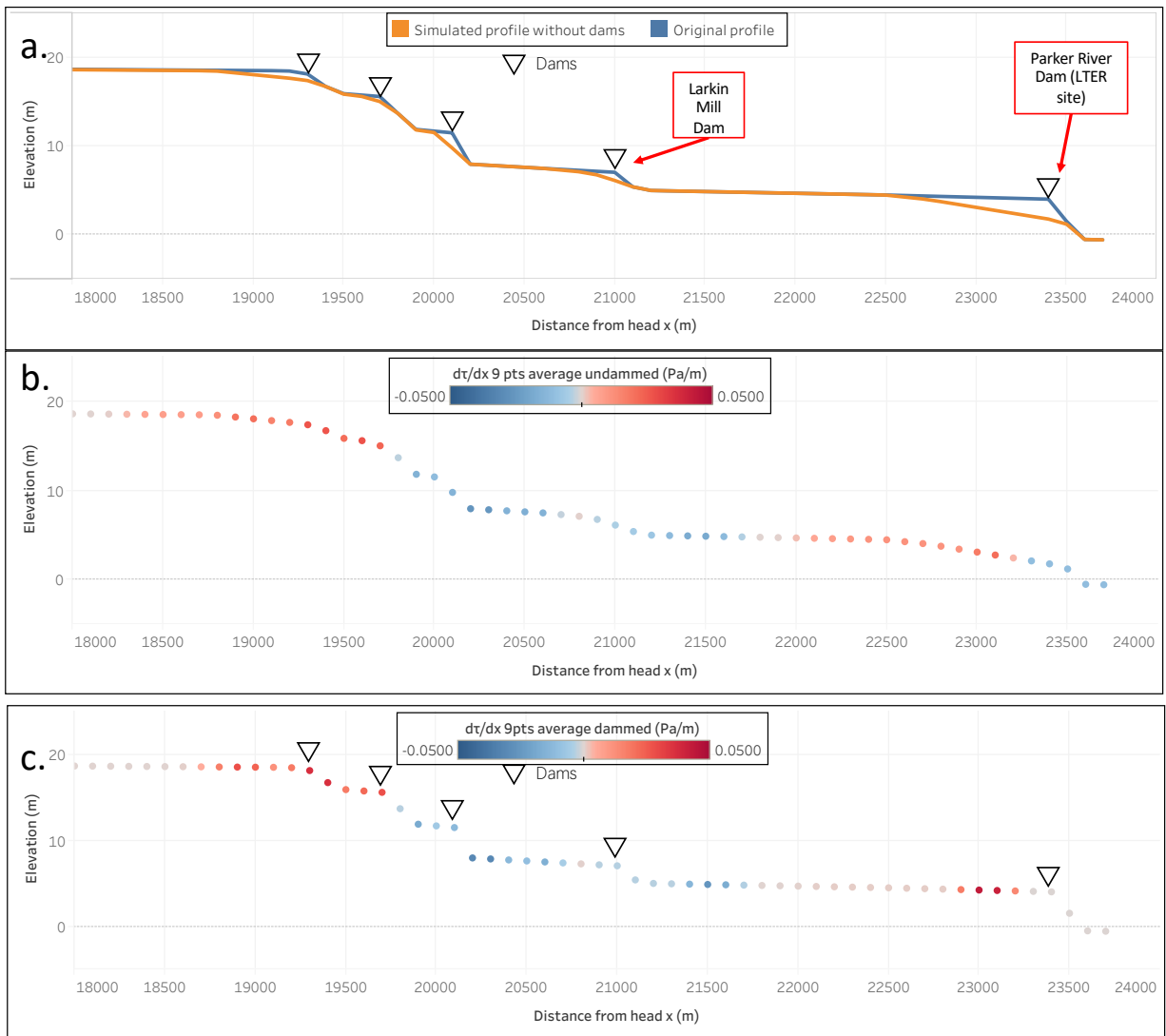


Figure 25. The longitudinal profile of the Parker main stem (blue) and its simulated undammed scenario (orange) (a). Change in shear stress ( $\frac{d\tau_b}{dx}$ ) is identified throughout the longitudinal profile with positive values as red and negative values as blue for undammed (b) and dammed (c) scenarios.

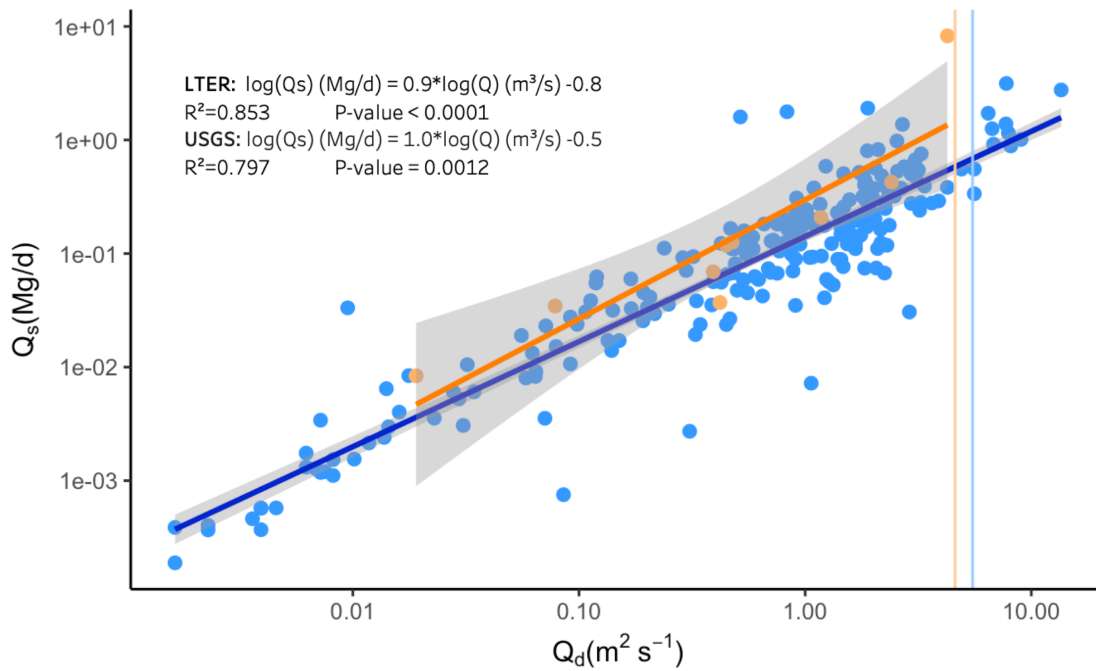


Figure 26. Suspended sediment rating curves at the Parker River Dam (LTER, blue) and USGS gage (modified from Nadeau, 2010, orange) are used for suspended sediment discharge estimate. Reference lines indicate the bankfull discharge at the USGS gage (light orange,  $4.6 \text{ m}^3 \text{ s}^{-1}$ ) and the LTER site (light blue,  $5.5 \text{ m}^3 \text{ s}^{-1}$ ).

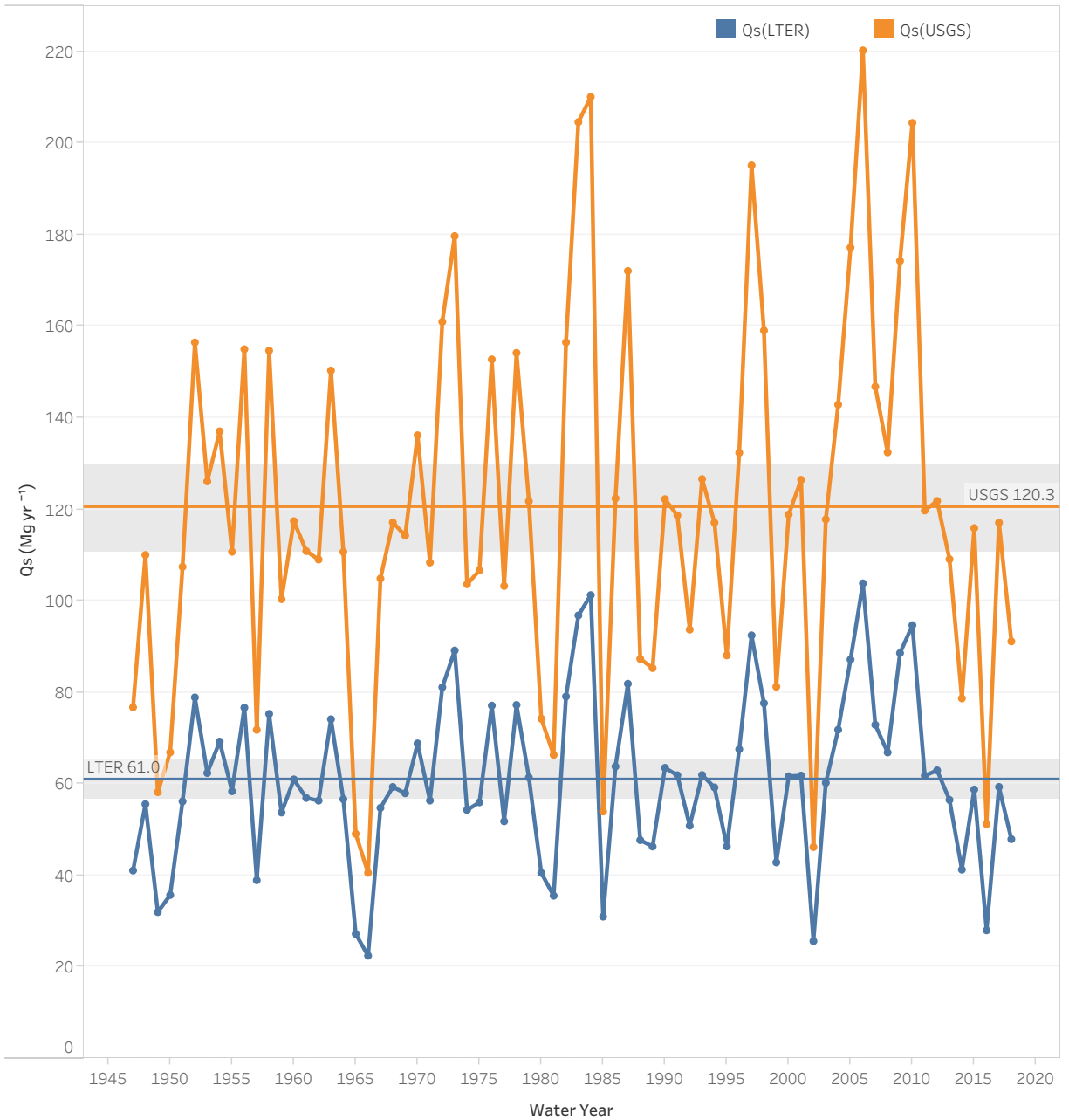


Figure 27. Sediment load at USGS gauge (orange dotted line) and Parker River Dam (LTER, blue dotted line) for each water year from 1947 to 2017. The average  $Q_s$  is  $120.3 \text{ Mg yr}^{-1}$  at USGS gauge (orange line) and  $61.0 \text{ Mg yr}^{-1}$  at LTER site (blue line). Grey banding is indicating the 95 % confidence interval for the average calculation.

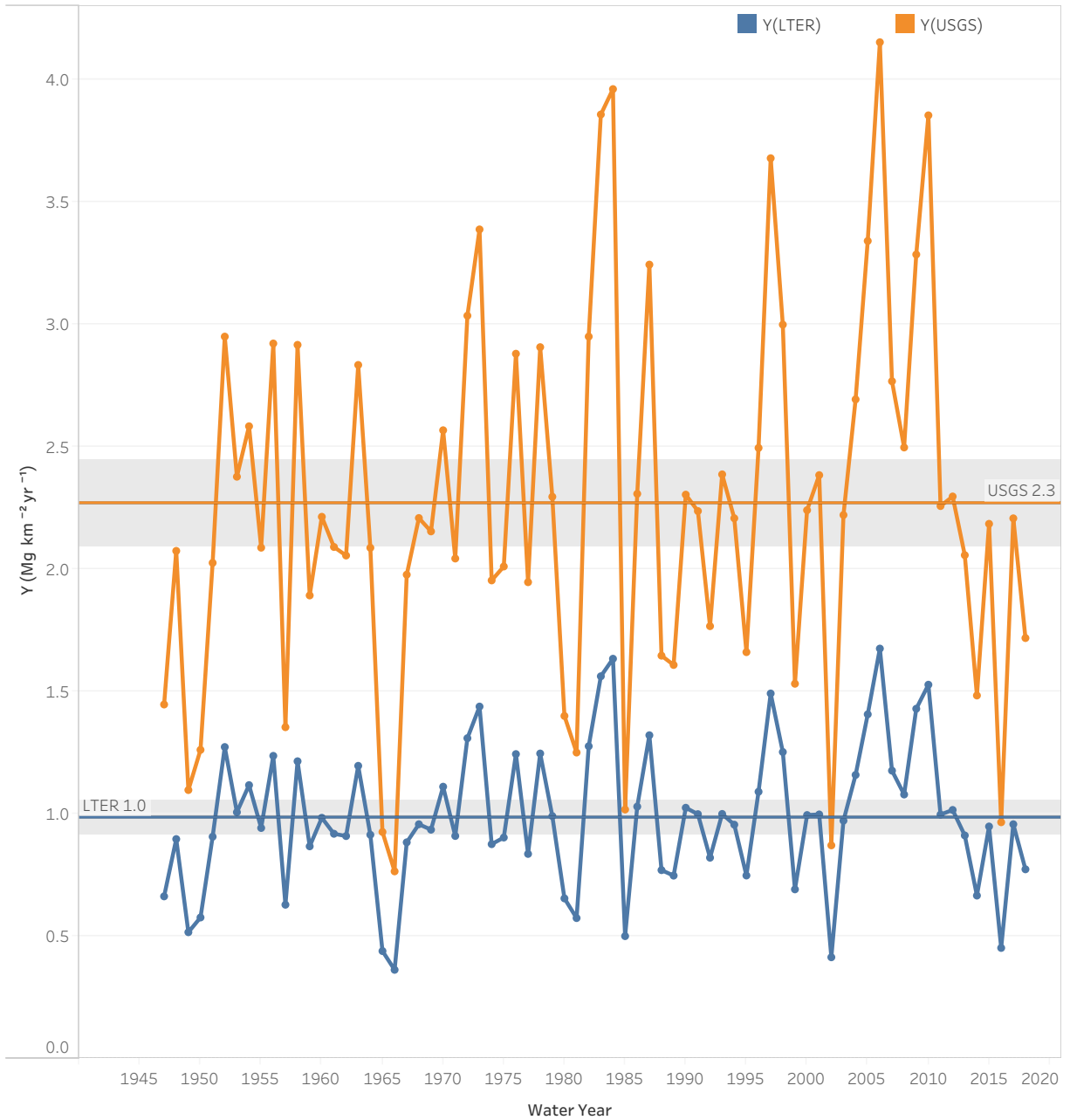


Figure 28. Sediment yield at USGS gauge (orange dotted line) and Parker River Dam (LTER, blue dotted line) for each water year from 1947 to 2017. The average Y is 2.3 Mg km<sup>-2</sup> yr<sup>-1</sup> at USGS gage (orange line) and 1.0 Mg km<sup>-2</sup> yr<sup>-1</sup> at LTER site (blue line). Grey banding is indicating the 95% confidence interval for the average calculation.

Mg yr<sup>-1</sup> at the Parker River Dam. The average  $Y$  is 2.3 Mg km<sup>-2</sup>yr<sup>-1</sup> at the USGS gage and 1.0 Mg km<sup>-2</sup>yr<sup>-1</sup> at the Parker River Dam. Higher  $Q_s$  and  $Y$  at the USGS gage could indicate deposition between the USGS gage and the Parker River dam, but these results are not significantly different from each other based on the available data. The values of  $Q_s$  and  $Y$  at the LTER site are more robust estimate because of the number of observations and the range of  $Q_d$  conditions at which the  $SSC$  samples were taken.

Nadeau (2010) measured 400 Mg of sediment passing through at the USGS gage from 2008 to 2010. Transferring this value into  $Y$  is equivalent to about 3.7 Mg km<sup>-2</sup>yr<sup>-1</sup>. This value is larger than my average  $Y$  at the USGS gage (2.3 Mg km<sup>-2</sup>yr<sup>-1</sup>). The overall  $Y$  estimated by Hopkinson et al. (2018) for the Ipswich and Parker Rivers (3.1 Mg km<sup>-2</sup>yr<sup>-1</sup>; Hopkinson et al, 2018) is also higher than my estimates. The values of  $Y$  calculated in Ames (2018) are 36.8 Mg km<sup>-2</sup>yr<sup>-1</sup> for glaciated basins and 50.5 Mg km<sup>-2</sup>yr<sup>-1</sup> for unglaciated basins in northeastern US. The values of  $Y$  at the two Parker River sites are about 1-2 orders smaller than the average in northeastern US. Thus, the sediment delivery capability of the fluvial portion of the Parker River is small.

### 6.2.2 SSC Spatial Pattern Analysis

Field suspended sediment data were collected at six sites (Fig. 1c) on two separate dates: October 26<sup>th</sup>, 2018 and May 14<sup>th</sup>, 2019. October 26<sup>th</sup>, 2018 was a sunny day with a temperature of 2-6 °C. The value of  $Q_d$  was 0.40 m<sup>3</sup> s<sup>-1</sup> at the USGS gage, representing a base flow condition ( $RI = 0.70$  year) of the Parker River. For a sample size of 250 mL,  $m_{ds}$ ,  $m_s$  and  $SSC$  values are relatively consistent over all sites with little visible variations (Fig. 29). All values are not significantly different from zero.  $SSC$  at all locations were also similar to the blank sample, DI water. The slight decrease from  $m_{ds}$  to  $m_s$  indicates that even if there were anything in the water

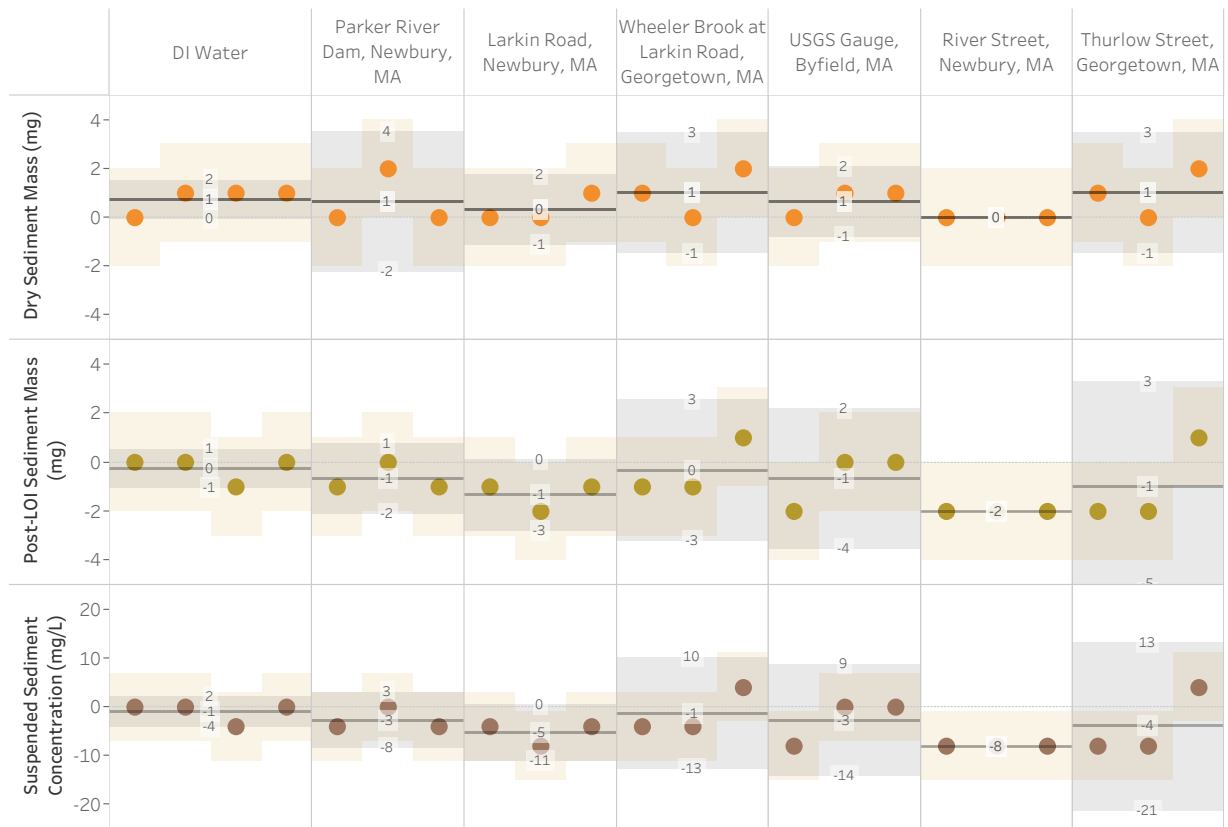


Figure 29. Dry sediment mass ( $m_{ds}$ , upper panel, orange dots), post-LOI sediment mass ( $m_s$ , middle panel, olive dots), and suspended sediment concentration (SSC, lower panel, brown dots) measured and calculated from a 250-mL water sample collected in 1-L bottles at the Parker River at Parker River Dam, Larkin Road, River Street, Newbury, MA, Thurlow Street, Georgetown, MA, Wheeler Brook at Larkin Road, Georgetown, MA, and USGS gage at Byfield, MA on October 26<sup>th</sup>, 2018. DI water was used as a blank reference. Yellow bandings indicate the uncertainty calculated from the accuracy of the measurement ( $\pm 2$  mg for  $m_{ds}$ , and  $m_s$  and  $\pm 7$  mg/L for SSC) and gray bandings indicate the 95% confidence intervals for the average of three samples at each site (dark gray line). The average daily flow ( $Q_d$ ) was  $0.40 \text{ m}^3/\text{s}$  and the weather was sunny with a temperature at 2-6 °C.

sample, it must be organic material. These results indicate that the base flow of the Parker River carries little to no suspended sediment for all six sites I sampled.

May 14<sup>th</sup>, 2019 had light rain with a temperature at 5-6 °C. The value of  $Q_d$  is  $1.68 \text{ m}^3 \text{ s}^{-1}$  at the USGS gage, representing an 0.89-year event flow condition of the Parker River. For a sample of 250 mL,  $m_s$  values are smaller than  $m_{ds}$ , indicating that most of the suspended material were organic (Fig. 30). Only the samples at the Parker River Dam and Wheeler Brook have values above zero (Fig. 30). Other samples have comparable values to the blank samples. These results indicate that the 0.89-year event flow on May 14<sup>th</sup>, 2019 did not carry much sediment at most sample locations.

In general, both sets of field data indicate a low suspended sediment load carried by the Parker River. Because the values are too small and not significantly different from zero, I cannot make any inferences about spatial variations in  $SSC$ . The limited change from the base flow to the event flow conditions indicate that the watershed might have limited sediment sources to start with. The change in  $RI$  is very small between the selected base flow and event flow conditions. Also,  $Q_d$  on both days were much smaller than  $Q_{bf}$  at the USGS gage ( $\sim 4.6 \text{ m}^3 \text{ s}^{-1}$ ). Sampling on a higher-flow day might reveal more substantial variations in  $SSC$ .

### 6.2.3 Remote Sensing Data Analysis

I used combination of  $Q$  data, precipitation data, and satellite images to look for evidence of sedimentation at the Crane Pond WMA. Between 2016 and 2018, only three high discharge events had  $Q > Q_{bf}$  at the USGS gage ( $\sim 4.6 \text{ m}^3 \text{ s}^{-1}$ ). Cloud-free satellite images from Planet.com were identified for these three events (Fig. 31-33). The values of  $Q$  are  $7.362 \text{ m}^3 \text{ s}^{-1}$  ( $RI = 2.53$  years) during the event between March 28<sup>th</sup> to April 17<sup>th</sup>, 2017,  $4.927 \text{ m}^3 \text{ s}^{-1}$  ( $RI = 1.62$  years) during the event between April 16<sup>th</sup> to April 25<sup>th</sup>, 2018, and  $6.513 \text{ m}^3 \text{ s}^{-1}$  ( $RI = 2.17$  years) during the event

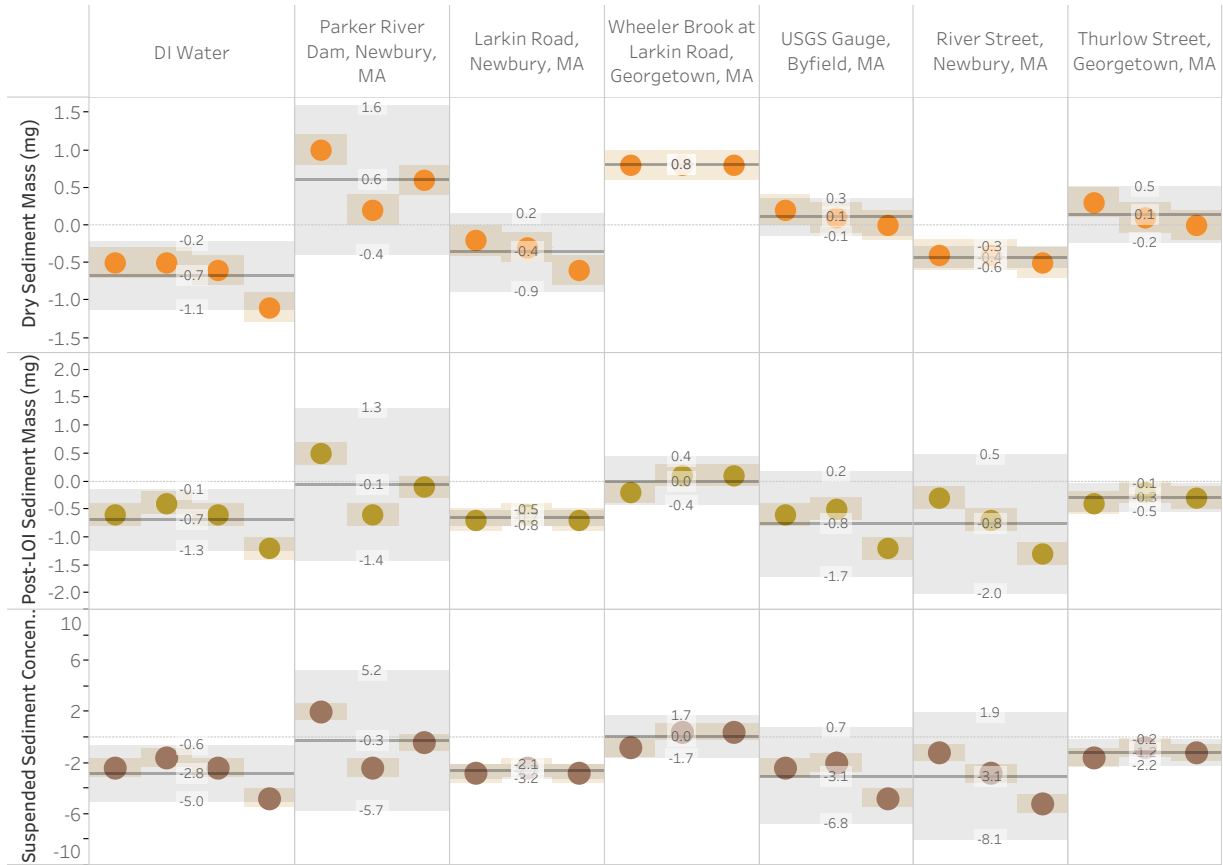
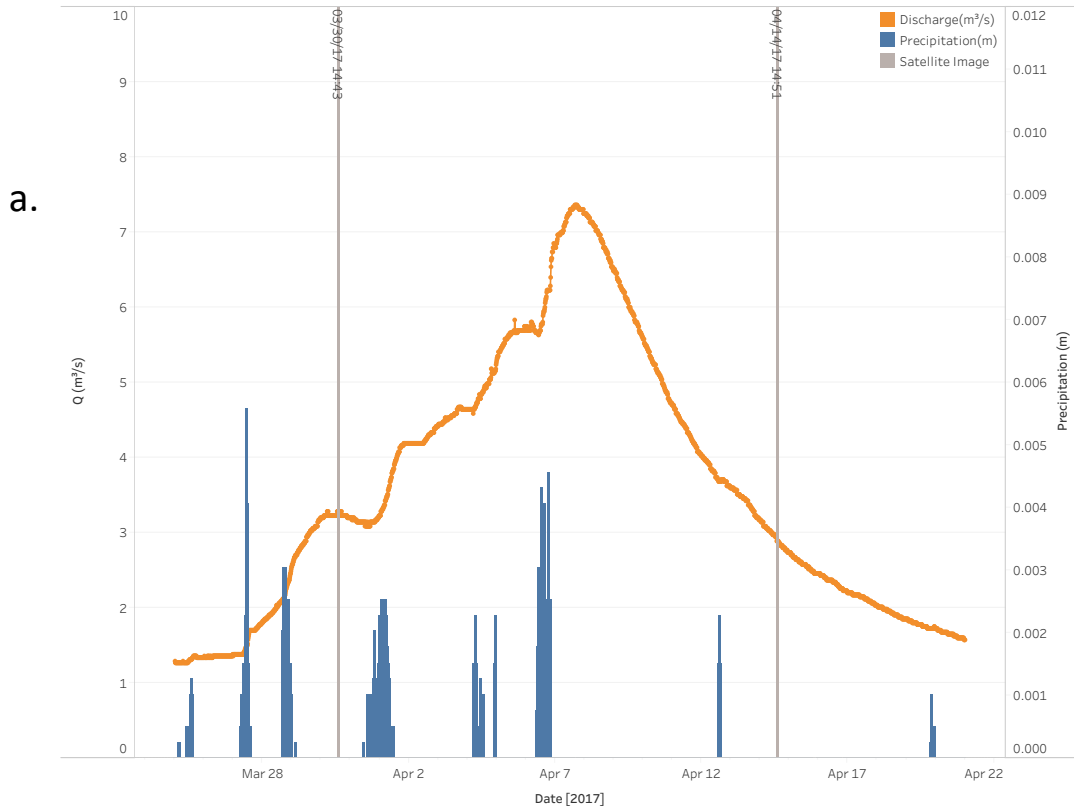


Figure 30. Dry sediment mass ( $m_{ds}$ , upper panel, orange dots), post-LOI sediment mass ( $m_s$ , middle panel, olive dots), and suspended sediment concentration (SSC, lower panel, brown dots) measured and calculated from a 250-mL water sample collected in 1-L bottles at Parker River at the Parker River Dam, Larkin Road, River Street, Newbury, MA, Thurlow Street, Georgetown, MA, Wheeler Brook at Larkin Road, Georgetown, MA, and USGS gage at Byfield, MA on May 14<sup>th</sup>, 2019. DI water was used as a blank reference. Yellow bandings indicate the uncertainty calculated from the accuracy of the measurement ( $\pm 0.2$  mg for  $m_{ds}$  and  $m_s$ , and  $\pm 0.7$  mg/L for SSC) and gray bandings indicate the 95% confidence intervals for the average of three samples at each site (dark gray line). The average daily flow ( $Q_d$ ) was  $1.68$  m<sup>3</sup>/s and the weather was light rain with a temperature at 5-6 °C.



March 30th, 2017



April 14th, 2017



Figure 31. (a) High discharge event between March 28th, 2017 to April 17th, 2017 at Parker River. Orange dots are 15-min discharges ( $Q_{15\text{-min}}$ ) measured at the USGS gauge, Byfield, MA with the peak discharge ( $Q_{\text{peak}}$ ) at  $7.362 \text{ m}^3/\text{s}$  ( $RI=2.52$  years). Blue bars are precipitations measured at Lawrence Municipal Airport, MA. Grey lines annotated the time with available satellite images from Planet.com. (b) (c) satellite images from Planet.com. Ice cover (red rectangle) presented on Crane Pond on March 30<sup>th</sup>, 2017 and the inlet is indicated (red arrow) (b).

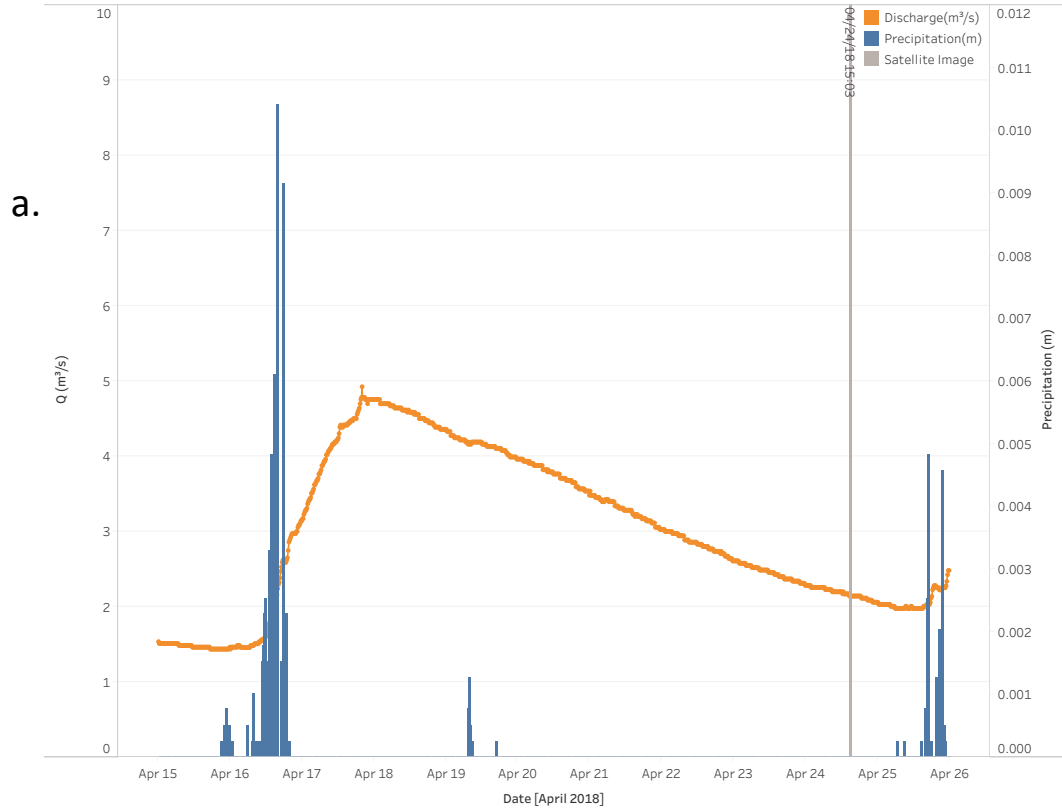


Figure 32. (a) High discharge event between April 16<sup>th</sup>, 2018 to April 25<sup>th</sup>, 2018 at Parker River. Orange dots are 15-min discharges ( $Q_{15\text{-min}}$ ) measured at the USGS gauge, Byfield, MA with the peak discharge ( $Q_{\text{peak}}$ ) at 4.927 m<sup>3</sup>/s ( $RI=1.62$  years). Blue bars are precipitations measured at Lawrence Municipal Airport, MA. Grey lines annotated the time with available satellite images from Planet.com. (b) satellite images from Planet.com with the inlet location indicated (red arrow).

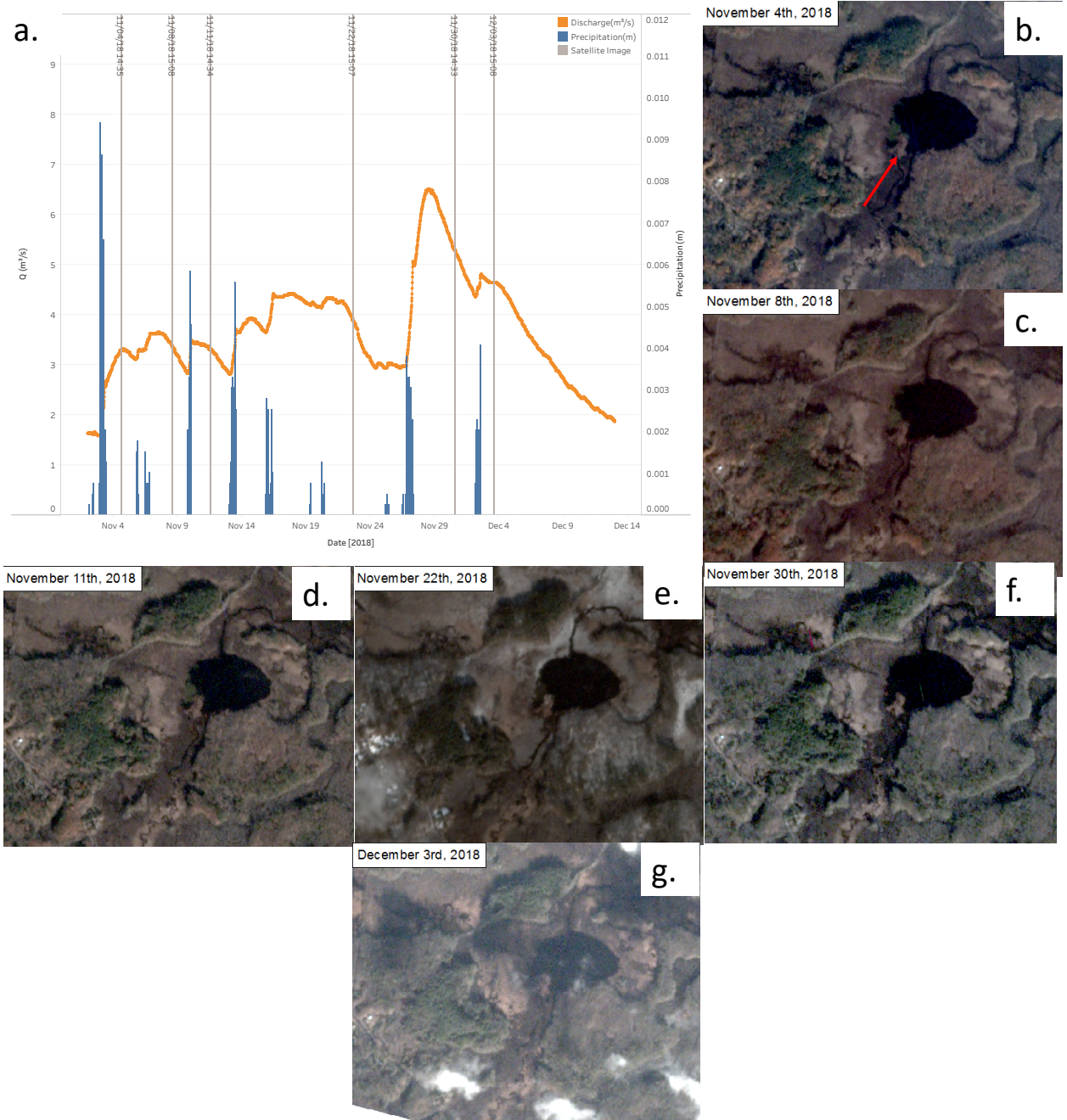


Figure 33. (a) Three consecutive high discharge events between November 4<sup>th</sup>, 2018 to December 9<sup>th</sup>, 2018 at Parker River. Orange dots are 15-min discharges ( $Q_{15-min}$ ) measured at the USGS gauge, Byfield, MA with the peak discharge ( $Q_{peak}$ ) at 6.513  $m^3/s$  (RI=2.17 years). Blue bars are precipitations measured at Lawrence Municipal Airport, MA. Grey lines annotated the time with available satellite images from Planet.com. (b-g) satellite images from Planet.com with the inlet location indicated (red arrow).

between November 4<sup>th</sup> to December 4<sup>th</sup>, 2018. From satellite images for all three events, no visual evidence of a suspended sediment plume is found following the high event flow. This observation indicates three possibilities. (1) The basin upstream of the Crane Pond is sediment starved and thus leaves no available sediments to be transported during high flows. (2) The stream profile upstream of the Crane Pond provides lots of opportunities for sediment deposition and thus traps any eroded sediments before they reach the Crane Pond. (3) The *SSCs* during the events are too low to be visible in the satellite images. Orthophotographs from 1995 to 2018 show little evidence of growth of the inlet delta in Crane Pond (Fig. 34). Lack of delta change indicates that the sediment sources from the upstream basin during this period were not sufficient to cause delta progradation.

### **6.3 Empirical Analysis: Trap Efficiency**

Two sets of *Te* were calculated using different reservoir areas. One set determined reservoir areas using the same reservoir extent as in the theoretical analysis (Fig. 25a) and the LiDAR DEM (Fig. 35). All derived *C/I* values are less than 0.001, and thus *Te* values fall outside the range of Brune's (1953) curves (Table 5, Fig. 36). Another set determined reservoir areas using the reservoir polygons in the USGS 25k water bodies (Fig. 37). Only the *C/I* value for the Parker River Dam is larger than 0.001 and the corresponding *Te* is 6.3% (Table 6, Fig. 36). These results suggest that most dams are not trapping any sediments. The Parker River Dam might be the only exception but the trapping capability is still minimal.

## **7 Discussion**

### **7.1 Are Dams Trapping Sediment and therefore Reducing Sediment Load to the Estuary?**

The results of this study suggest that dams on the Parker River main stem are not trapping sediment. The modeled variations in *P* and  $\tau_b$  indicate that the regions immediately downstream

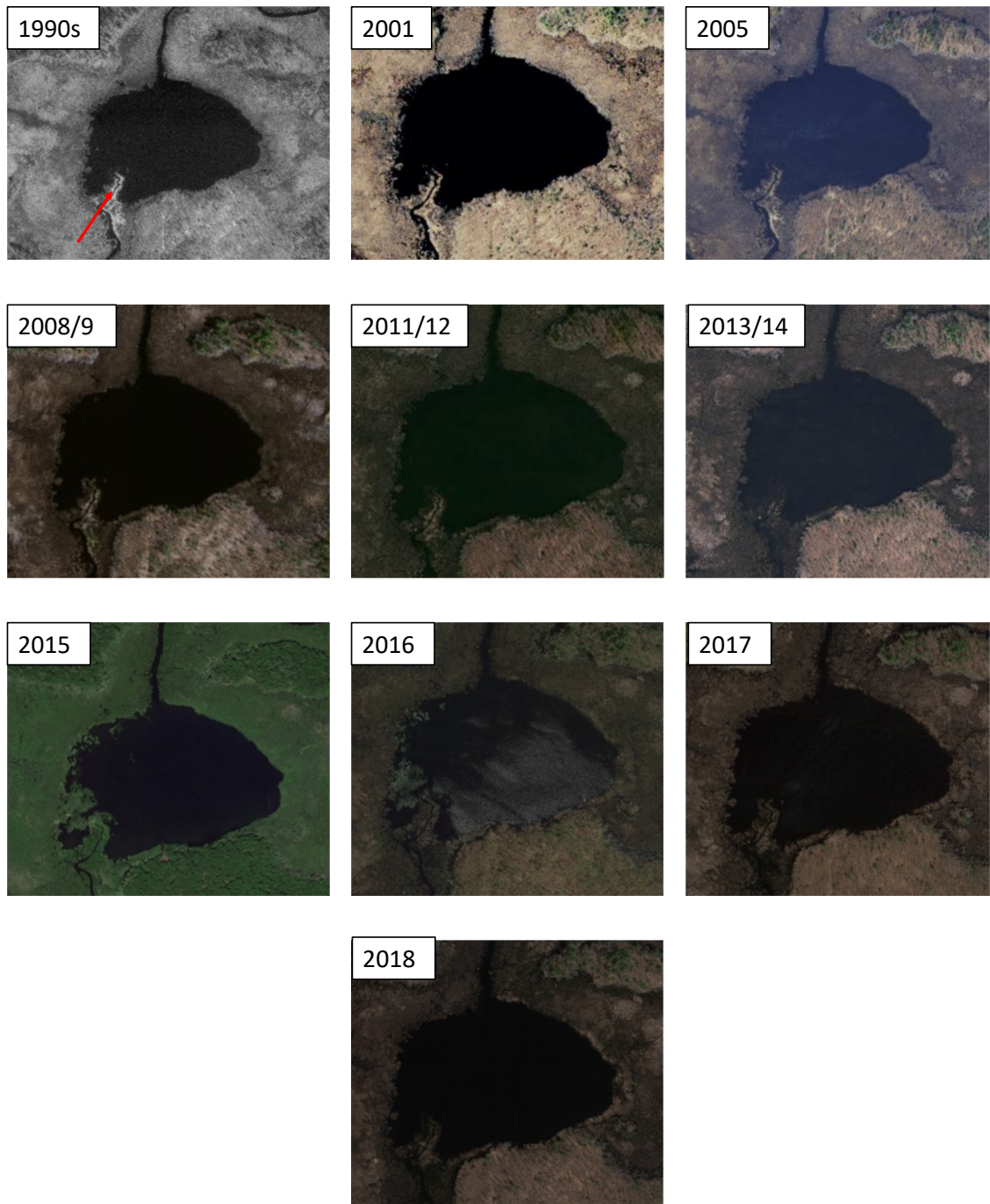


Figure 34. Aerial photos of Crane Pond from 1990s to 2018 signaling little to no delta evolution (MassGIS, 2019) with the inlet location indicated (red arrow). The figure for 2016 was impacted by cloud cover.

- ▽ dams
- reservoir extent
- ▭ reservoir area
- ▭ parker watershed
- ▬ parker main stem
- ▭ lakes and reservoirs
- ▭ wetlands
- Elevation (m)**
- High : 106.799
- Low : -2.1

Base map:  
2011 LIDAR DEM  
overlaying hillshade

Bankfull discharge  
(USGS gage)

Reservoir extent  
determined by  
the slope jump  
in the connected  
minimum profile

1:12,000  
500  
Meters

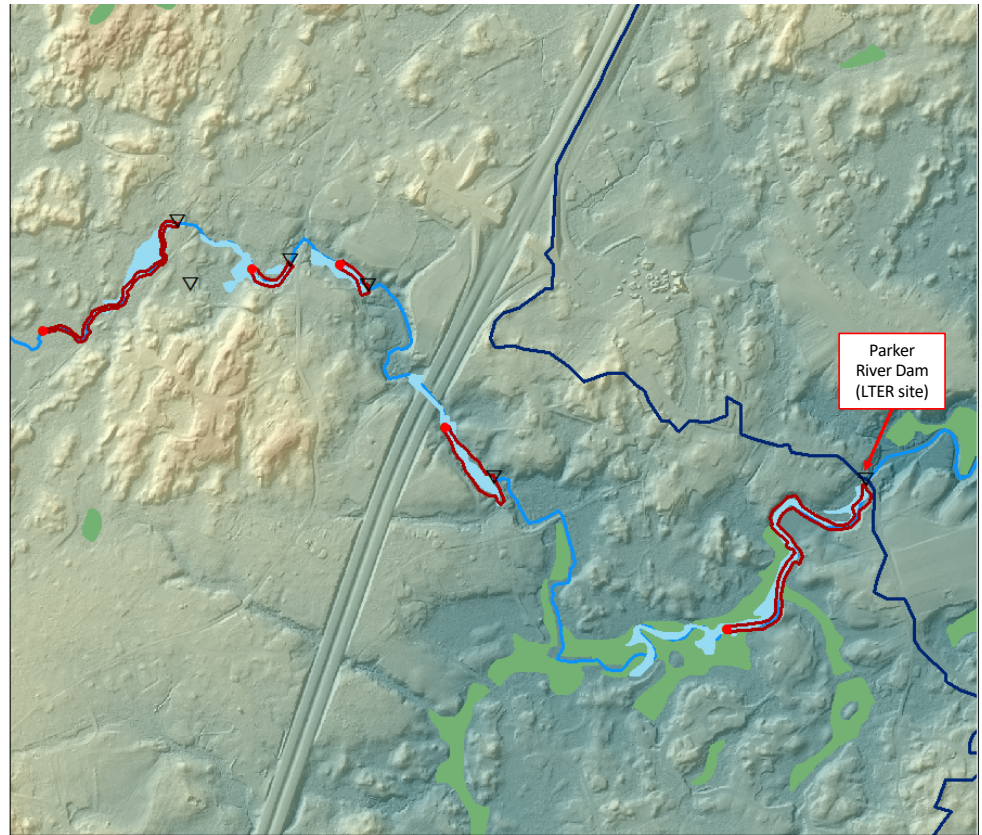


Figure 35. The reservoir area (A, red line) and reservoir extent (red dots) determined by the slope jump in the minimum profile.

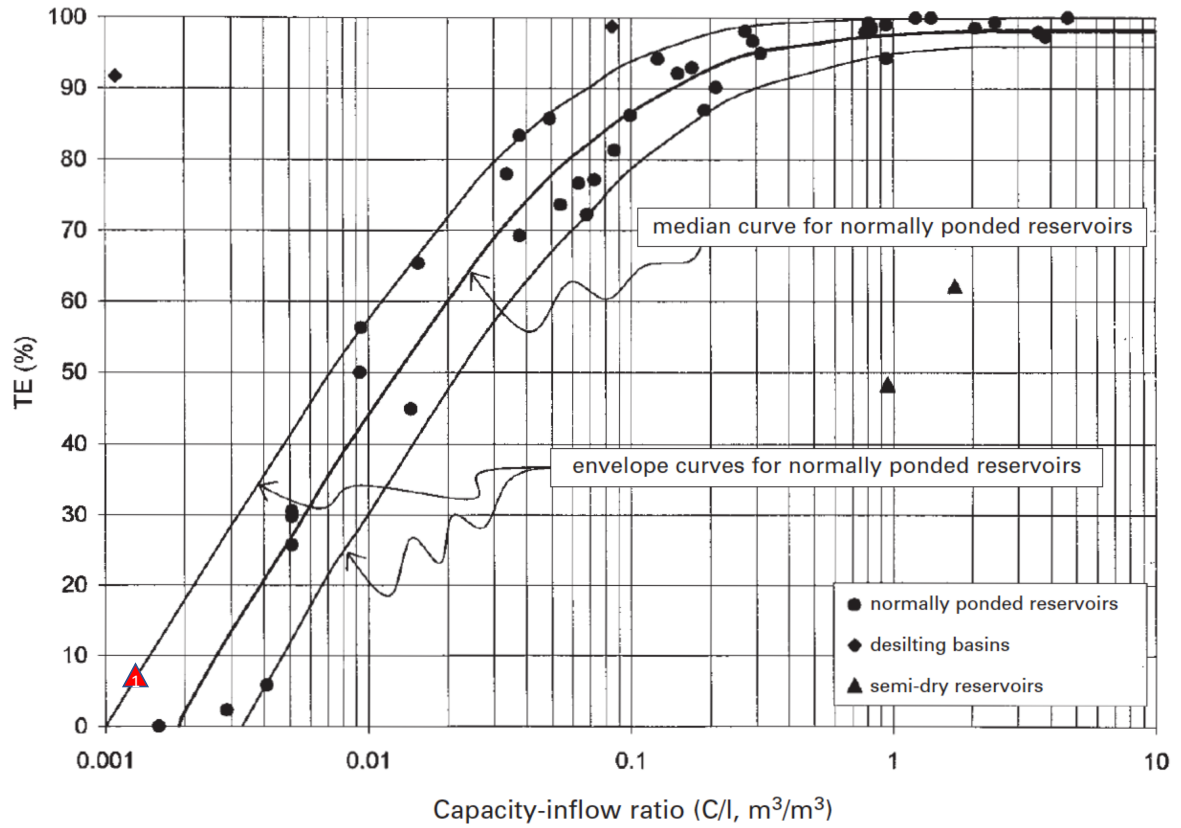


Figure 36. The corresponding trap efficiency (Te) for each dam given capacity-inflow ratio ( $C/I$ ) (modified by Verstraeten and Poesen, 2000 from Brune, 1953). The red triangle with number one inside denotes the trap efficiency and capacity-inflow ( $C/I$ ) ratio for the Parker River Dam, Newbury, MA when the reservoir area is determined using the reservoir polygons in the USGS 25k water bodies. All reservoir areas determined using LiDAR DEM and other reservoir areas from USGS 25k water bodies are not identifiable using this graph because the  $C/I$  ratios are less than 0.001.

- ▽ dams
  - ▭ parker watershed
  - parker main stem
  - ▭ USGS reservoir area
  - ▭ wetlands
- Elevation (m)**
- High : 106.799
  - Low : -2.1

Base map:  
2011 LiDAR DEM  
overlaying hillshade

Bankfull discharge  
(USGS gage)

Reservoir extent  
determined by  
reservoir polygons  
in USGS 25k water  
bodies

1:12,000  
500  
Meters

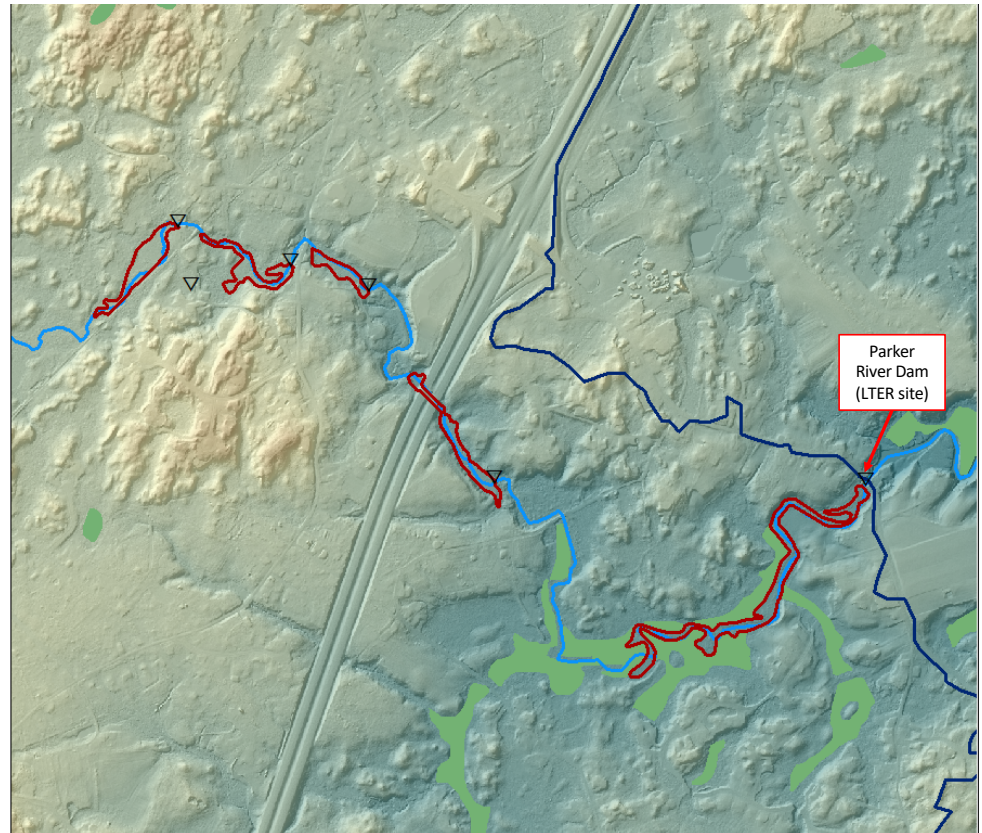


Figure 37. The reservoir area (A, red line) determined by reservoir polygons in USGS 25k water bodies.

Table E. The calculation for the empirical analysis based on the reservoir areas determined by the interpolated minimum slope profile.

<b>Road/Name</b>	<b>Area (m<sup>2</sup>)</b>	<b>Dam height (m)</b>	<b>Storage capacity (m<sup>3</sup>)</b>	<b>Drainage area (km<sup>2</sup>)</b>	<b>Mean annual flow (m<sup>3</sup>)</b>	<b>C/I</b>	<b>Te (%)</b>
<b>Parker River</b>							
<b>Dam</b>	17079.5	3.0	25619.2	62	39651492.7	6.46E-04	NA
<b>Larkin Mill</b>							
<b>Dam</b>	9237.8	1.6	7390.3	53	33895630.9	2.18E-04	NA
<b>Little River</b>							
<b>Dam</b>	2394.9	2.8	3352.9	52.8	33767722.9	9.93E-05	NA
<b>Main Street</b>	2776.1	1.4	1873.9	52.3	33447952.7	5.60E-05	NA
<b>River Street</b>	7129.5	1.0	3564.8	52.1	33320044.7	1.07E-04	NA

Table F. The calculation for the empirical analysis based on the reservoir areas determined by the connected minimum profile.

<b>Road/Name</b>	<b>Area (m<sup>2</sup>)</b>	<b>Dam height (m)</b>	<b>Storage capacity (m<sup>3</sup>)</b>	<b>Drainage area (km<sup>2</sup>)</b>	<b>Mean annual flow (m<sup>3</sup>)</b>	<b>C/I</b>	<b>Te (%)</b>
<b>Parker River</b>							
<b>Dam</b>	33694.1	3.0	50541.1	62	39651492.7	1.27E-03	6.3%
<b>Larkin Mill</b>							
<b>Dam</b>	12119.5	1.6	9695.6	53	33895630.9	2.86E-04	NA
<b>Little River</b>							
<b>Dam</b>	6086.0	2.8	8520.4	52.8	33767722.9	2.52E-04	NA
<b>Main Street</b>	11026.8	1.4	7443.1	52.3	33447952.7	2.23E-04	NA
<b>River Street</b>	13947.0	1.0	6973.5	52.1	33320044.7	2.09E-04	NA

of a dam headwall could serve as potential locations for sediment deposition (Fig. 14, 18, 20), but silt size or smaller particles are too small to be trapped given the calculated  $\tau_b$  from the stream profile. As indicated by the  $P$  values for 20  $\mu\text{m}$  grains, silt size or smaller particles will be transported downstream as wash load (Fig. 21) and thus the variation of  $P$  and  $\tau_b$  will not lead to sediment trapping. Sand-sized sediments are more likely to be trapped in the reservoirs as the  $P$  values for 200  $\mu\text{m}$  grains indicates a section of 50% suspended load between the Parker River dam and the Larkin Mill Dam (Fig. 19). Positive  $\frac{dP}{dx}$  and negative  $\frac{d\tau_b}{dx}$  downstream of the Larkin Mill dam could lead to the trapping of sand-sized sediments in the reservoir of the first dam (Fig. 14, 18). However, the grain sizes that build up downstream marshes are mud to silt sizes (e.g., Vinagre et al., 2008; Kirwan et al., 2011), which is better represented by the analysis for 20  $\mu\text{m}$  grains (Fig. 20, 21, 24). Thus, based on the results of the longitudinal profile analysis, dams do not appear to be trapping the grain sizes of most concern.

If the dams are not trapping much sediment, then removing them from the profile will not release much historically trapped sediments to the downstream estuary. Furthermore, if the removal of dams causes little change to the stream profile, then it will also have little effect on improving the future sediment delivery. The values of  $\frac{d\tau_b}{dx}$  remain in a similar pattern for the undammed scenario as that of the original profile (Fig. 25), because most of the dams were built on natural knickpoints along the stream profile. Thus, dam removal is not likely to change the sediment transport pattern of the main stem and increase the sediment transport to the estuary.

Field analysis also supports the findings from the theoretical analysis. The average values of  $Q_s$  and  $Y$  decrease from the USGS gaging station (120.3  $\text{Mg yr}^{-1}$ , 2.3  $\text{Mg km}^{-2}\text{yr}^{-1}$ ) to Parker River Dam (61  $\text{Mg yr}^{-1}$ , 1.0  $\text{Mg km}^{-2}\text{yr}^{-1}$ ), indicating that sediment trapping might take place in the reservoir of the Parker River dam (Fig. 27-28). However, the sediment rating curves of these

two locations are not significantly different (Fig. 26) and thus the calculated  $Q_s$  and  $Y$  are also not significantly different from each other. Also,  $SSC$  measurements collected in the dammed reach indicate little variation of  $SSC$  on base and event flow days (Fig. 29, 30). Thus, the evidence of the field analysis suggests little impact of dams on sediment availability downstream.

Except for the Parker River dam, none of the dams studied have a positive  $Te$ , which indicates that these dams do not trap sediments. The result at the Larkin Mill Dam is consistent with a previous study. Using the model from Wade (2008), Nadeau (2010) estimated a net erosion rather than deposition between 2008 and 2010 at the Larkin Mill Dam. In that study, cross sections directly upstream of the I-95 bridge abutments and at Larkin Mill Dam did show net sediment deposition, most cross-sections across the impoundment showed net erosion, resulting a negative change (-69 Mg) in storage from 2008 to 2010 (Nadeau, 2010). One of the two reservoir area estimates derived a positive, but small  $Te$  value (Table 6). Thus, the trapping capacity of the Parker River Dam is also limited and removing this dam will most likely not increase sediment delivery to the estuary.

Despite the strong evidence suggesting little to no impact of dams on sediment budget downstream, limitations still exist. The theoretical modeling and trap efficiency calculations only consider the active channel and reservoirs. It is possible that dams raise the water level and increase the frequency of overbank sedimentation. A more detailed hydraulic model (e.g., HEC-RAS in Wade, 2008) or more  $SSC$  observations during high flow events might better address the sediment transport pattern at these locations, but both are beyond the scope of this project. In the Wade (2008) study at the Larkin Mill Dam, a different  $n$  was used for the overbank areas (0.1), but the value was uncalibrated because the water level rarely reached overbanks. Using the model of Wade (2008), Nadeau (2010) found good correspondence in overbank areas and the general channel

shape in the majority of cross sections between 2008 and 2010. The results of these hydraulic models indicate that overbank sedimentation might play a limited role at the Larkin Mill Dam site.

## 7.2 What Portion of the Watershed can Contribute Sediments to the Estuary?

This study suggests that only a small portion of the watershed could contribute sediments to the estuary. In the drainage basin upstream of the Crane Pond, sediments need to pass through the Crane Pond to reach farther downstream. Thus, I separate the watershed into two portions to discuss their contributions to downstream sediment budget: the drainage basin upstream of the Crane Pond (39.6 km<sup>2</sup>, 62.3%) and the drainage basin of the dammed reach (23.9 km<sup>2</sup>, 37.7%).

Sediments from the basin upstream of the Crane Pond are unlikely to contribute to the estuary. The Crane Pond can serve as an effective sediment sink. The values of  $P$  for 200  $\mu\text{m}$  grains are highest around Crane Pond, where sediment transport mode switch from 50% suspension to bed load (Fig. 18, 19). As a result, sand-sized sediments are unlikely to pass through the Crane Pond. The  $P$  values for 20  $\mu\text{m}$  indicates that silt-sized grains will be transported as wash load throughout (Fig. 20, 21). However, the values of  $P$  are likely underestimated at the Crane Pond because the model assumption of a fluvial channel scaling underestimates the actual depth and  $\omega$  of the pond and thus overestimates  $\tau_b$ .

Remote sensing analysis provides little evidence for active sediment transport into Crane Pond. No visible sediment plumes exist on satellite images in the Crane Pond during high flow events, and the delta of the Crane Pond has remained essentially the same over the past two decades based on the orthophotographs (Fig. 31-34). The range of  $SSC$  (on the order of 1-10 mg/L) that I looked to identify are small values compared to other regions. It is possible that these values are too small to cause visible variations in orthophotographs. For the paired examples in Zhang et al. (2020) where the sole influence of  $SSC$  was interpreted to be river discharge, the spatial variations of  $SSC$

predicted from spectral remote-sensing reflectance in the PIS were not visible from unprocessed Landsat images (Fig. 38). This lack of evidence for sediment input to the Crane Pond could indicate that the upstream watershed is either starved of sediments to be transported, or has many other locations of sediment deposition, but it is also likely that more sophisticated analysis of remote sensing data (e.g., Zhang et al., 2020) is necessary to identify these changes.

The watershed downstream of Crane Pond, including the dammed reach, also has limited sediment supply. The *SSC* values for the sites in this portion of the watershed are not significantly different from that for DI water on both base flow and event flow days (Fig. 29, 30). The *Y* at the Parker River Dam, Newbury, MA ( $1.0 \text{ Mg km}^{-2} \text{ yr}^{-1}$ ) is also lower than the numbers reported in past compilations. The global average is  $120 \text{ Mg km}^{-2} \text{ yr}^{-1}$  (Syvinski et al., 2005) with a range of  $5 - 1,460 \text{ Mg km}^{-2} \text{ yr}^{-1}$  (Lane et al., 2005). The average *Y* in the northeastern US is  $36.8 \text{ Mg km}^{-2} \text{ yr}^{-1}$  for glaciated basins with an error range (one standard deviation) of 9.98 to  $136 \text{ Mg km}^{-2} \text{ yr}^{-1}$  and the smallest *Y* recorded is  $1.7 \text{ Mg km}^{-2} \text{ yr}^{-1}$  at the McDonalds Branch, NJ (Ames, 2018). The *Y* value at the Parker River Dam is 3 orders smaller than the global average, and 1-2 order smaller than the northeastern average. Thus, the Parker River watershed is undoubtedly sediment starved.

The *Y* value is also smaller than previous estimates in the study area:  $3.7 \text{ Mg km}^{-2} \text{ yr}^{-1}$  at the Larkin Mill Dam (Nadeau, 2010) and  $3.1 \text{ Mg km}^{-2} \text{ yr}^{-1}$  for both Ipswich and Parker River watersheds (Hopkinson et al., 2018). The *Y* values reported in Nadeau (2010) and Hopkinson et al. (2018) were both calculated based on the discharge conditions in the 21<sup>st</sup> century, while my value is an average over the past 82 years (1947-2018). Hopkinson et al. (2018) reported that the average discharge during the 8-year *SSC* record (2007-2014) was approximately 10% higher than the USGS 80-year average. Indeed, the average *Y* for water year 2007-2014 ( $1.100 \text{ Mg km}^{-2} \text{ yr}^{-1}$ ) is

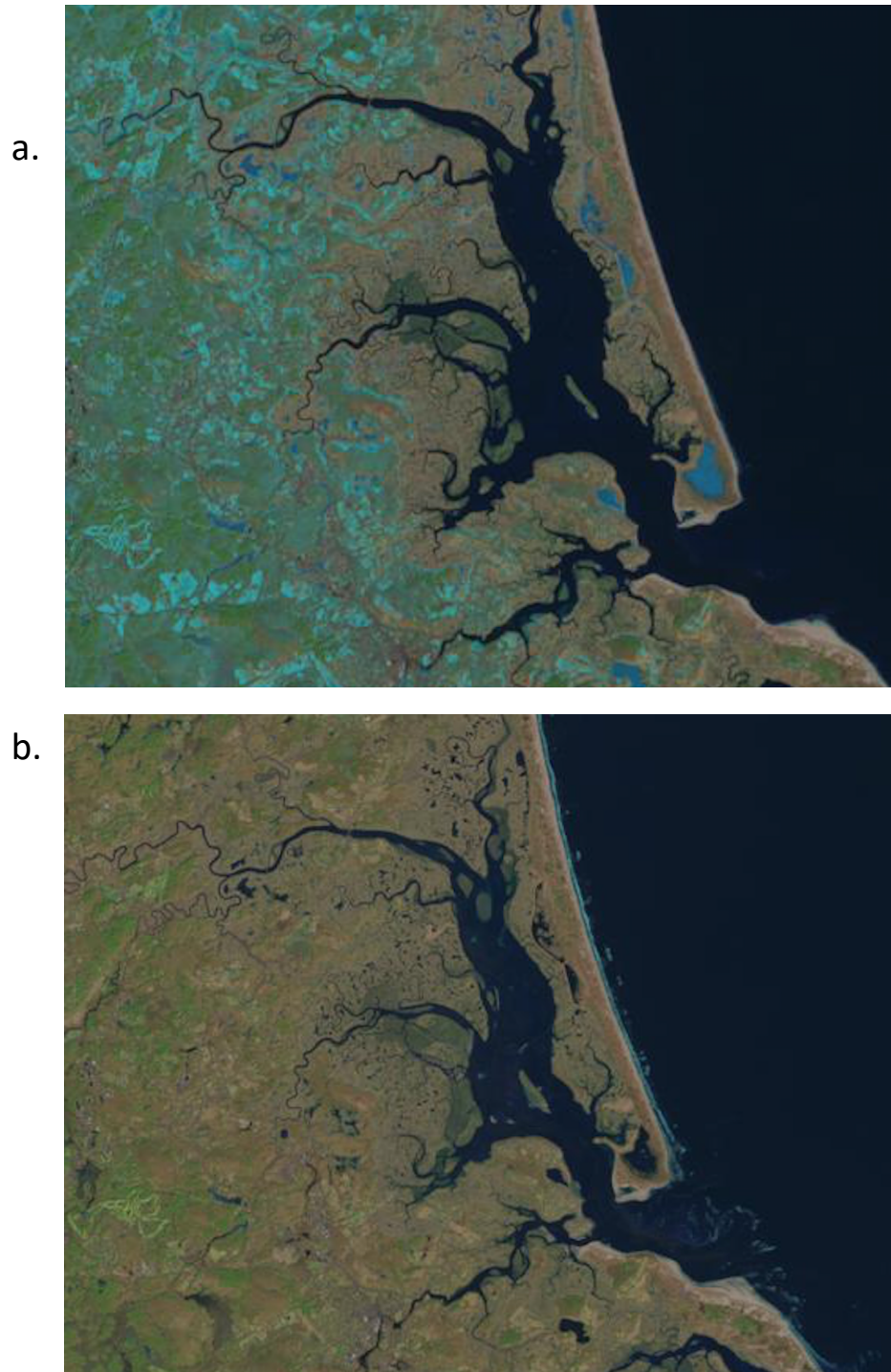


Figure 38. The Landsat Scenes in 1-2-3 [Blue-Green-Red] of Plum Island Sound (PIS) on March 18th, 2014 (SSC = 1.72 mg/L) (a) and April 3rd, 2014 (SSC = 9.72 mg/L) (b) (EarthExplorer, 2020).

about 12% higher than the 82-year average, and the average  $Y$  for water years 2009-2010 ( $1.478 \text{ Mg km}^{-2}\text{yr}^{-1}$ ) is about 50% higher. Thus, the shifting baseline of  $Q_d$  condition could contribute to a part of the gap between values in previous literature and this study.

In addition, the  $Y$  calculated in Nadeau (2010) is also based on the less-robust sediment rating curve at the USGS gage (orange line, Fig. 26). Thus, the  $Y$  value of Nadeau (2010) is comparable to the average  $Y$  of water year 2009-2010 estimated using the USGS sediment rating curve ( $3.6 \text{ Mg km}^{-2}\text{yr}^{-1}$ ). To better understand the sediment contribution of the dammed reach, developing a robust estimate of  $Q_s$  and  $Y$  at the USGS gage site would be useful. The change of the  $Q_s$  and  $Y$  from the USGS gauge to Parker River Dam could help evaluate whether Wheeler Brook can serve as an important sediment source and whether the Parker River Dam is a sediment sink (Fig. 1c).

The Parker and Ipswich River watersheds together have a  $Q_s$  of  $3210 \text{ Mg yr}^{-1}$  and a  $Y$  of  $3.1 \text{ Mg km}^{-2}\text{yr}^{-1}$  between 2007-2014 (Hopkinson et al., 2018), while the upland Parker River watershed defined in this study ( $63.5 \text{ km}^2$ ) has a  $Q_s$  of  $68.2 \text{ Mg yr}^{-1}$  and a  $Y$  of  $1.1 \text{ Mg km}^{-2}\text{yr}^{-1}$  between 2007-2014. The difference between the  $Q_s$  and  $Y$  values reported in this study and the Hopkinson et al. (2018) study may be a result of differences in calculation methods and datasets. It is not entirely clear how Hopkinson et al. (2018) calculated  $Q_s$  and  $Y$ , but several possibilities can be postulated. First, the difference in watershed extent could lead to this slight variance in  $Y$ . The calculations of Hopkinson et al. (2018) included the whole Parker and Ipswich River watersheds, including the tidal portions, while the watershed defined in this study is much smaller only upstream of the Parker River Dam. Second, using different discharge data for sediment discharge calculation could result in different values. I used  $Q_d$  for my calculation of  $Q_s$ , but it is possible that Hopkinson et al. (2018) used instantaneous discharge ( $Q_{15-min}$ ) which would likely yield a higher value of  $Q_s$  as  $Q_d$  often dampens the peak represented in  $Q_{15-min}$ . Third, it could also

reflect discharge data from a different period, as noted above. Regardless of the reason behind the differences in  $Q_s$  and  $Y$ , these two sets of values are both low and thus reflect the limited sediment production of the watersheds.

Additional work might shed more light on variations in sediment transport within the watershed. The sediment transport pattern in the theoretical analysis assumes bankfull discharge, and thus to analyze the spatial patterns of  $SSC$ , samples with  $Q_d > Q_{bf}$  would provide best validations to the model results. This study only has 11 LTER data points of  $SSC$  at the Parker River Dam with a  $Q_d > Q_{bf}$ . The LTER dataset contains  $SSC$  data from 0.1 to 39.8 mg/L and  $Q_d$  with  $RI$  of 0.65 to 7.9 years. The log regression of  $SSC$  and  $Q_d$  yielded a negative slope (Fig. 39). For data points with  $Q_d > Q_{bf}$  ( $5.5 \text{ m}^3 \text{ s}^{-1}$ ,  $RI > 1.53$ ) ( $n = 11$ ),  $SSCs$  range between 0.68 to 4.6 mg/L (Fig. 40). For four highest  $SSCs$  (11.4 - 39.8 mg/L),  $Q_d$  ranges between 0.009 ( $RI = 0.65$ ) and  $1.9 \text{ m}^3 \text{ s}^{-1}$  ( $RI = 0.93$  years) (Fig. 39). Thus, existing datasets imply that  $SSCs$  stay low and do not vary much (mostly within 1~10 mg/L) despite the variations of  $Q_d$  over ~4 orders. Thus,  $Q_s$  and  $Y$  calculated from the sediment rating curve of this dataset are not what one would expect. The negative correlation indicates that increasing discharge is probably diluting a relatively constant sediment inputs from the watershed and thus the landscape is sediment starved. Close examinations of the hydrograph, seasonality, and land use changes of individual cases with high  $SSC$  could potentially provide more understanding of what factors are contributing to the high  $SSC$  events ( $SSC > 10.0$  mg/L, Fig. 39) that occur despite a relatively low discharge.

### 7.3 Sediment Sources to the PIS Estuary

Evaluating potential sediment sources for the estuary is critical to model the resilience of marshes under SLR. For the PIS estuary, the threshold rate of SLR is predicted to be at  $5 \text{ mm yr}^{-1}$ , given an  $SSC$  of 3 mg/L and a tidal range of 3 m (Kirwan et al., 2010). With the current acceleration

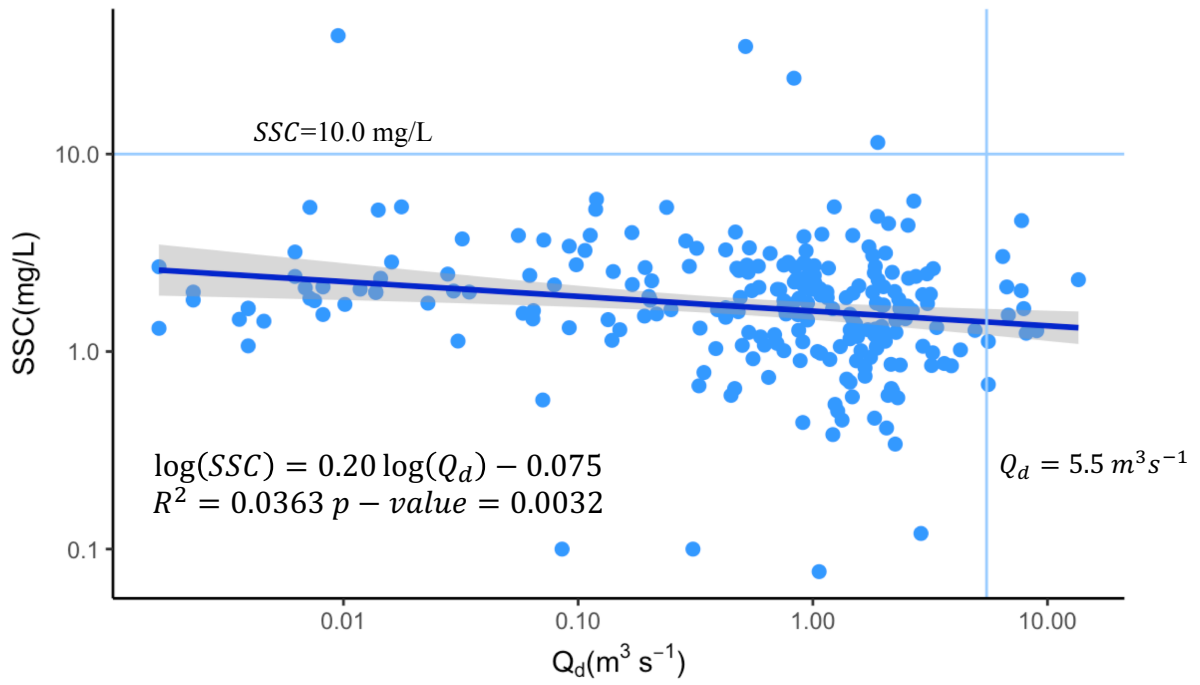


Figure 39. The relationship between  $SSC$  and  $Q_d$  at the Parker River Dam (LTER site). The blue line indicates the log-regression relationship between the two variables and the grey band shows the 95% confidence interval. The light blue reference line indicates the bankfull discharge (vertical,  $5.5 \text{ m}^3/\text{s}$ ) and the splitting line for the highest four  $SSC$ s (horizontal,  $10 \text{ mg/L}$ ) at Parker River Dam.

of SLR, the drowning of the marsh is expected to happen in less than 30-40 years (Kirwan et al., 2010). The threshold rate of SLR can increase to more than  $20 \text{ mm yr}^{-1}$  with an order increase in SSC ( $30 \text{ mg/L}$ ) in the PIS estuary (Kirwan et al., 2010). The resulting resilience of marshes could postpone the drowning for at least about a century as the SLR rate is projected to reach  $20 \text{ mm yr}^{-1}$  earliest around 2100 (Fig. 7, 8). Thus, finding additional sediment sources to the estuary is critical for the resilience of marshes against SLR.

The sediment loads from the Parker and Ipswich River watersheds are considered to be an important sediment source to the PIS system, accounting for about 10% of total sediment load needed to maintain marsh accretion (Hopkinson et al., 2018). However, in contrast with McCusker and Daniels (2008) who estimated a total yearly sedimentation rate of five dams in Connecticut to be  $7664 \text{ m}^3 \text{ yr}^{-1}$ , the dams in the Parker River watershed are hardly trapping sediments and might even be sediment sources, as indicated by Nadeau (2010). These outcomes might not be a result of the size of the watershed, but rather a result of the low sediment availability of the watershed and the lack of effectiveness of the stream profile for eroding and transporting sediments. The Parker River watershed has average  $Q_s$  ( $61.0 \text{ Mg yr}^{-1}$ ) and  $Y$  ( $1.0 \text{ Mg km}^{-2}\text{yr}^{-1}$ ) that are significantly below the average in the northeastern US ( $36.8 \text{ Mg yr}^{-1}\text{km}^{-2}$ ; Ames, 2018) and the overall  $Q_s$  ( $3210 \text{ Mg yr}^{-1}$ ) and  $Y$  ( $3.1 \text{ Mg km}^{-2}\text{yr}^{-1}$ ) for the Ipswich and Parker Rivers (Hopkinson et al., 2018). Also, the difference in topographic environment can impact the effectiveness of the hillslope and fluvial processes to erode sediments. In the Willis and Griggs (2003) study, the steep topography of the small coastal drainages in California prime the exceptionally high sediment loads, which are reduced by 25% by over 500 dams on these drainages.

Kirwan et al. (2011) suggested a 6 to 9  $\text{km}^2$  wetland expansion in the PIS during the European settlement due to the land clearing in the Rowley watershed (Fig. 1b) and argued for the capacity

of the watershed to provide substantial amount of sediments ( $SSC \sim 10 \text{ mg/L}$ ) allowing marsh expansion. The platform evolution model indicates that marshes can expand quickly (<100 years) with increasing sediment supply (from  $\sim 1 \text{ mg/L}$  to  $\sim 10 \text{ mg/L}$ ) and maintain a metastable equilibrium despite sediment supply reduction (from  $\sim 10 \text{ mg/L}$  to  $\sim 1 \text{ mg/L}$ ) (Kirwan, et al. 2011). Thus, a short-term increase in fluvial sediment supply during past land-clearing might also exist for the Parker River watershed and legacy sediments could have been stored behind dams.

The surficial geology categories in the Rowley River watershed are the same as those in the Parker River watershed, but the proportions of each type are different (Table 2; Fig. 3). Both watersheds have a significant portion of sand and gravel deposits, but the dominant geologic unit in the Parker River watershed is till or bedrock (Table 2), which does not provide much sediment for erosion and transport. In the Rowley River watershed, fine-grained deposits (10%) and floodplain alluvium (22%) are also much more available than those of the Parker River watershed (a total of 10%, Table 1). Thus, this difference in surficial geology could lead to a difference in sediment availability of the watersheds.

Also, the Parker River watershed as defined in this study only incorporates the part that transport sediments purely through hillslope and fluvial processes. In contrast, the Rowley River watershed analysis in the Kirwan et al. (2011) study included the entire watershed with both fluvial and tidal portions. Zhang et al. (2020) suggested that water level and tidal flow are the two dominant factors controlling  $SSC$  in the PIS: water level explains 34% of overall  $SSC$  variations and 60% of variation during tidal ebb, while tidal flow explains 19% of variations during tidal flood and 49% of variations when water levels are low during tidal flood. Thus, it is possible that the historically elevated sediment transport in the Rowley River was a result of the synergy between tidal processes and land clearing.

Despite the difference between the two watersheds and the scope of two studies, the results of Kirwan et al. (2011) remain debatable (Priestas et al., 2012) and field observations also suggest visible marsh degradation under large reductions in sediment supply (e.g., Cahoon et al., 1995; Kearney et al., 2002; Yang et al., 2005). It is possible that land clearing never boosted  $Y$  of the Rowley watershed during the European period and the present-day marsh extent has existed since early 1700s. If this was also true for the Parker River watershed, little legacy sediment could be found behind the old mill dams in the dammed reach. For the several field sites of this study in the dammed reach, no evidence for legacy sediment storage was found adjacent to the channel. Thus, removing dams will likely not release past sediments to the marsh.

The fluvial contribution to the sediment budget in the PIS estuary only represents one piece of information within the whole story. The  $Q$  of the Parker River can only explain 19% of  $SSC$  variations within the marsh (Zhang et al., 2020). Fluvial sediment loads together comprise only 10% of total sediment needed for marsh accretion in PIS estuary under  $2.8 \text{ mm yr}^{-1}$  of SLR, while erosion of marsh shoreline comprises 29% (Hopkinson et al., 2018). Given that the PIS estuary has accreted at rates comparable to SLR in past decades, the contribution from the ocean and tidal flats are much more important factor in the marsh accretionary sediment budget system, making up about 61% of total sediment needed (Hopkinson et al., 2018).

The Merrimack River is a likely source of oceanic sediments. It is the fourth largest river by drainage area in New England and enters the western Gulf of Maine north of the Plum Island. The formation of Plum Island was linked to the reworking of the lowstand deposits from Paleo-Merrimack River (e.g., Hein et al., 2012). The abundant sand supply from the Merrimack River and the longshore currents gradually built sand landward and southward (e.g., McIntire and Morgan, 1962; Hein et al., 2012). Modelling the wetland-estuarine-shelf interaction processes in

the PIS and Merrimack River system, Zhao et al. (2010) predicted a complex recirculation loop around the Merrimack River, shelf, and Parker River. Conducting a Lagrangian neutral-buoyant particle-tracking experiment using their model of river-estuarine-shelf system, particles released at maximum flood tide in the Merrimack River during both spring and neap tidal cycles followed the main trajectory flowing onto the shelf and then turned clockwise to flow southward (Zhao et al., 2010). In most modelled conditions, more than 10% of the modelled particles ( $n=50$ ) would enter PIS and sediment transport from Merrimack to PIS is most effective under spring tide without wind forcing (See Fig. 9 from Zhao et al., 2010). Clues for this recirculation can be found on the Landsat orthophotograph of the PIS and Merrimack River mouth after Hurricane Irene on September 2<sup>nd</sup>, 2011: an evident suspended sediment plume came out of the Merrimack River and curved down south towards the PIS (Fig. 40). Based on the sediment rating curve and  $Q_d$  during Hurricane Irene, the sediment load for the watershed upstream USGS gage at Lowell, MA (USGS 01100000) was about 1000 Mg/d at the peak of this event (Fig. 41). Thus, a conservative estimate of 10 Mg/d of sediments could be delivered from Merrimack River to the PIS system during this event.

Finally, although SLR threatens the resilience of marshes, climate change might increase the *SSC* in the PIS in an unexpected way. As the intensity and frequency of extreme precipitation continues to increase (Easterling et al., 2000), the Gulf of Maine might expect more Nor'easter storms. The consequential river flooding and strong northeast wind might raise *SSC* within the estuary to a level that is critical for marsh accretion ( $\sim 10$  mg/L; Kirwan et al., 2011). For a river flood on April 3, 2014 with a river discharge of  $6.17 \text{ m}^3/\text{s}$  ( $RI = 2$  years), the *SSC* in PIS was 4-5 times larger (9.87 mg/L vs. 1.72 mg/L) when compared to a river discharge of  $1.83 \text{ m}^3/\text{s}$  (Zhang et al., 2020; Fig. 38). Based on the *SSC* data collected at the LTER site, *SSCs* during high flow



Figure 40. The Landsat Scenes in band 1-2-3 [Blue-Green-Red] of Plum Island Sound and Merrimack River mouth on September 2<sup>nd</sup>, 2011 (after Hurricane Irene) (Earth Explorer, 2020).

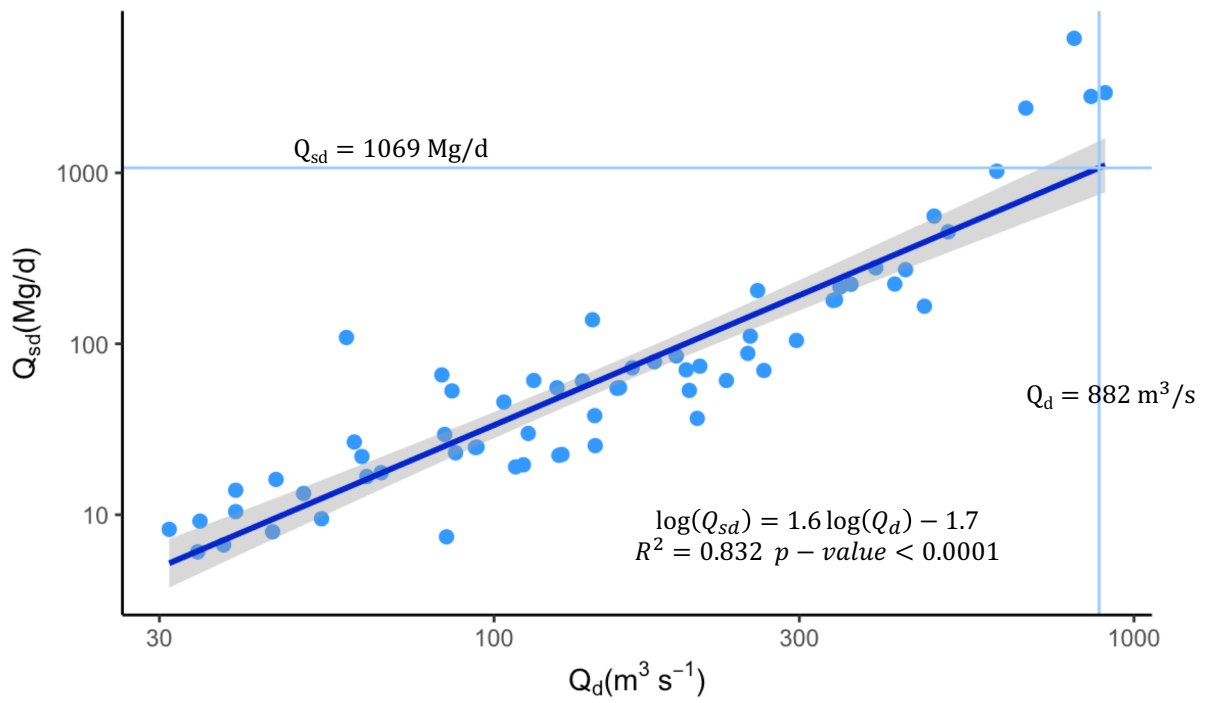


Figure 41. The sediment rating curve for the USGS gage at Lowell, MA (USGS 01100000) on the Merrimack River. Light blue lines indicate the  $Q_d$  during Hurricane Irene ( $882 \text{ m}^3/\text{s}$ ) and its corresponding  $Q_{sd}$  ( $1069 \text{ Mg/d}$ ) estimated from this curve.

events ( $> 5 \text{ m}^3/\text{s}$ ;  $RI > 1.64$  years) remain small (an average of  $1.96 \text{ mg/L}$  with a range of  $0.68 - 4.6 \text{ mg/L}$ ). Though high *SSCs* ( $> 10 \text{ mg/L}$ ) were recorded, they were mostly recorded during a base flow condition (an average of  $0.81 \text{ m}^3/\text{s}$  [ $RI = 0.75$  years] with a range of  $0.0094 - 1.89 \text{ m}^3/\text{s}$ ). Thus, the increase in *SSC* observed by Zhang et al. (2020) during a high flow may be a result of turbulent fluxes remobilizing sediments within the marsh rather than a result of the watershed delivering sediments. Also, strong northeast wind during the storm of March 26<sup>th</sup>, 2018 triggered sediment resuspension along the shoreline and in the bay, doubling the *SSC* ( $4.08 \text{ mg/L}$  vs.  $1.82 \text{ mg/L}$ ) when comparing to a similar condition with northwest wind (Zhang et al., 2020). It is unclear whether a strong northeast wind would further aid sediment transport through the Merrimack-shelf-PIS recirculation loop, and it is worthwhile for future study to explore the interaction of high river discharge, strong northeast wind, and the recirculation loop of the riverine-estuarine-shelf system to better understand the influence of climate change on the sediment budgets of the watershed.

#### **7.4 Insights on Management**

As part of the Parker River/Essex Bay ACEC, the PIS estuary attracts management interests from different stakeholders to maintain its marsh extent under the influence of various anthropogenic factors. Concerns over the impacts of climate change, SLR, and human-made structures are mounting overtime, and management practices such as dam removal are proposed (e.g., Schottland et al., 2017; Kelder, 2018; DER, 2020). However, these assessments only focus on the ecological impacts (mostly concerning fish passage) and infrastructure failure risks of the dams (e.g., Schottland et al., 2017; Kelder, 2018; DER, 2020), ignoring their potential roles in trapping past and current sediments that could be used for marsh accretion. The results of my study reveal that removing dams on the Parker River would lead to limited change in the sediment budget

of the downstream marsh. The methods used in this study can be systemized and integrated into the existing Restoration Potential Model Tool, that evaluates the relative ecological benefits of dams in Massachusetts (DER, 2020).

Furthermore, the results of this study reveal a need to assess the management efforts against climate change and SLR from a more holistic scope of the whole riverine-estuarine-shelf system. As a big portion of marsh sediment supply comes from the marsh shoreline along the main channels of the estuary, the shelf and the Merrimack River, management practices along the shoreline and within the Merrimack River watershed can also impact the long-term sustainability of the PIS estuary. The interests in armoring shoreline with either living shorelines or hard stabilization structures (e.g., Schottland et al., 2017) might actually lead to the opposite preservation effect as most of sediment sources of PIS come from the ocean and tidal flat (61%) and erosion from the shoreline is essential to maintaining elevation of marsh to SLR (Hopkinson et al., 2018). Dams on the Merrimack River are found to have trapped significant amount of sediments (e.g., Pearson et al., 2011; Shawler et al., 2019). Thus, dam removal projects within the Merrimack River watershed could potentially help the resilience of PIS by releasing sediments to the shelf that might then recirculate into the PIS estuary. Collaborative efforts to manage the watersheds of PIS and Merrimack River could help better develop future management practices.

## **8 Conclusions**

This study combines theoretical, field, and empirical analyses using remote sensing and field data to determine the impact of dams on sediment transport, and evaluate the capability of the Parker River watershed as a sediment source. Sediment transport patterns are modelled through the calculations of  $P$  and  $\tau_b$  along the Parker River main stem using DEMs. The values of  $SSC$ , aerial photos, and satellite images provide field-based evidence of whether active sediment

transport exists along the Parker River. Empirical calculation of  $Te$  provides a reference value for the sediment trapping capability of the dams.

Contrary to the conclusions of previous studies (Willis and Griggs, 2003; McCusker and Daniels, 2008), the results support H1 (Upstream dams have no impact on the sediment supply of the Parker River watershed to the PIS and thus, no role in influencing the threshold sea level rate and resilience of salt marshes). The patterns of  $\frac{d\tau_b}{dx}$  are similar between the dammed and undammed scenarios (Fig. 25) and  $Te$  of the dams are negligible (Table 5-6). The limited influence of dam removal could be contributed to three reasons. First, the dams were built on natural knickpoints along the river, and therefore dam removal does not significantly change the river profile. Second, the watershed is sediment starved. 50% of the watershed is consist of till or bedrock, which supplies limited amount of sediments. The average  $Q_s$  and  $Y$  of the Parker River watershed (Fig. 27, 28) are significantly below the average in the northeastern US (Ames, 2018).  $SSC$  data on a base flow day and a 0.87-year event day are also not significantly different from those of a blank DI water sample (Fig. 29, 30). Thus, little sediments are available for erosion from hillslopes. Third, Crane Pond likely serves as an effective sediment sink preventing sediments from 63% of the watershed to transport downstream.

Consistent with previous studies, this study reveals a limited influence of fluvial contribution to the sediment budget of the PIS estuary. Sediment sources from the ocean and tidal flats are more important factors (e.g., Hopkinson et al., 2018; Zhang et al., 2020). In particular, the Merrimack River is most likely a source of oceanic sediments (Hopkinson et al., 2018), given the recirculation mechanism existing among the Merrimack River, the shelf, and the PIS estuary (Zhao et al., 2010). Climate change might also interact with this riverine-estuarine-shelf system through more extreme floods and strong northeast wind events that may boost  $SSC$  within the estuary.

The proposed method of this study provides an additional scope to assess the ecological benefits of removing a dam, and could be systemized and integrated into current assessment tools for dam removal. These analyses could then contribute to better understand the implications of upland land use management to the habitat and environment of downstream communities. Future studies should assess the sediment dynamics and management practices from a holistic scope of the riverine-estuarine-shelf system.

## Bibliography

- Ames, E. M. (2018). *A Comparison of Glacial and Land-use Controls on Erosion in the Northeastern United States* (Master's thesis). Master's thesis shared by Noah Snyder (Boston College).
- Bagnold, R.A. (1966). An approach to the sediment transport problem from general physics. *United States Geological Survey Prof. Paper* 422-1: 231-291.
- Bent, G.C., and Waite, A.M. (2013). *Equations for estimating bankfull channel geometry and discharge for streams in Massachusetts: U.S. Geological Survey Scientific Investigations Report 2013–5155*. 62 p.. <http://dx.doi.org/10.3133/sir20135155>.
- Bindoff, N.L., J. Willebrand, V. Artale, A. Cazenave, J. Gregory, S. Gulev, K. Hanawa, C. Le Quéré, S. Levitus, Y. Nojiri, C.K. Shum, L.D. Talley and A. Unnikrishnan. (2007). *Observations: Oceanic Climate Change and Sea Level*. In: *Climate Change 2007: The Physical Science Basis. Contribution of Working Group I to the Fourth Assessment Report of the Intergovernmental Panel on Climate Change* [Solomon, S., D. Qin, M. Manning, Z. Chen, M. Marquis, K.B. Averyt, M. Tignor and H.L. Miller (eds.)]. Cambridge University Press, Cambridge, United Kingdom and New York, NY, USA
- Boon, J. D. (2012). Evidence of Sea Level Acceleration at U. S. and Canadian Tide Stations, Atlantic Coast, North America. *Journal of Coastal Research*, 28(6), 1437–1445. <https://doi.org/10.2112/JCOASTRES-D-12-00102>.
- Borsje, B. W., Kranenburg, W. M., Roos, P. C., Matthieu, J., & Hulscher, S. J. M. H. (2014). The role of suspended load transport in the occurrence of tidal sand waves. *Journal of Geophysical Research: Earth Surface*, 119(4), 701-716.
- Brown, C. B. (1943). Discussion of "Sedimentation in reservoirs " by B . J. Witzig, *Proc , Amer . Soc. Civ. Eng.*, v. 69, no. 6, pp. 793-815, 1493-1499.
- Brune, G. M. (1953), Trap efficiency of reservoirs, *Eos Transactions AGU*, 34(3), 407–418, doi:10.1029/TR034i003p00407.
- Buchsbaum, R., Purinton, T., and Magnusson, B. (2002). *The Marine Resources of the Parker River-Plum Island Sound estuary: An update after 30 years*. Massachusetts Office of Coastal Zone Management. 172p. <https://www.mass.gov/files/documents/2016/08/ug/marine-resources-preb.pdf>.
- Bureau of Geographic Information (MassGIS) (2017). *MassGIS Data Layers*. [www.mass.gov/service-details/massgis-data-layers](http://www.mass.gov/service-details/massgis-data-layers). Accessed 3 November 2017.
- Bureau of Geographic Information (MassGIS) (2019). *MassGIS Data Layers*. [www.mass.gov/service-details/massgis-data-layers](http://www.mass.gov/service-details/massgis-data-layers). Accessed 15 March 2019.
- Cahoon, D. R., D. J. Reed, and J. W. Day Jr. (1995), Estimating shallow subsidence in microtidal salt marshes of the southeastern United States: Kaye and Barghoorn revisited, *Mar. Geol.*, 128, 1–9, doi:10.1016/0025-3227(95)00087-F.
- Church, J. A., & White, N. J. (2011). Sea-Level Rise from the Late 19th to the Early 21st Century. *Surveys in Geophysics*, 32, 585–602. <https://doi.org/10.1007/s10712-011-9119-1>
- Craft, C., Clough, J., Ehman, J., Joye, S., Park, R., Pennings, S., Guo, H. & Machmuller, M. (2009). Forecasting the effects of accelerated sea-level rise on tidal marsh ecosystem services. *Frontiers in Ecology and the Environment*, 7(2), 73–78. doi: 10.1890/070219
- D'Alpaos, A., Lanzoni, S., Marani, M., & Rinaldo, A. (2007). Landscape evolution in tidal embayments: Modeling the interplay of erosion, sedimentation, and vegetation dynamics. *Journal of Geophysical Research*, 112, F01008. <https://doi.org/10.1029/2006JF000537>

- Dada, O. A., Li, G., Qiao, L., Asiwaju-Bello, Y. A., & Anifowose, A. Y. B. (2018). Recent Niger Delta shoreline response to Niger River hydrology: Conflict between forces of nature and humans. *Journal of African Earth Sciences*, 139, 222–231.  
doi:10.1016/j.jafrearsci.2017.12.023
- Dangendorf, S., Marcos, M., Wöppelmann, G., Conrad, C. P., Frederikse, T., & Riva, R. (2017). Reassessment of 20th century global mean sea level rise. *Proceedings of the National Academy of Sciences of the United States of America*, 114(23), 5946–5951.  
<https://doi.org/10.1073/pnas.1616007114>
- Davis, B.E. (2005). A Guide to the Proper Selection and Use of Federally Approved Sediment and Water-Quality Samplers: Vicksburg, MS, *U.S. Geological Survey. Open File Report 2005-1087*, 20 p.
- Division of Ecological Restoration (DER) (2014). *Estimates of Ecological Services Values from Ecological Restoration Projects in Massachusetts*. 40 p. Accessed on 23 February 2020.  
<https://www.mass.gov/doc/phase-2-estimates-of-ecosystem-service-values-from-ecological-restoration-projects-in-0/download>.
- Division of Ecological Restoration (DER) (2020). *DER's Restoration Potential Model Tool Description*. Accessed on 3 April 2020.  
<https://www.mass.gov/service-details/ders-restoration-potential-model-tool-description>.
- Dunne, T. & Leopold, L. B. (1978). *Water in environmental planning*. San Francisco: W. H. Freeman.
- Earth Explorer (2020). *Landsat 8 OLI*. Accessed on March 16th, 2020 from <https://earthexplorer.usgs.gov/>.
- Easterling, D.R., Meehl, G.A., Parmesan, C., Changnon, S.A., Karl, T.R. and Mearns, L.O. (2000). Climate extremes: observations, modeling, and impacts. *Science*, 289(5487), pp.2068-2074.
- Executive Office of Environmental Affairs (2005). *Parker River Watershed Year 5 Watershed Action Plan (2005-2010)*. 79 p.  
<https://www.mass.gov/files/2017-07/Parker%20River%20Watershed%20Action%20Plan.pdf>.
- Forbes, D.L., and Syvitski, J.P.M. (1994). *Paraglacial coasts*. In *Coastal evolution: Late quaternary shoreline morphodynamics*. Edited by R.W.G. Carter and C.D. Woodroffe. Cambridge University Press, Cambridge. pp. 373–424.
- Fredsøe, J., and Deigaard, R. (1992). Mechanics of coastal sediment transport. *World Scientific*.
- Gartner, J. D., Dade, W. B., Renshaw, C. E., Magilligan, F. J., & Buraas, E. M. (2015). Gradients in stream power influence lateral and downstream sediment flux in floods. *Geology*, 43(11), 983–986. <https://doi.org/10.1130/G36969.1>
- Granato G.E., Ries, K.G., III, and Steeves, P.A. (2017) Compilation of streamflow statistics calculated from daily mean streamflow data collected during water years 1901-2015 for selected U.S. Geological Survey streamgages: *U.S. Geological Survey Open-File Report 2017-1108*, 17 p.
- Hay, C. C., Morrow, E., Kopp, R. E., & Mitrovica, J. X. (2015). Probabilistic reanalysis of twentieth-century sea-level rise. *Nature*, 517(7535), 481–484.  
<https://doi.org/10.1038/nature14093>
- Hein, C. J., FitzGerald, D. M., Carruthers, E. A., Stone, B. D., Barnhardt, W. A., & Gontz, A. M. (2012). Refining the model of barrier island formation along a paraglacial coast in the Gulf of Maine. *Marine Geology*, 307, 40-57.

- Hill, K. M., Gaffney, J., Baumgardner, S., Wilcock, P., & Paola, C. (2017). Experimental study of the effect of grain sizes in a bimodal mixture on bed slope, bed texture, and the transition to washload. *Water Resources Research*, 53(1), 923-941.
- Hopkinson, C.S., Morris, J.T., Fagherazzi, S., Wollheim, W.M., Raymond, P.A., (2018). Lateral marsh edge erosion as a source of sediments for vertical marsh accretion. *J. Geophys. Res. Biogeosci.* 123, 2444–2465.
- Horton, R. E. (1945). Erosional development of streams and their drainage basins: hydro-physical approach to quantitative morphology. *Geological Society of America Bulletin*, 56 (3): 275–370.
- Jevrejeva, S., Moore, J. C., Grinsted, A., Matthews, A. P., & Spada, G. (2014). Trends and acceleration in global and regional sea levels since 1807. *Global and Planetary Change*, 113, 11–22. <https://doi.org/10.1016/j.gloplacha.2013.12.004>
- Kearney, M.S., Rogers, A.S., Townsend, G., Rizzo, E., and Stutzer, D. (2002). Landsat imagery shows decline of coastal marshes in Chesapeake and Delaware Bays. *American Geophysical Union*, v. 83, p. 173–178. doi: 10.1029/2002EO000112.
- Kelder, B. (2018). *Great Marsh Barriers Assessment*. Ipswich River Watershed Association, Ipswich, MA. <http://pie-rivers.org/barriers>.
- Kemp, G. P., Day, J. W., Rogers, J. D., Giosan, L., & Peyronnin, N. (2016). Enhancing mud supply from the Lower Missouri River to the Mississippi River Delta USA: Dam bypassing and coastal restoration. *Estuarine, Coastal and Shelf Science*, 183(B), 304–313. <https://doi.org/10.1016/j.ecss.2016.07.008>
- Kirwan, M. L., Guntenspergen, G. R., Alpaos, A. D., Morris, J. T., Mudd, S. M., & Temmerman, S. (2010). Limits on the adaptability of coastal marshes to rising sea level. *Geophysical Research Letters*, 37, L23401. <https://doi.org/10.1029/2010GL045489>
- Kirwan, M. L., & Murray, A. B. (2007). A coupled geomorphic and ecological model of tidal marsh evolution. *Proceedings of the National Academy of Sciences of the United States of America*, 104(15), 6118–6122. <https://doi.org/10.1073/pnas.0700958104>.
- Kirwan, M. L., & Murray, A. B. (2012). Forum Reply: Rapid wetland expansion during European settlement and its implication for marsh survival under modern sediment delivery rates. *Geology*, e286.
- Kirwan, M. L., Murray, A. B., Donnelly, J. P., & Corbett, D. R. (2011). Rapid wetland expansion during European settlement and its implication for marsh survival under modern sediment delivery rates. *Geology*, 39(5), 507–510. <https://doi.org/10.1130/G31789.1>
- Kasprak, A., Magilligan, F.J., Nislow, K.H., Renshaw, C.E., Snyder, N.P., and Dade, W.B. (2013). Differentiating the relative importance of land cover change and geomorphic processes on fine sediment sequestration in a logged watershed. *Geomorphology*, 185: 67–77. doi: 10.1016/j.geomorph.2012.12.005.
- Lane, L., Hernandez, M., & Nichols, M. (1997). Processes controlling sediment yield from watersheds as functions of spatial scale. *Environmental Modeling and Software*, 12(4), 355–369. [https://doi.org/10.1016/S1364-8152\(97\)00027-3](https://doi.org/10.1016/S1364-8152(97)00027-3)
- McCusker, M. H., & Daniels, M. D. (2008). The Potential Influence of Small Dams on Basin Sediment Dynamics and Coastal Erosion in Connecticut. *Middle States Geographer*, 41, 82–90.
- McFadden, L., Spencer, T., & Nicholls, R. J. (2007). Broad-scale modelling of coastal wetlands: what is required? *Hydrobiologia*, 577, 5–15. <https://doi.org/10.1007/s10750-006-0413-8>

- McIntire, W. G., & Morgan, J. P. (1962). *Recent geomorphic history of Plum Island. Massachusetts and adjacent coasts* (No. TR-19-PT-A). LOUISIANA STATE UNIV BATON ROUGE COASTAL STUDIES INST.
- Meade, R.H. (1982). Sources, sinks, and storage of river sediment in the Atlantic drainage of the United States. *J. Geology*, 90(3): 235–252. doi: 10.1086/628677.
- Merritts, D., Walter, R., Rahnis, M., Hartranft, J., Cox, S., Gellis, A., Potter, N., Hilgartner, W., Langland, M., Manion, L., Lippincott, C., Siddiqui, S., Rehman, Z., Scheid, C., Kratz, L., Shilling, A., Jenschke, M., Datin, K., Cranmer, E., Reed, A., Matuszewski, D., Voli, M., Ohlson, E., Neugebauer, A., Ahamed, A., Neal, C., Winter, A., and Becker, S. (2011). Anthropocene streams and base-level controls from historic dams in the unglaciated mid-Atlantic region, USA. 369. *Philosophical Transactions of the Royal Society A: Mathematical, Physical and Engineering Science*. <https://doi.org/10.1098/rsta.2010.0335>.
- Middleton, G., & Southard, J. (1984). Chapter 6 Dynamics of Sediment Movement. *Mechanics of Sediment Movement* (p. 165-239). Tulsa, Oklahoma: Society of Economic Paleontologists and Mineralogists.
- Morris, J. T., Sundareshwar, P. V., Nietch, C. T., Kjerfve, B., & Cahoon, D. R. (2002). Responses of coastal wetlands to rising sea level. *Ecology*, 83(10), 2869–2877.
- Mudd, S. M., Howell, S. M., & Morris, J. T. (2009). Impact of dynamic feedbacks between sedimentation, sea-level rise, and biomass production on near-surface marsh stratigraphy and carbon accumulation. *Estuarine, Coastal and Shelf Science*, 82(3), 377–389. <https://doi.org/10.1016/j.ecss.2009.01.028>
- Nadeau, P., (2010). *Larkin Mill Dam Sediment Transport Characterization*. Hollings Scholarship Internship Report.
- National Oceanic and Atmospheric Administration (NOAA). 2017. *Tides and currents products*. <http://tidesandcurrents.noaa.gov/products.html> Accessed 25 October 2017.
- National Oceanic and Atmospheric Administration (NOAA) (2018). *Datums for 8441241, Plum Island South MA*. <https://tidesandcurrents.noaa.gov/datums.html?units=1&epoch=0&id=8441241&name=Plum+Island+South&state=MA>. Accessed 28 April 2018.
- Nienhuis, J.H., Ashton, A. D., Edmonds, D. A., Hoitink, A. J. F., Kettner, A. J., Rowland, J. C., & Törnqvist, T.E. (2020). Global-scale human impact on delta morphology has led to net land area gain. *Nature*, V. 577: 514-518.
- Paola, C., Parker, G., Mohrig, D. C., and Whipple, K. X. (1999). The influence of transport fluctuations on spatially averaged topography on a sandy, braided fluvial fan. Numerical Experiments in Stratigraphy: Recent Advances in Stratigraphic and Sedimentologic Computer Simulations, *Society for Sedimentary Geology (SEPM) Spec. Publ.*, edited by J. Harbaugh et al., pp. 211–218, SEPM (Society for Sedimentary Geology).
- Panin, N., & Jipa D., (2002). Danube river sediment input and its interaction with the north-western Black Sea. *Estuarine, Coastal and Shelf Science* 54: 551-562.
- Park, K.-D., R. S. Nerem, J. L. Davis, M. S. Schenewerk, G. A. Milne, and J. X. Mitrovia, (2002). Investigation of glacial isostatic adjustment in the northeast U.S. using GPS measurements. *Geophysical Research Letters*, 29(11). doi: 10.1029/2001GL013782.
- Pearson, A.J., Snyder, N.P., and Collins, M.J. 2011. Rates and processes of channel response to dam removal with a sand-filled impoundment. *Water Resour. Res.* 47(8): 1–15. doi: 10.1029/2010WR009733.

- Priestas, A. M., Fagherazzi, S., Wilson, C. A., & FitzGerald, D. M. (2012). Forum Comment: Rapid wetland expansion during European settlement and its implication for marsh survival under modern sediment delivery rates. *Geology Forum*, e284–e285. <https://doi.org/10.1130/G32597C.1>
- Rahmstorf, S. (2007). A semi-empirical approach to projecting future sea-level rise. *Science*, 315(January), 368–370. <https://doi.org/10.1126/science.1135456>
- Restrepo, J. D., Kettner, A. J., & Syvitski, J. P. M. (2015). Recent deforestation causes rapid increase in river sediment load in the Colombian Andes. *Anthropocene*, 10(October), 13–28. <https://doi.org/10.1016/j.ancene.2015.09.001>
- Rickards, B., Lund, K., and Cooper, A. (2002). *An Assessment of Resource Management Strategies in the Parker River/Essex Bay Area of Critical Environmental Concern*. Massachusetts Office of Coastal Zone Management. 97 p. <https://www.mass.gov/files/documents/2016/08/sd/an-assessment-of-resource-management-strategies-in-the-parker-river-essex-bay-acec-rickards.pdf>.
- Sallenger Jr, A. H., Doran, K. S., & Howd, P. A. (2012). Hotspot of accelerated sea-level rise on the Atlantic coast of North America. *Nature Climate Change*, 2(12), 884–888. <https://doi.org/10.1038/nclimate1597>
- Schottland, T., Merriam, M. G., Hilke, C., Grubbs, K., and Castonguay, W. (2017). *Great Marsh Coastal Adaptation Plan*. National Wildlife Federation Northeast Regional Office, Montpelier, VT. [www.nwf.org/GreatMarshAdaptation](http://www.nwf.org/GreatMarshAdaptation).
- Snyder, N. P. (2009). Studying Stream Morphology with Airborne Laser Elevation Data. *EOS, Transactions American Geophysical Union*, 90(6), 45–52.
- Snyder, N. P., Nesheim, A. O., Wilkins, B. C., & Edmonds, D. A. (2013). Predicting grain size in gravel-bedded rivers using digital elevation models: Application to three Maine watersheds. *Geological Society of America Bulletin*, 125(1/2), 148–163. <https://doi.org/10.1130/B30694.1>
- Snyder, N. P., Whipple, K. X., Tucker, G. E., & Merritts, D. J. (2000). Landscape response to tectonic forcing: Digital elevation model analysis of stream profiles in the Mendocino triple junction region, northern California. *Geological Society of America Bulletin*, 112(8), 1250–1263.
- Stokes, G. G. (1851). On the effect of internal friction of fluids on the motion of pendulums. *Transactions of the Cambridge Philosophical Society*. 9, part ii, p. [52], equation (127).
- Strahler, A. N. (1952). Hypsometric (area-altitude) analysis of erosional topology. *Geological Society of America Bulletin*, 63 (11): 1117–1142.
- Strahler, A. N. (1957). Quantitative analysis of watershed geomorphology. *Transactions of the American Geophysical Union*, 38 (6): 913–920.
- Syvitski, J. P. M., Kettner, A. H., Overeem, I., Hutton, E. W. H., Hannon, M., Brakenridge, R., Day, J., Vorosmarty, C., Saito, Y., Giosan, L., and Nicholls, R. J. (2009). Sinking Deltas due to Human Activities. *Nature Geoscience*. 2. 10.1038/ngeo629.
- Syvitski, J., Vorosmarty, C. J., Kettner, A., & Green, P. (2005). Impact of humans on the flux of terrestrial sediment to the global coastal ocean. *Journal of Geology*, 115, 1–19.
- Temmerman, S., Govers, G., Meire, P., & Wartel, S. (2003). Modelling long-term tidal marsh growth under changing tidal conditions and suspended sediment concentrations, Scheldt estuary, Belgium. *Marine Geology*, 193, 151–169.
- U. S. Geological Survey (USGS) (2017). *The National Map*. Accessed 3 November 2017. [nationalmap.gov](http://nationalmap.gov)

- U. S. Geological Survey (USGS) (2018a). *USGS 01101000 Parker River at Byfield, MA*. Accessed 24 April 2018. [https://waterdata.usgs.gov/nwis/uv?site\\_no=01101000](https://waterdata.usgs.gov/nwis/uv?site_no=01101000).
- U. S. Geological Survey (USGS) (2018b). *USGS Sediment Data Portal*. <https://cida.usgs.gov/sediment/>. Accessed 13 June 2018.
- U. S. Geological Survey (USGS) (2019). *Stream Stats Data-Collection Station Report*. Accessed 5 September 5, 2019. <https://streamstatsags.cr.usgs.gov/gagepages/html/01101000.htm>.
- Van Rijn L.C. (1984)/ Sediment transport, part I: bed load transport. *Journal of hydraulic engineering* 110(10): 1431- 1456.
- Verstraeten, G., & Poesen, J. (2000). Estimating trap efficiency of small reservoirs and ponds: methods and implications for the assessment of sediment yield. *Progress in Physical Geography: Earth and Environment*, 24(2), 219–251. <https://doi.org/10.1177/030913330002400204>
- Wade, L. (2008). *Larkin Mill Dam Removal: Monitoring and Modeling*. Not Published. Student field project shared by Matt Collins (NOAA).
- Wang, H., Yang, Z., Saito, Y., Liu, J. P., Sun, X., & Wang, Y. (2007). Stepwise decreases of the Huanghe (Yellow River) sediment load (1950 – 2005): Impacts of climate change and human activities, *Global and Planetary Change*, 57, 331–354. <https://doi.org/10.1016/j.gloplacha.2007.01.003>
- Wikipedia (2011). *Flussordnung.svg*. Accessed 23 October 2017. [https://commons.wikimedia.org/wiki/File:Flussordnung\\_\(Strahler\).svg](https://commons.wikimedia.org/wiki/File:Flussordnung_(Strahler).svg).
- Wilkins, B. C., & Snyder, N. P. (2011). Geomorphic comparison of two Atlantic coastal rivers: Toward an understanding of physical controls on Atlantic salmon habitat. *River Research and Application*, 27, 135–156. <https://doi.org/10.1002/rra.1343>.
- Willis, C.M. & Griggs, G.B. (2003). Reductions in Fluvial Sediment Discharge by Coastal Dams in California and Implications for Beach Sustainability. *Journal of Geology*, 111: 167-182.
- Whipple, K. (2004). IV. *Essentials of Sediment Transport* (PDF). 12.163/12.463 Surface Processes and Landscape Evolution: Course Notes. MIT OpenCourseWare, Retrieved 2018-7-12.
- Wollheim, W., & Hopkinson, C. (2016). *Dissolved nutrient and particulate concentrations of freshwater inputs to the Plum Island estuarine system, taken approximately monthly*. Plum Island Ecosystems LTER Database. <http://ecosystems.mbl.edu/PIE/data/WAT/WAT-VA-Inputs.html>
- Yang, S.L., Zhang, J., Zhu, J., Smith, J.P., Dai, S.B., Gao, A., & Li, P. (2005). Impacts of dams on Yangtze River sediment supply to the sea and delta intertidal wetland response. *Journal of Geophysical Research* 110: F03006.
- Zhang, X., Fichot, C.G., Baracco, C., Guo, R., Neugebauer, S., Bengtsson, Z., Ganju, N. and Fagherazzi, S. (2020). Determining the drivers of suspended sediment dynamics in tidal marsh-influenced estuaries using high-resolution ocean color remote sensing. *Remote Sensing of Environment*, 240, p.111682.
- Zhao, L., Chen, C., Vallino, J., Hopkinson, C., Beardsley, R. C., Lin, H., & Lerczak, J. (2010). Wetland-estuarine-shelf interactions in the Plum Island Sound and Merrimack River in the Massachusetts coast. *Journal of Geophysical Research: Oceans*, 115(C10).

## Appendix: Parameters and Constants

Table A.1. Parameters, corresponding symbols and units.

Parameters	Symbols	Units
drainage area	$A$	km <sup>2</sup> or m <sup>2</sup>
discharge	$Q$	m <sup>3</sup> s <sup>-1</sup>
bankfull discharge	$Q_{bf}$	m <sup>3</sup> s <sup>-1</sup>
channel width	$w$	m
bankfull channel width	$w_{bf}$	m
channel slope	$S$	-
elevation	$z$	m
distance	$x$	m
basal shear stress	$\tau_b$	Pa
downstream change of basal shear stress	$\frac{d\tau_b}{dx}$	Pa m <sup>-1</sup>
median bed grain size	$D$	m
grain size	$d$	m
Shields parameter	$\varphi$	-
critical Shields parameter	$\varphi_c$	-
Rouse number	$P$	-
downstream change of Rouse number	$\frac{dP}{dx}$	m <sup>-1</sup>
settling velocity	$w_s$	m s <sup>-1</sup>
shear velocity	$u^*$	m s <sup>-1</sup>
recurrence interval	$RI$	years
suspended sediment yield	$Y$	Mg km <sup>-2</sup> yr <sup>-1</sup>
sediment discharge	$Q_s$	Mg yr <sup>-1</sup>
suspended sediment concentration	$SSC$	mg L <sup>-1</sup>
mass of suspended sediments	$m_s$	mg
mass of dry sediments and organics	$m_{ds}$	mg
volume of water sample	$V_{ws}$	L
daily mean flow discharge	$Q_d$	cfs or m <sup>3</sup> s <sup>-1</sup>
instantaneous discharge (15-min)	$Q_{15\ min}$	cfs or m <sup>3</sup> s <sup>-1</sup>
peak discharge	$Q_{peak}$	cfs or m <sup>3</sup> s <sup>-1</sup>
daily sediment discharge	$Q_{sd}$	Mg d <sup>-1</sup>
trap efficiency	$Te$	-(%)
capacity-drainage area ratio	$C/W$	-(%)
capacity-inflow ratio	$C/I$	-(%)
mean annual inflow	$Q_{avg}$	m <sup>3</sup>
storage capacity of the reservoir	$V$	m <sup>3</sup>
reservoir area	$A_d$	m <sup>2</sup>
height of dam	$H_d$	m
slope of the sediment rating curve	$a$	-
intercept of the sediment rating curve	$b$	-

Table A.2. Constants, corresponding symbols, and values with units.

<b>Constants</b>	<b>Symbols</b>	<b>Values with Units</b>
density of water	$\rho$	1000 kg m <sup>-3</sup> at 20 °C
sediment density	$\rho_s$	2650 kg m <sup>-3</sup>
acceleration by gravity	$g$	9.81 m s <sup>-2</sup>
Manning's coefficient of channel roughness	$n$	0.04 for gravel-bedded rivers
bankfull discharge at the USGS gauge	$Q_{bf\ usgs}$	4.62 m <sup>3</sup> s <sup>-1</sup>
drainage area at the USGS gauge	$A_{usgs}$	$5.52 \times 10^7\ m^2$
empirical, dimensional coefficient for the power-law relation between bankfull discharge and drainage area	$k_q$	$8.20 \times 10^{-8}\ m\ s^{-1}$
exponent constant for the power-law relation between bankfull discharge and drainage area	$c$	1
empirical, dimensional coefficient for the power-law relation between bankfull channel width and drainage area	$k_w$	$1.918 \times 10^5\ m^{1.2382}$
exponent constant for the power-law relation between bankfull channel width and drainage area	$e$	0.4038
von Karman constant	$\kappa$	0.41
molecular viscosity	$\mu$	0.001 kg m <sup>-1</sup> s <sup>-1</sup> for water at 20 °C